NUMERICAL AND EXPERIMENTAL ANALYSIS OF MAGNETIC PULSE WELDING FOR JOINING SIMILAR AND DISSIMILAR MATERIALS

Angshuman Kapil

A Dissertation Submitted to
Indian Institute of Technology Hyderabad
In Partial Fulfillment of the Requirements for
The Degree of Master of Technology

Department of Mechanical and Aerospace Engineering

December, 2015

Declaration

I declare that this written submission represents my ideas in my own words, and where others ideas or words have been included. I have adequately cited and referenced the original sources. I also declare that I have adhered to all principles of academic honesty and integrity and have not misrepresented or fabricated or falsified any idea/data/fact/source in my submission. I understand that any violation of the above will be a cause for disciplinary action by the Institute and can also evoke penal action from the sources that have thus not been properly cited, or from whom proper permission has not been taken when needed.

Angshuman Kapil

Angshuman Kapil

ME13M0001

Approval Sheet

This thesis entitled "Numerical and experimental analysis of magnetic pulse welding for joining similar and dissimilar materials" by Angshuman Kapil is approved for the degree of Master of Technology from IIT Hyderabad.

Dr. Abhay Sharma
Department of Mechanical and Aerospace Engineering
IIT Hyderabad
Adviser

Dr. S Surya Kumar
Department of Mechanical and Aerospace Engineering
IIT Hyderabad
Examiner

Dr. Bharat Bhooshan Panigrahi
Department of Materials Science and Metallurgical Engineering
IIT Hyderabad
Examiner

Acknowledgements

It is a privilege for me to write the following few lines in acknowledgement of those who enabled me to carry out the project work upto this stage. I express my deep sense of gratitude to my thesis adviser **Dr. Abhay Sharma**, Associate Professor, Department of Mechanical and Aerospace Engineering, Indian Institute of Technology Hyderabad for his guidance, help and support to my project. His affability boosted my moral towards the working of the project. I express my deep and sincere gratitude, regards and thanks to him for his excellent guidance, invaluable suggestions and continuous encouragement at all the stages of my research work. His wide knowledge and logical way of thinking have been of great value for me.

I would also like to thank my batch mates, MTech friends and PhD scholars who at one point or the other have given their moral support and shared their knowledge which has been helpful to me so far. I would like to specially thank **Murugesh** and **Ramesh** for providing technical inputs and constantly helping me in the experimental work.

It was a great pleasure for me to be a part of the Department of Mechanical and Aerospace engineering, IIT Hyderabad and I would like to thank all the staff members and my friends for helping me in all stages of my work. The stay at IITH has developed me both personally and professionally and has inculcated in me numerous skills.

Above all, I extend my deepest gratitude to **my parents** for their invaluable love, affection, encouragement and support.

Dedicated to

This little endeavour is dedicated to all those who have technically made this world a better place to live in.

Abstract

Magnetic pulse welding, a high speed joining process using electromagnetic forces, because of clean and multi-material operation has a wide range of possibilities for further development and application. Unlike conventional joining processes, the weld interface does not melt keeping the material properties intact without generation of hazardous emissions in form of heat, fume, and spatters. The present investigation deals with the feasibility study of the magnetic pulse welding technology for joining of similar and dissimilar materials through numerical modelling and simulation work followed by experimental validation of the obtained results. A finite element model was developed and validated with results available in literature. The model developed in this study helped predict accurate values of weld validation criteria for a wide range of process parameters and for different combinations of similar and dissimilar materials with varying geometry. Based on the model suitable and shop floor applicable weldability windows considering one or more than one of the available weld validation criteria were developed for varying material and process parameter combination. The weldability windows would enable the end user to conduct magnetic pulse welding at parameters where successful weld occurrence is highly possible. Predictive models for impact velocity were developed for two different material combinations viz. Al-SS 304 and AA 2219-SS 321 using artificial neural network and the same were able to predict values within ±10 % probable error. The developed neural networks could handle a large data set and predict accurate impact velocities in a very less time which would otherwise take lot of effort and time through finite element modelling or experimentation. Sensitivity analysis highlighted that coil c/s area, coil turns, voltage and air gap effect the magnetic pulse welding process in a major way followed by coil length and resistance. This was followed by experimental validation of the results of the numerical models. The AA 2219- SS321 were welded with an electroforming machine but upon examination it was observed that all the joints failed and no visible bonding was observed among the mating members. A limitation on the electrical parameters viz. voltage, capacitance, frequency and inductance and

material parameters viz. skin depth led to the failure of the joints. The Al-SS 304 members were then welded in a machine with enhanced capacity. The pulse welded Al-SS 304 specimen was subjected to mechanical and metallurgical tests. The Al-SS 304 MPW joint subjected to lap shear tests resulted in fracture occurring out of the welded region and broke at the weaker of the base metals i.e. pure Al. Maximum pull-off strength of 111 MPa corresponding to a pull-off force of 1.697 kN was obtained for the joint which was greater than that of the weaker of the base metals i.e. Al. The obtained hardness results were in close agreement with results available in literature; an increase in the hardness value was recorded in and around the weld interface. The optical and scanning microscopy images showed the presence of a welded centre zone with a characteristic wavy pattern and unbonded zones on either side of it which is a characteristic of a tubular pulse welded joint, thus proving the weldability of the Al-SS 304 joint using magnetic pulse welding. Surface energy dispersive spectroscopy map of the Al-SS 304 joint gave clear evidence of material transfer between the two mating members. The increase in hardness near the interface could be related to the material transfer phenomena in magnetic pulse welding and intermetallic phase formation. Energy dispersive spectroscopy line analysis results suggested that the interface layer in the investigated joint had varying widths (5 μm to 12 μm) along the length of the welded zone. It can be concluded that some intermetallics, such as $FeAl_3$ is likely to have formed in this region and other similar parts of the diffusion zone. The welded bonds in the present investigation were aided by mechanical interlocking. The wave vortices took part in mechanical interlocking and the same acted as a joining mechanism.

The experimental results (optical imaging and scanning electron microscopy) have much similarity with the finite element model developed in the present study. Both the finite element model and experimental results showed similar weld interface characteristics which are in complete agreement with the available literature. It was found that a tubular magnetic pulse welded joint has separate bond and no-bond zones, the same being well predicted by the finite element model which validated the same. The closeness in the results predicted by the finite element model gives the end user the confidence to use to predict suitable process parameters for

successful welding, at the same time making the model practical and shop floor applicable. Future aspects of the simulative work should focus on development of models for MPW that would include thermodynamic simulation at micrometre scale to understand the short range diffusion and phase transformation along the welded interface during high pressure impact. The measurements of the wave pattern must be compared to the finite element simulations. Further research for detailing the microstructural changes in the parent materials and the mechanical properties of dissimilar welds including transmission electron microscopy work to study the structure of the mixture, composition, structure, arrangement and extent of the intermetallics formed along the welded interface must be carried out.

Nomenclature

Symbols

Symbol	Unit	Description
A	-	Material constant
$\vec{A}$	-	Vector potential
a_i	-	Predicted value
B	-	Material constant
$\vec{B}$	T	Magnetic flux density
C	μF	Capacitance of the system
C_0	-	Strain rate constant
c	-	Number of model covariates
d	mm	Distance between two long parallel conductors of infinite length
E	kJ	Discharge energy
F	N	Force existing between two long parallel conductors
$\vec{f}$	N	Magnetic force in unit volume of medium
G	GPa	Shear modulus
H_f	Kgf/mm^2	Hardness of the flyer tube
H_t	Kgf/mm^2	Hardness of the target tube
I	-	Unit matrix
I_1	A	Primary current passing through the coil
I_2	A	Secondary current
J	-	Jacobian matrix
$\vec{J}$	A/m^2	Coil current density
K	GPa	Bulk modulus
K_m	-	A constant
K_0	-	Constant depending on the geometry of the coil
k	-	Number of cells in the hidden layer
L	H	Inductance and resistance of the discharge circuit
l_w	mm	Length of the coil working zone

m	-	Material parameter
N	-	Number of turns of the coil
n	-	Strain hardening constant
net_j	-	Linear activation of the neuron
n_1	-	Number of data
o_i	-	Input activation of the *i*th neuron in the preceding layer
o_j	-	Output of the *j*th neuron
P	-	Material parameter
P_c	N/m^2	Critical impact pressure for jet formation in the subsonic state
p	-	Number of cells in the input layer
q	-	Number of cells in the output layer
R	ohm	Resistance of the discharge circuit
R^2	-	Coefficient of determination
Re	-	Reynolds number
S	m/s	Bulk sound velocity
s	-	Number of terms in full model
SQ_{model}	-	Sum of squares of predicated values of the model
SQ_{Total}	-	Sum square of actual process outcome
S_1	m/s	Speed of sound in the flyer sheet/tube
S_2	m/s	Speed of sound in the base sheet/tube
t	sec	Time
t_i	-	*i*th target value
t_v	-	Target value
U	kV	Charging voltage
U_T	m/s	Minimum impact velocity required for successful welding to occur
u	-	A positive number
V	-	Weights passed from hidden layer to output layer
V_{damage}	m/s	Velocity at which damage occurs to the impact members
$V_{threshold}$	m/s	Threshold impact velocity

V_w	m/s	Stagnation point velocity
V_{WT}	m/s	Transition velocity
v_w	m/s	Collision velocity
W	-	Weights passed from input layer to hidden layer
w_{ij}	-	Component of the weight vector
x	-	Number of input connections
Y	GPA	Young's modulus
Y_0	MPa	Tensile yield stress
y	-	Value predicted by the neural network
Z_{eq}	-	Equivalent acoustic impedance of the colliding sheets/tubes
Z_1	-	Flyer sheet/tube acoustic impedance
Z_2	-	Base sheet/tube acoustic impedance
β	-	Damping exponent
δ	mm	Skin depth
ε_{pl}	-	Equivalent plastic strain
$\dot{\varepsilon}$	1/s	Strain rate
$\dot{\varepsilon}_p$	-	plastic strain rate for $\dot{\varepsilon}$= 1.0/s
Υ	S/m	Conductivity of the medium
$\Upsilon(\partial\vec{A}/\partial t)$	A/m^2	Current density
σ	MPa	Yield stress
σ_D	MPa	Dynamic yield stress
σ_{pl}	MPa	von Mises yield stress
σ_{TU}	MPa	Ultimate tensile stress
σ_y	MPa	Quasi-static flow stress
ν	-	Poisson's ratio
μ	H/m	Absolute magnetic permeability of the conductor
μ_0	H/m	Permeability of free space (vacuum)
ρ	ohm m	Resistivity of conductor
ρ_1	kg/m^3	Material density of the flyer sheet/tube
ρ_2	kg/m^3	Material density of the base sheet/tube

ρ_f	kg/m^3	Density of the flyer tube
ρ_t	kg/m^3	Density of the target tube
ω	rad/s	Angular frequency of the current
Φ		Critical angle for jet formation
θ	K	Absolute temperature when the stress is applied
θ_{trans}	K	transition temperature defined as the one at or below which there is no temperature dependence on the expression of the yield
θ_{melt}	K	Reference melt temperature
π	-	Mathematical constant Pi

Physical constants

Symbol	Value	Description
μ_0	$4.\pi. 10^{-7}$ H/m	Permeability of free space (vacuum)

Abbreviations

Abbreviation	Description
ADALINE	Adaptive linear network
ANN	Artificial neural network
CT	Computerised Tomography
DOE	Design of experiments
EDS	Energy dispersive spectroscopy
EMPT	Electromagnetic pulse technology
EMF	Electromagnetic forming
EXW	Explosive welding
FEA	Finite element analysis
FEM	Finite element model
FESEM	Field electron scanning electron microscope
HEL	Hugoniot elastic limit
HEDM	Hole drilling electric discharge machine
IML	Intermediate layer

IP	Intermetallic phases
LM	Levenberg-Marquardt
MLP	Multi-layer perceptron
MPW	Magnetic pulse welding
MSE	Mean squared error
NDT	Non-destructive testing
OM	Optical microscope
PDV	Photon Doppler Velocimetry
PLC	Programmable logic controller
RBF	Radial basis function network
TEM	Transmission electron microscopy
UT	Ultrasonic testing
WEDM	Wire-cut electric discharge machine

Publications

Refereed Journal Articles

[1] **Kapil, A.** and Sharma, A.: "Magnetic Pulse Welding: An efficient and environmentally friendly multi-material joining technique", Journal of Cleaner Production, 2015, 100, 35-58.

[2] **Kapil, A.** and Sharma, A.: "Understanding weld interface in magnetic pulse welded dissimilar Al-SS 304 tubular joint through numerical and experimental investigation", Materials and Design **(submitted)**

[3] **Kapil, A.** and Sharma, A.: "Investigation of weld validation criterion for magnetic pulse welded dissimilar Al-SS 304 tubular joint by artificial neural networks and numerical simulations" **(under preparation)**.

Book Chapter

[4] **Kapil, A.** and Sharma, A.: Coupled Electromagnetic Structural Simulation of Magnetic Pulse welding, Advances in material forming and joining, Edited by Uday Shanker Dixit and R. Ganesh Narayanan, Chapter 13: Pages 255-272; DOI 10.1007/978-81-322-2355-9_13, ISBN: 978-81-322-2354-2.

Conference proceedings

[5] **Kapil, A.** and Sharma, A.: Coupled Electromagnetic Structural Simulation of Magnetic Pulse welding, Proceedings of the 5th International and 26th All India Manufacturing Technology, Design and Research Conference, IIT Guwahati, 2014, 249(1)-249(6).

Contents

List of Figures **Page No.**

List of Tables **Page No.**

Chapter 1

Introduction

With improvements and development in technology, the use of a single material no longer suits the ever-increasing demands for sophisticated and versatile products and equipment's. Thus, a mix of variety of materials provides the desired technological characteristics required for the industries. Product designers and manufacturers of automobiles, aerospace and railway are often constrained by the restrictions of traditional joining technologies that limit the materials, type of joint that can be joined and the quality of the process [1, 2]. MPW allows manufacturers to significantly improve their product designs and production results by making it possible to weld dissimilar metals thus enabling the use of lighter and stronger material combinations. Joining of dissimilar materials by conventional fusion welding processes is impossible in certain cases due to huge differences in melting point, thermal conductivity, volumetric specific heat, and coefficient of thermal expansion. MPW being a cold process, therefore, makes it possible to use it for welding dissimilar metals. The production of high strength joints economically is a major challenge for the manufacturing sector nowadays [3]. An alternative to conventional welding is joining by electromagnetic welding since the achievable joint strength is within the range of the strength of the weakest joining partner [3].

MPW is a high speed joining process using electromagnetic forces to cause the impact of one metal onto other to form a solid state cold weld. The process is a variant of impact welding, which deals with the welding of workpieces by application of a striking force and is analogous to explosive welding (EXW) [1]. The analogy of MPW with other impact welding processes is quite evident and literature proving the same is available. MPW is a part of the larger window called the Electromagnetic pulse technology (EMPT). It can be employed for various purposes depending upon the geometry and need of the job. The process has been successfully applied to weld sheet metals, plates and tubes in the recent past.

MPW is a process that been known since 70's. The use of MPW in industries is limited due to lack of knowledge about the physics of the process. Inspite of the

process been known for more than 40 years, the industrialization of the process took place only at the end of the twentieth century. The use of magnetically driven welding has gained much importance over the past few years owing to its various advantages over conventional welding processes. Unlike conventional welding processes the weld interface does not melt keeping the material properties intact. As the time for a weld to occur is very less, usually in microseconds [4], the heat generated is not sufficient to melt the workpieces thus limiting the problem of heat affected zone and prevents localized annealing and corrosion in and around the weld zone. MPW allows joining of dissimilar metals and at the same time minimizes the chances of formation of continuous intermetallic phases (IP). In the case of joining dissimilar materials, one should consider the process which does not lead to formation of intermetallics compounds and other fragile phases. The use of MPW results in the reduction of manufacturing costs compared to conventional welding processes as it does not employ consumable materials like filler wire/rod or shielding gases. The process is a forward step into the future of welding having widespread application in automotive, aerospace, ordnance, consumer products, packaging and electrical industry due to its unique ability to join dissimilar metals as well it being an environment friendly process. It allows the user to look into further possibilities that are beyond scope of conventional welding processes. Although the process has been known for a long time, there lies a wide range of possibilities for further development and application.

1.1 The Process

1.1.1 Welding set up and principle of operation

The MPW consists (Fig. 1) of a high voltage power supply, a bank of capacitors and a gap switch which is capable of opening and closing very fast. There is a control system and a trigger system outside whereas the work area is composed of a coil and the workpiece where the weld takes place.

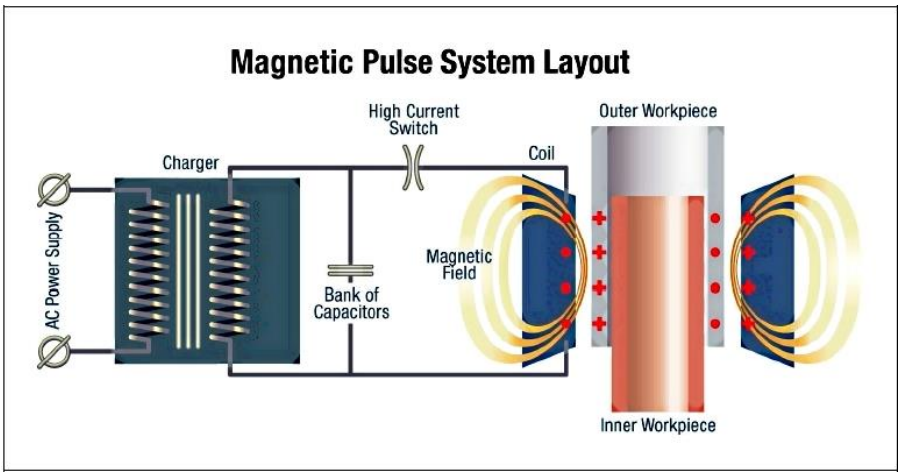

Fig. 1 MPW Process [5]

The schematic of the MPW set up for tubular geometry is shown in the Fig. 2. The whole set up can be divided into four units namely Pulse generator, Control cabinet, Workstation and an Operational unit [6]. The Pulse generator unit includes a bank of capacitors that store and discharge electrical energy through the electromagnetic coil very rapidly. The control cabinet consists of charging unit (DC power supply) and a high voltage trigger switch. The work station consists of the electromagnetic coil, workpiece, electrical cables and field shaper (optional).

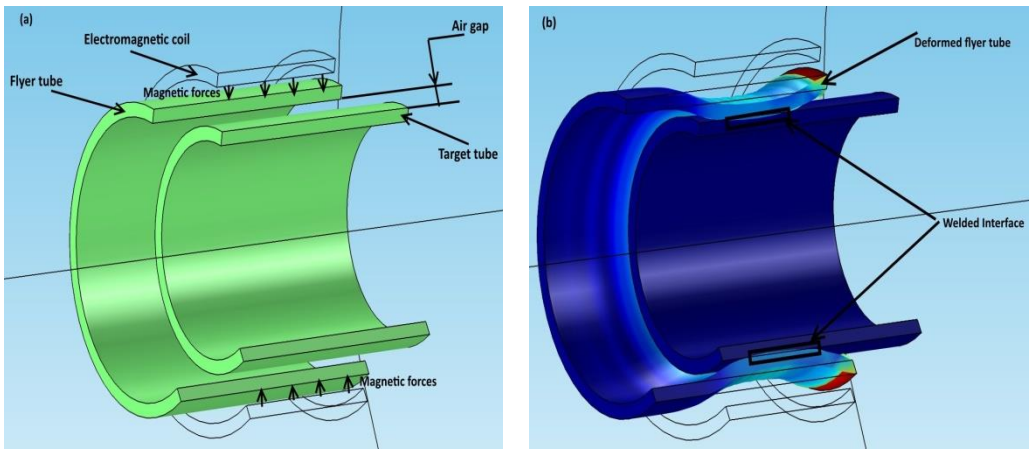

Fig. 2 MPW set-up for two tubes (a) before the application of pulsed current and (b) after application of current

MPW is centred on Ampere's law which states that the force existing between two long parallel conductors of infinite length carrying currents I_1 and I_2 and separated from each other by distance'd' may be written as:

$$F = \frac{\mu_0}{2\pi d} I_1 I_2 \tag{1}$$

When both the currents flow in opposite directions the force between the electromagnetic coil and workpiece is repulsive in nature and vice versa. An electrically conducting workpiece material is subjected to a force called the Lorentz force when a current is applied to it in presence of a magnetic field. The current itself generates a magnetic field.

As the current passes through the coil, a magnetic field is created around the coil, and due to the eddy currents on the surface of the workpiece material (conductor) a second magnetic field of opposing nature is created as shown in Fig. 3. These two magnetic fields interact with each other and an electromagnetic force is exerted on the flyer metal causing it to impact against the parent metal at high velocity. This causes the plastic deformation of the colliding metal and under certain conditions; a solid state weld is created between the two materials. The velocity of impact of the workpiece is in the range of 250-500 m/s [7] and thus the process is being named as high velocity forming process. After the discharge of energy, the trigger system automatically operates the gap switch that in turn starts converting the current from AC to DC. In the meantime, the processed parts are taken out of the system and the capacitors are charged to the desired energy level, and the system becomes ready for its next operation.

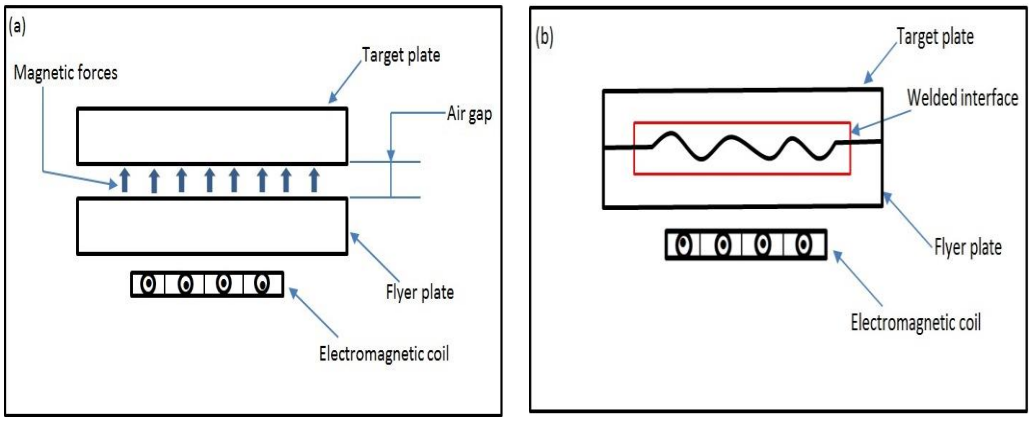

Fig. 3 Schematic illustration of MPW process (a) initial MPW set-up for flat plates and (b) deformed geometry after the application of magnetic forces MPW scheme

Welding of tubes is much similar to that of plate/sheet welding where current is discharged through the electromagnetic coil by operating a trigger. For MPW of tubular geometry the tube with higher electrical conductivity should be made the flyer and made to impact with the tube with lower electrical conductivity. The tube with

lower electrical conductivity or the base tube must be strong enough to resist the impact without damage.

1.1.2 Processing parameters

The MPW process parameters can be divided into a number of categories viz. electromagnetic, geometrical and material properties, the process being affected by a combination of these parameters.

1.1.2.1 Electromagnetic parameters

a) Discharge energy

Energy stored at the capacitor bank is discharged through the coil and this discharge should happen very rapidly in order to generate very high velocities during the impact of the flyer metal onto the target metal. Fig. 4 below shows the discharge of capacitor bank energy with time.

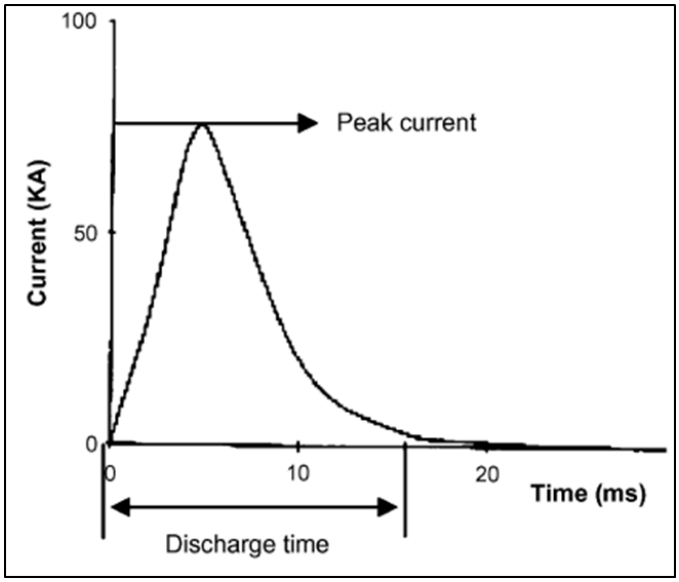

Fig. 4 Current discharging diagram [9]

With increase in charging voltage the discharge energy also increases and with this increase the shearing strength of the metals and the wavelength of the bond zone also increase as shown in Fig. 5. During the MPW, energy discharged by the capacitor bank is directly proportional to the square of the input voltage for a given value of capacitance as given in Eq. (2) [10]. With an increase in discharge energy, the energy of the flyer tube also increases and so does the impact velocity.

$$E = CU^2/2 \quad (2)$$

where E is the discharge energy, C is the capacitance of the system and U is the charging voltage.

For each material combination whether it is similar or dissimilar there is a particular range of energy required for joining the metals and there is a maximum energy beyond which tearing or weld failure occurs [11]. As the gap between the flyer and the base tube/plate increases the discharge energy should also be increased [5, 11].

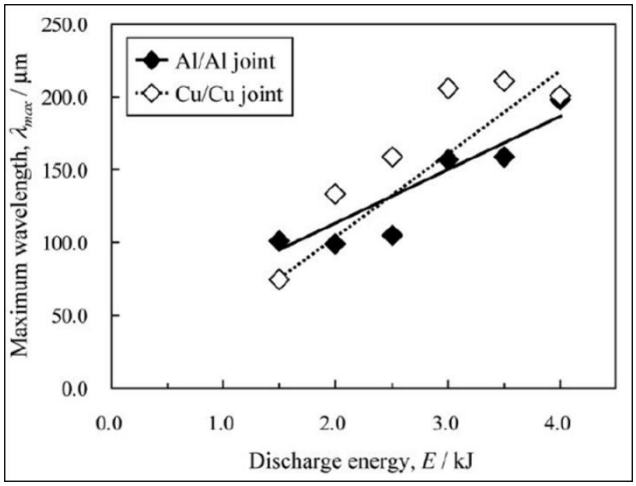

Fig. 5 Relationship between discharge energy and wavelength [8]

b) Magnetic pressure

Magnetic pressure causes the impact of the flyer plate/tube with the target plate/tube to form a joint. For a successful weld to occur it is necessary that the magnetic pressure is high or else the flyer does not attain sufficient velocity required for bonding to take place successfully. Higher magnetic pressure is obtained by increasing the discharge energy or by using a high frequency current. When there is an increase in standoff distance, the discharge energy must be increased in order to increase the magnetic pressure and maintain bond quality. At a given value of standoff distance increase in magnetic pressure increases the tensile shear strength of the joint [12].

For a tubular geometry, the magnetic pressure P generated due to the eddy current pulse in the coil is expressed as [10]:

$$P = \frac{\mu_0 K_0^2 N^2 U^2 C \sin^2\left((1/2\pi\sqrt{LC})t\right) exp(-(R/L)t)}{2Ll_w^2} \quad (3)$$

where μ_0 is the magnetic permeability, K_0 is a constant depending on the geometry of the coil, N is the number of turns of the coil, U is the input voltage, C is the capacitance of the system, L and R are the inductance and resistance of the discharge circuit respectively, l_w is the length of the coil working zone and t is the time.

c) Impact velocity

The energy used in the process and the standoff distance between the mating members directly influences the impact velocity. Fig. 6 shows the variation of impact velocity with increase of discharge energy. With an increase in discharge energy the impact velocity increases.

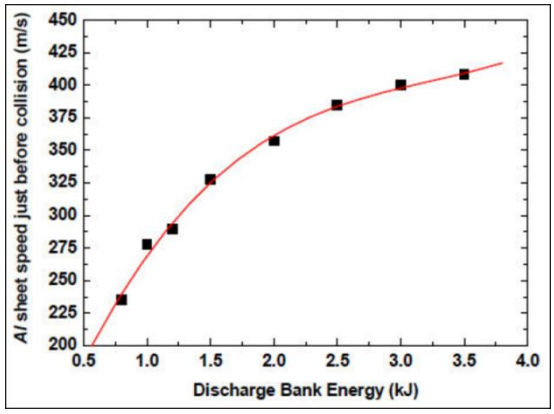

Fig. 6 Variation of flyer metal velocity with discharge energy [13]

The discharge energy and the time of discharge from the capacitor directly affect the impact velocity of the flyer. The energy transfer at low velocity leads to the collapse of the flyer and no bonding takes place. Fig. 7 shows the relationship between the energy discharged by the capacitor bank and impact velocity attained by the workpiece (flyer).

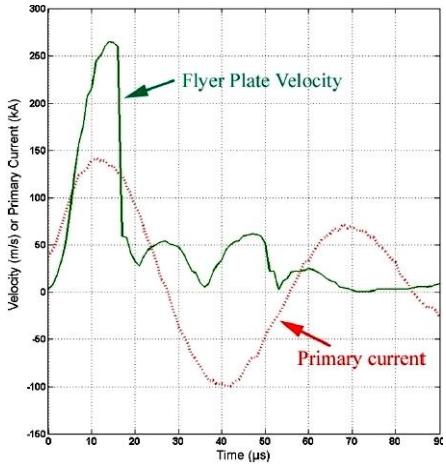

Fig. 7 Relationship between impact velocity and discharge energy [1]

One of the major requirements of conducting a successful weld through MPW is that the surfaces of the mating members are free of any oxide layers and contaminations. The impact velocity plays a crucial role in making the surfaces suitable for bonding due to the jetting action that removes any contaminants and makes the surfaces oxide free [5]. If the impact velocity is excessively high, intermetallic compounds might be formed at the interface of the mating members or brittle damage might occur whereas on the other hand if the velocity is too low the jet formed is not sufficient to remove the contaminants and oxide layer from the surface of the workpiece which does not allow successful weld to occur. It has also been proved that a minimum impact velocity has to be reached to ensure the weldability of the joint [14].

1.1.2.2 Geometrical parameters

a) Coil geometry

Coils are designed and manufactured in diverse ways and can be employed as flat forming coils, compression coils and expansion coils. The coils are classified into three main types depending upon the total number of turns, shape and material of the coil. The coil may be single and multi-turn. Depending upon its shape there are a variety of coils e.g. flat coil (I–shape, H-shape, E-shape), helical coil (solenoid), coils with rectangular and tapered cross section, spiral flat coil, tapered cross section coil, bifilar coil, and round coil. Based on material the coils can be further classified, e.g. brass coil, copper coil, copper alloy–chromium coil, copper-beryllium alloys coil and high strength aluminium alloys coil [15-17].

b) Standoff Distance/Air gap

The standoff distance is the distance between flyer plate and target plate or between flyer tube and core as shown in Fig. 8. It is normally between 0.5 and 3 times the thickness of the flyer plate/tube [18].

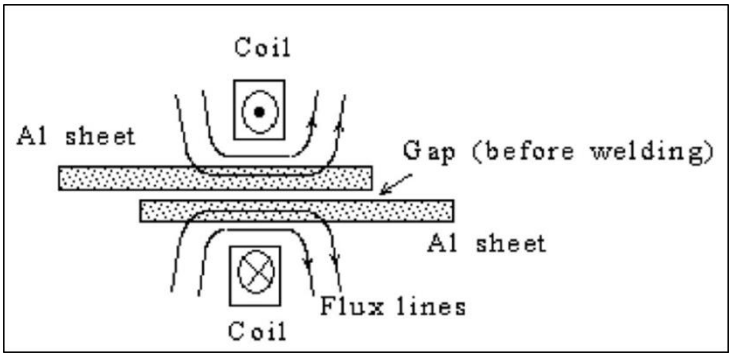

Fig. 8 Standoff Distance [19]

The gap between the mating parts must be present so that when electromagnetic force is supplied to the flyer workpiece, it must have requisite space and time to acquire the minimum required impact velocity for successful weld to happen [20]. When the gap between the mating parts is less the flyer does not attain maximum possible velocity while in the cases where the gap is more the velocity drops to a lower value during collision. For different materials there are different optimum values of standoff distance and any deviation beyond these values leads to decrease in width and shearing strength of the weld [5, 11] as shown by Fig. 9.

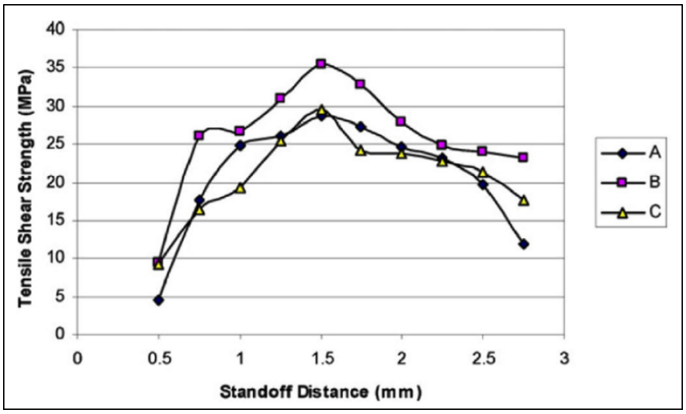

Fig. 9 Shear strength as a function of standoff distance on. B - Sample cut from centre of welded zone; A and C - samples cut from edges of the weld zone [11]

Fig. 10 shows the influence of standoff distance on the bond characteristics. It shows the weld zone interface during welding of aluminium and titanium at various

standoff distances. The standoff distance and energy increase from left to right (Fig. 10). The optimum value occurs at section 3. Before section 3 the standoff distance was very less, no bonding took place, and beyond section 3, as the standoff distance increased intermetallic formation was observed.

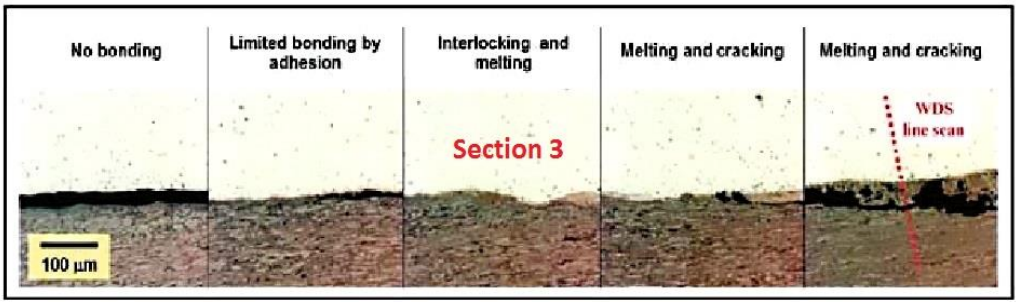

Fig. 10 Bonding interface as a function of standoff distance [21]

c) Impact angle

This is the angle formed by the target plate and the flyer plate on impact. For MPW the angle starts small and ends big for a parallel setup of the tubes. The impact angle normally is somewhere between 3° and 30°. For a fixed impact angle, the impact velocity is mainly responsible for the variations occurring in the bonding. As the impact angle increases, the impact velocity also increases.

1.1.2.3 Material properties

a) Workpiece materials

The electrical properties of material that affect the process are conductivity and permeability of the material. When the product of the conductivity and magnetic permeability for a given material is low then the skin depth of that material will be very high. As a result, the shielding of the magnetic field by the flyer metal will be poor and sufficient radial forces will not be set up on the flyer thus resulting in an inefficient process. The permeability of a material defines the degree of magnetisation [22]. The electrical conductivity influences the magnitude of eddy currents generated in the workpiece. Higher values of electrical conductivity cause the induced current values to be higher thus generating a larger opposing magnetic field. A larger value of induced magnetic field increases the magnetic pressure that is important to cause bonding.

The mechanical properties to be considered before selecting a material for performing the welding operation are yield strength, strain hardening and strain rate hardening. The yield stress of the selected material together with strain hardening defines the pressure required for deforming the flyer workpiece. As the deformations take place at very high velocity the dependence of the elastic plastic properties on the strain rate are of much importance. The constitutive behaviour of almost all the metals changes at strain rates above 10^{-4} s^{-1}. Beyond these strain rate values the apparent strain rate sensitivity of the metals change prominently [23]. A material constitutive law expresses the influences of strain and strain-rate hardening. A commonly used constitutive law is the Johnson-Cook model that can be expressed as [22]:

$$\sigma_{pl} = \left[A + B.\varepsilon_{pl}^{n}\right]\left[1 + C_0.ln\left(\dot{\varepsilon}_p\right)\right]\left[1 - \frac{\theta - \theta_{trans}}{\theta_{melt} - \theta_{trans}}\right] \quad (4)$$

where σ_{pl} is the von Mises yield stress (MPa), ε_{pl} is the equivalent plastic strain, $\dot{\varepsilon}_p$ is the plastic strain rate for $\dot{\varepsilon}$= 1.0/s, A, B, n are yield and strain hardening constants, C_0 is the strain rate constant, θ is the absolute temperature when the stress is applied (K), θ_{trans} is the transition temperature defined as the one at or below which there is no temperature dependence on the expression of the yield (K) and θ_{melt} is the temperature when the stress is applied (K).

b) Skin depth

Skin depth can be defined as the depth upto which the magnetic field penetrates inside the flyer metal form the top of its surface, the magnetic field being highest at the surface of the conductor (flyer) and decays exponentially as it moves towards the other edge. In other words it is the depth beneath the surface of the workpiece at which the current density decays to $1/e$ of the current density at the surface. As the capacitors are discharged a magnetic field is induced around the coil which reaches the surface of the workpiece (flyer) and induces a current on it. The eddy current limits the penetration of the magnetic field from the coil and creates its own induced magnetic field that diffuses through the thickness of the workpiece (flyer). Due to this skin effect, the repulsive magnetic field produces electromagnetic forces that exert the requisite pressure on the workpiece (flyer). These electromagnetic forces help the workpiece (flyer) attain the required impact velocity and cause impact of the same with the base metal at a very high pressure and velocity. The mathematical representation of skin depth is shown [24]:

$$\delta = \sqrt{\frac{2\rho}{\omega\mu}} \tag{5}$$

where δ is the skin depth (m), ρ resistivity of conductor (ohm m), μ is the absolute magnetic permeability of the conductor (H/m) and ω is the angular frequency of the current (rad/s).

The variation of skin depth of several materials as a function of current frequency is shown in Fig. 11. It can be seen that for a low conductive material like stainless steel the skin depth is very high at lower frequencies. Thus, it becomes very important to employ a high frequency when low conductive materials are employed for MPW. As higher frequency values are employed, the skin depth values start decreasing as seen in Fig. 11. When hollow workpieces or thin workpieces are used, the frequency employed should be high such that the skin depth is less than the workpiece wall thickness.

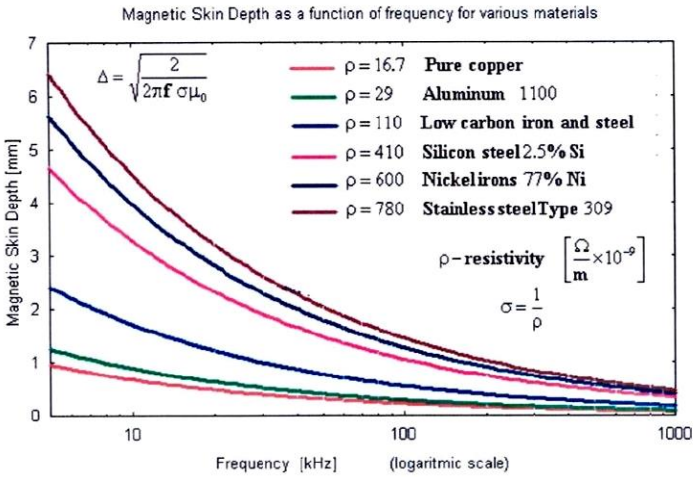

Fig. 11 Skin depth as a function of the frequency for several [25]

1.1.3 Bonding mechanism

The phenomenon of formation of a wavy interface occurs in the case of both EXW as well as MPW. The fact that the same wavy bond zone occurs in both these processes supports the analogy between them [26, 27]. The temperature in the interface rises because of jetting action and substantial plastic deformation of the surfaces occur under the impact. Under certain circumstances the melting and solidification takes place in a similar manner as in EXW [28-30]. The rise in the interface temperature leading to the softening of the interface and its vicinity supports

the formation of a wavy pattern. Very few attempts have been reported in literature [8, 31, 32] that explain the mechanisms governing the wave formation in MPW, but no detailed model has been developed specific to MPW as a process is identical to EXW [33]. Thus, the well-defined mechanisms for wave formation in EXW can also be applied to MPW.

An explosively welded joint is usually characterized by the presence of two distinct interfaces; a waveless (straight) and a wavy interface as shown in Figs. 12 (a) and (b). A regular wavy interface is however often seen in EXW and this transition from straight to wavy interface is governed by impact parameters like collision velocity, impact angle etc. In MPW also a similar interface having wavy shape similar to EXW process can be seen. The interface waves are periodic in nature and are characterized by well-defined wavelength and amplitude values. The nature of the wavy interface is dependent on several process parameters like the energy of collision, the angle of impact, and the geometrical features of the welded joint. The strength of the joints produced in case of impact welding whether by the use of explosives or magnetic pulses, the strongest joints produced will be in the case where waves are formed at the surface [34].

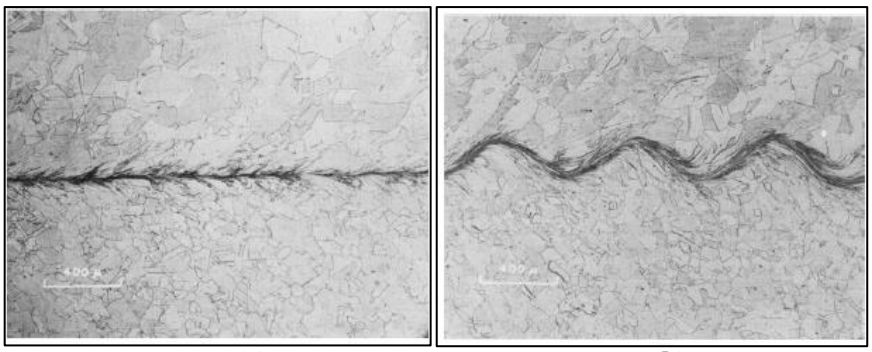

(a) **(b)**

Fig. 12 (a) a straight interface (b) a typical wavy interface [28]

Inspite of striking similarities between the above two processes they cannot be termed to be entirely same. An inherent assumption of EXW is that it considers the angle of impact to be constant whereas the same is not the case in MPW where there is a change in the impact angle as the welding progresses. Thus as mentioned in [35] “if an EXW weldability window prescribes certain values for the angle of impact, the weld produced by MPW will only occur in that part of the workpiece where these conditions are met”. In practical sense the above statement implies that due to the variation in angle of impact there are different zones in MPW in which weld may or

may not occur. This directly contradicts the fact that in EXW process, the angle of impact is constant and bond formation or a successful weld occurs along the whole workpiece.

The mechanism of bonding and the events occurring at the interface in MPW or EXW is a complicated subject and not much research has been done in this area. Similar to EXW, in MPW an impact force acts between the two mating surfaces. This impact force is the cause of the formation of jet between the two bonded surfaces. The surface contaminants and all traces of oxides on the surface of the metal plates are removed due to this jetting action. The high impact forces due to the detonation of the explosives or due to magnetic force as in MPW cause the plastic deformation of the metals for a short period and force the surfaces of the members together to form a bond. The two metal surfaces cleaned by the jet of its oxide layers are then made to come in close contact with each other due to the application of very high pressures. The pressing of the metal plates together then initiates the forces at the atomic level subsequently bringing the atoms of mating members into contact with each other. A large number of explanations to explain the mechanism occurring at the point of collision have been suggested, but all have concluded that metals involved behave like liquids momentarily, in spite of the fact that they remain solid. As the process is very rapid and fast too, the interface temperatures do not rise much and thus, it has become possible to bond dissimilar metals with widely varying properties permanently. Parameters like the magnetic pressure, impact angle, impact velocity and the standoff distance etc. decide the interface phenomenon and the quality of the bond. The collision point is subjected to very high pressures and these pressures are typically in the order of 100,000 MPa [36].

1.1.3.1 Collision jetting

In impact welding, formation of a high velocity jet occurs when the mating members collide with a high velocity and when the collision angle and collision velocity cross a critical value required for bonding to occur. The oxide films found on the surface layers of the metals are a hindrance to the successful formation of a bond that is metallurgical by nature. The forward moving jet helps in removing the oxide layer and renders the surface clean and suitable for bonding (Fig. 13). The oxide free metal surfaces owing to the forward jet action, now under the action of very high pressures are joined internally. This high-pressure region can be called the collision region. The metal plates being subjected to very high pressures are subjected to a

considerable amount of plastic deformation that is localized in the area where bonding occurs. The bond thus created is by nature metallurgical and usually is stronger than the weaker parent metal [28, 37].

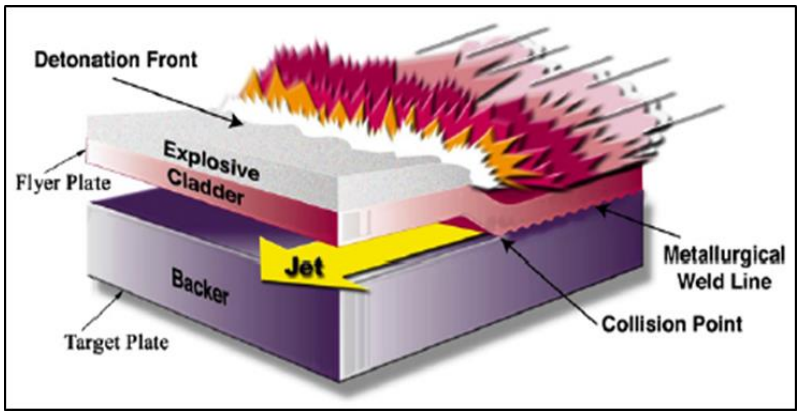

Fig. 13 Schematic diagram showing the forward moving jet in EXW [1]

Fig. 14 defined by Wittman and Deribas [36], shows a possible window in which MPW can occur successfully. Within the closed area abcdef and with correct parameters the welding can occur. The Curves 6-6 and 7-7 represent the upper and lower flyer plate velocity limits for welding to occur. A combination of critical values of collision velocity and collision angle defines a curve 5-5 to the right of which no jetting can occur, while jetting can occur to its left. The minimum and maximum angles of incidence required for jetting to occur are defined by Abscissas 3-3 and 4-4, while 1-1 and 2-2 respectively define the lowest velocity for which conditions for welding can be created and the velocity above which excessive kinetic energy is produced, which will give rise to excessive melting and thus produce unwanted intermetallic alloying. It is very much necessary that this envelope should be experimentally defined for all metal pairs to be welded.

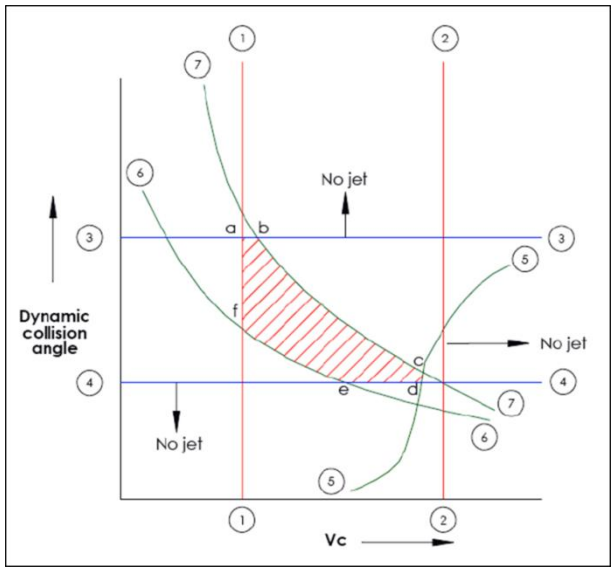

Fig. 14 Jetting envelope for any metal pair [36]

1.1.4 Wave formation mechanism

Over the past few years, several researchers have suggested mechanisms to explain how the waves at the interface are produced [38-40]. Few researchers [41, 42] have suggested the formation of local vortices in the plastic deformation zone due to the shearing action of the flyer and target plates/tubes. They suggested that these vortices are the source for wave formation at the interface. However some other researchers [43, 44] attributed this fact to the formation of a hump ahead of the stagnation point periodically. Another theory [45, 46] was suggested which stated that flow discontinuities across the weld interface was the reason behind the wavy pattern seen at the interface. One more theory explaining the formation of a wavy interface was also suggested [47, 48]. It was proposed that periodic interferences of the compressive waves produced at the point of collision point and redirected waves at the free surface of the target plate result in the formation of a wavy interface in MPW. However, there is no agreement till date which can represent the exact mechanism responsible for the wave formation. The mechanisms have been divided into four categories. These are:

(i) Indentation mechanism.

(ii) Helmholtz instability mechanism.

(iii) Rarefaction wave mechanism.

(iv) Vortex-shedding mechanism.

i) Indentation mechanism

The indentation mechanism [44] tries to explain the way the weld interface attains its characteristic wavy shape. The indentation of the parent plate that occurs periodically and formation of a hump ahead of the stagnation point *S* (Fig. 15) by the flyer plate and vice versa causes the interface to take the periodic wavy shape. The periodicity of the wavy interface is due to the influence of the period of instability of the re-entrant jet. The indentation occurs due to the high pressures which come into picture when stagnation point velocity (V_w) is in the vicinity of the parent plate "sound" speed and there is a decrease in this pressure when V_w goes on either side of the sound speed. The cause of periodicity in the indentation is assumed due the periodic oscillation of V_w about the local sound speed.

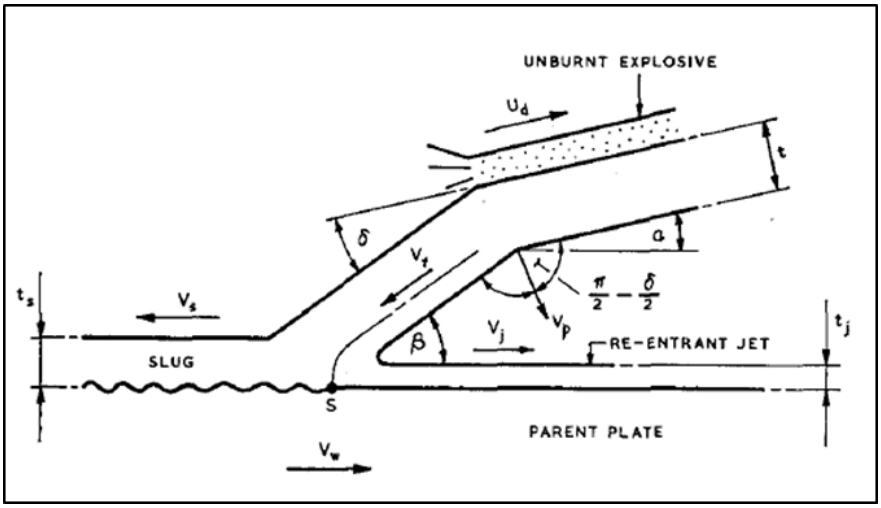

Fig. 15 Assumed flow configuration during cladding process [44]

ii) Helmholtz instability mechanism

The Kelvin–Helmholtz instability mechanism [37, 44] infers that interface waves are formed when there are discontinuities in the velocities of flow in the interface of the welded members. The interaction of two different fluids with different flow velocities causes interferences and as a result, instabilities occur at the interface of the weld due to the interferences. As a general rule a mass flow, mostly from the material with higher density to the material with lower density is the direct result of the instabilities. The instability with a certain direction and some definite value of velocity (energy) causes transfer of material along the weld interface (Fig. 16(a)), and thus to satisfy the law of conservation of energy of the system a flow of material from the side

with less concentration gradient occurs immediately (Fig. 16(b)). The velocity of both the metals influences the interface waves and gives directionality and shape to the newly created interface (Fig. 16(c)).

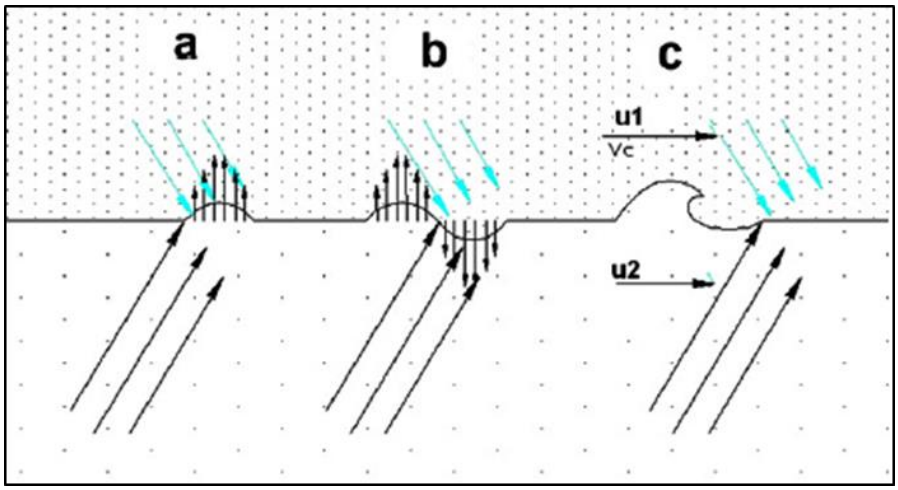

Fig. 16 Material transfer along the weld interface (u1 > u2) [44]

iii) Rarefaction wave mechanism

Rarefaction wave mechanism [37, 44] was another theory developed for explaining the mechanism of wave formation involved in impact welding. According to this theory the collision point is where the compressive waves are generated and are reflected back by the unobstructed surface of the target workpiece. As shown in Fig. 17 (a), the shock waves that are produced at the point of impact move in both the target and flyer materials carrying a radial front. The compression waves which are generated in the flyer plate/tube are then redirected as refraction waves from the back surface (blue arrows in Fig. 17 (b)). The welding set up used in the experiment [44] was axi-symmetric. Kore et al. [49] stated that it was the symmetricity of the set-up which makes the compression waves, compressed from the inner part to meet their corresponding waves at the center of the bar in a rigid collision. These are then reflected as compression waves towards the interface (black arrows in Fig. 17 (b))". At the collision point, pressure is at its peak as the velocity is higher at this point and as the weld progresses the speed decreases. The superposition p–x diagram of Fig. 17 (a) and (b) is shown in Fig. 17(c) as new shock waves are created with the origination of each new impact point. For generation of waves at the interface it is must that the interaction between the compressed and refracted waves, happen at the collision point and in its close by areas and this would be possible only in the case where there is a

match between their periods. It is necessary that the interaction between the compression and refracted waves take place alongside the propagation of the impact point. Due to extreme pressure and heat being put on the collision point, the combination of the interaction of the shock waves together with the movement of both the metals produced the waves at the interface (Fig. 17(d)).

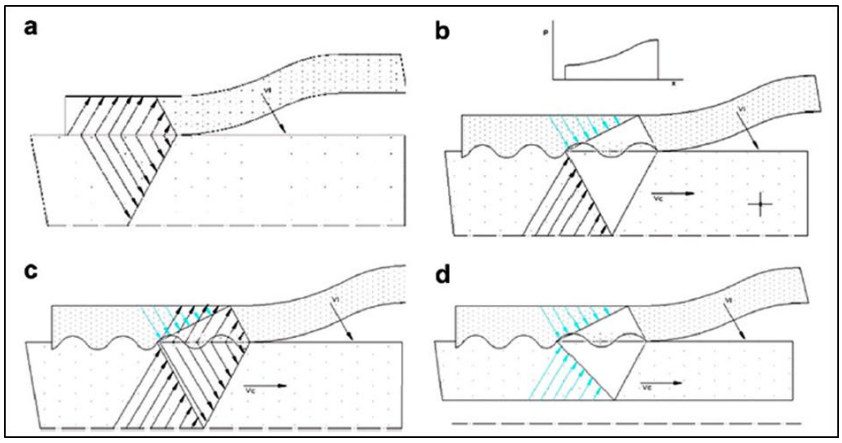

Fig. 17 Wave-creation model for MPW [44]

For the wave formation to be started, it is must that the shock waves meet at the point of impact, the point where the pressure together with the heat have a maximum value [44]. The first shock wave initiation is shown in Fig. 18(a). Due to higher collision velocity at this moment, the interference zone lags behind the collision point (Fig. 18(b)). There is a critical collision velocity beyond which waves are created, which has been depicted in Fig. 18(c). As the first wave is created, a Kelvin–Helmholtz instability occurs and periodical creation of waves takes place (Fig. 18(d)). From that instant, a constant generation of waves takes place due to the Kelvin–Helmholtz instability, until something decays it. As the interference continues further, waves are being created (Fig. 18(e)). As the weld progresses, the velocity of propagation, V_c goes on decreasing. As such, the interferences produced by the shock waves meet the impact point further along and thereby increases the wavelength (Fig. 18(f)). At a point of time due to the drastic reduction in propagation velocity V_c, no new waves can be generated as the collision point lags behind the interferences (Fig. 18(g)).

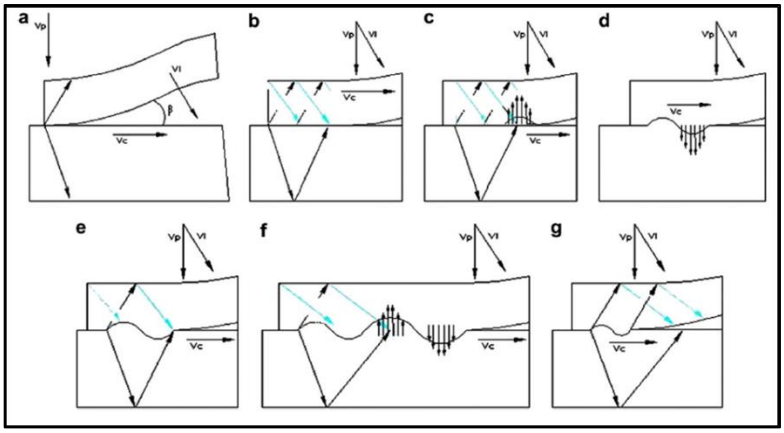

Fig. 18 Wave formation in MPW [44]

iv) Vortex-shedding mechanism

Cowan et al. [28] suggested that the formation of bond waves in explosion welding is analogous to flow of fluid about a barrier in which regular formation of eddies is observed. Reid [37, 44] considered "that the confluence of the flyer plate material and the parent plate material behind the re-entrant jet produced conditions similar to the flow of a viscous fluid around an obstacle". The re-entrant jet shears the surface of the parent plate. As a result, formation of a hump takes place at the point of impact and this hump causes the re-entrant jet to be deflected upwards into the flyer plate jet thus blocking off the re-entrant jet completely. As the re-entrant jet remains trapped a vortex is formed at the back of the hump, where kinetic energy is dissipated and is the cause of high temperatures created. This might cause phase changes and local melting.

Fig. 19 shows the vortex shedding mechanism as defined by Kowalick and Hay. The complete chocking of the re-entrant jet causes the stagnation point to move from the trough to the crest of the wave. The high pressure around the stagnation point goes on decreasing and causes the hump to elongate further until the extent a forward trunk is formed. The further movement of the hump downstream causes the stagnation point to be dependent on the forward slope of the hump, and as a result, an increase in the angle of inclination between the jet and the inclined side of the hump takes place. In the meanwhile, the velocity of the re-entrant jet is reduced. On further descend of the forward slope of the hump by the re-entrant jet, a new stagnation point forms at and as a part of the jet enters the cavity under the trunk, a new vortex is created.

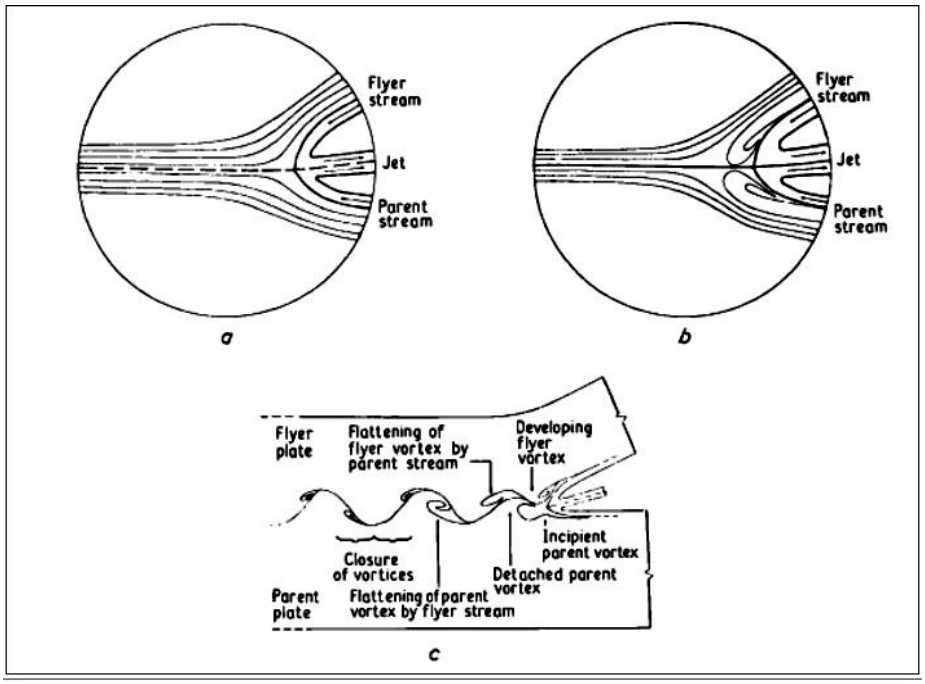

Fig. 19 Production of periodic waves by vortex shedding (a) laminar flow around jet at low Reynolds number, (b) vortex formation following flow separation, (c) generation of periodic wave formation by vortex shedding [37]

1.1.5 Process advantages and limitations

Every other process in the world has its advantages and limitations and MPW is no exception. Over the years it has been verified to be an efficient welding technique. With increased research and development the limitations of the process have been minimized and in some cases even being eliminated. The various advantages of the process are as listed below:

- The process allows joining of dissimilar material combinations, keeping their mechanical and chemical properties intact in a quick and cost-effective manner [50].
- The process is suitable for automation. Allows development of newer products and complex designs previously not possible with conventional joining processes.
- MPW being a cold welding process limits the temperature rise to 30-50°C at the outer surfaces of the workpieces. This allows the parts to be unloaded immediately and further processed with standard equipment.

- It offers the advantage of higher strength to weight ratio without the presence of any heat affected zone [51].
- The process is environmental friendly compared to other welding technologies and has a much lesser impact on the environment. There is no emission of heat, radiation, gas or smoke, shielding gas during the process. MPW does not also employ consumable materials like filler wire/rod.
- Consumption of energy during the process is less. The joining can also be done in hostile environments, minimizing the need of supplementary investments in operator safety. MPW being a clean and green process makes it possible to provide safer and cleaner working conditions for the operators [22].
- It is quite economical for the industries as it reduces the rework time, diminishes cycle time and enhances the process capability [52].
- Time consuming post weld activities like cleaning and finishing are not required for MPW [53].
- Highly suited for large volume production and automated feeding system due to its low maintenance costs and quick changeover.
- MPW is a good alternative to brazing because it offers greater repeatability.
- Apart from joining of metals, the applicability of MPW has been verified at powder compaction. Thus it provides a different means of producing parts with some level of complexity [54].
- Corrosion studies have reported that show no corrosion problem in the welded area of a magnetic pulse joint [55].

MPW has its limitations like any other welding process. Some of the limitations of the process are listed below:

- The MPW process is limited by the nature of the workpiece material. The process is successful only for electrically conducting materials.
- The thickness of job that can be welded is limited. For tubes possible diameters range from 5 to 254 mm [56]. As of date the largest tube diameter welded is 121 mm [57].
- The geometry and size of the parts that can be successfully welded are controlled by the shape and size of the coil or field shaper. It is very

cumbersome to find an optimal standoff distance between the mating members, which is vital to produce the suitable impact velocity.

- Coaxial positioning of the parts to be welded is also critical, as is the angle of impact.
- Accurate frequency of the pulse must be maintained which might not be possible every time. Successful welding occurs in the frequency range of 10 kHz to 200 kHz [10].
- The process is very sensitive to changes in input parameters. The input parameters are very part specific and the weld quality is quite sensitive to changes in the same.
- The entire set up is quite costly. The electromagnetic coil is quite expensive and needs to be replaced periodically.
- The process being a variant of high velocity impact processes, the inner or base tube needs to have sufficient structural strength in order to withstand the impact [58]. Therefore, it is not possible to pulse magnetic weld a thin-walled tube on another thin-walled tube unless there is a mandrel backing up the inner part.
- Due to very high levels of current and voltage during operation, the industrialization of the process requires higher security and safety levels which are quite costly.
- While speed is an advantage to assemblers, it can also be a limitation. The process is so fast that it does not lend itself to deep drawing of material since the material does not have time to stretch.
- Due to use of high intensity magnetic fields the process is possibly hazardous to the operator.

1.1.6 Magnetic pulse welding applications

The application of MPW is widespread in nuclear, automobile, aerospace, ordnance, packaging, consumer products and electrical industries owing to its large production capability, repeatability and reparability and ability to join dissimilar materials. MPW has been utilised in nuclear industry for various applications including welding of closing caps and end closers of nuclear fuel rods (Fig. 20), welding of metal canisters and nuclear fuel pins [12].

Fig. 20 End enclosures for nuclear fuel rods [12]

MPW is slowly developing as a potential and practicable technology in automotive sector owing to its capacity to join lightweight parts thus reducing the vehicles impact on the environment. Most of the modern day MPW machines developed by two companies namely PULSAR and DANA Corporation have been utilized for a variety of applications including joining of space frame structures made of combination of aluminium and steel , flange mufflers in the exhaust system drive-shafts (Figs. 21 (a) and (b)), components of air conditioners (Fig. 21 (c)) and tubular seats, components of fuel filters (Fig. 21 (d)) automotive earth connector (Fig. 22) , assembling air brake hoses, attaching reinforcing bands on oil filters and clamping rings over sleeves on shock absorbers [22].

(a) **(b)**

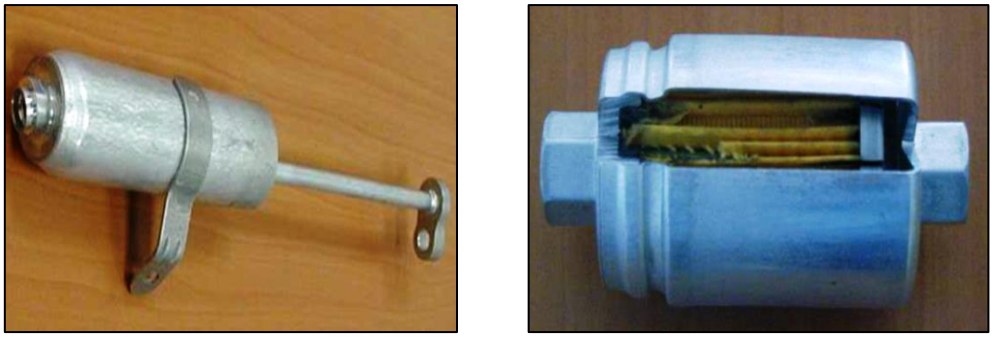

(c) **(d)**

Fig. 21 (a) MPW welded drive shaft (aluminium-steel joint), (b) MPW welded drive shaft (aluminium-aluminium joint), (c) MPW welded automotive A/C receiver-dryer, (d) MPW welded fuel filter (aluminium-aluminium joint) [22]

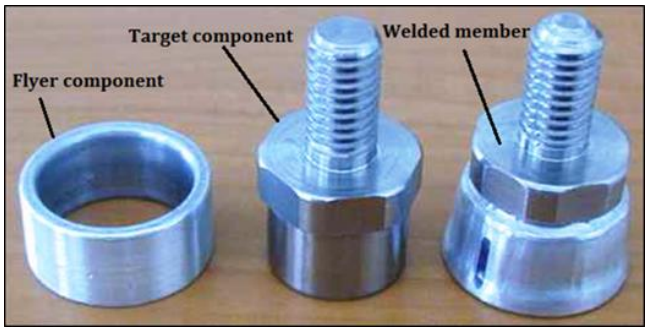

Fig. 22 MPW welded automotive earth connector [22]

The application of MPW has gained importance in aerospace industry of late. Figs. 23 (a) and (b) show some aircraft control tubes welded through MPW. These control tubes are torsional members subjected to very high levels of torque while in operation. These torque tubes have been successfully used in aircraft operations without any signs of damage to the weld zone inspite of such high torque levels.

(a) **(b)**

Fig. 23 (a) aircraft flight control tubes, (b) aircraft flight control tubes in use [22]

The use of MPW can also be seen in electronics industry. Researchers have successfully utilised the process to provide metallurgical and electrical bonds between flexible printed circuit boards (FPCB). They concluded that the joint produced had a good quality devoid of any damage or heat affect in polyimide substrates of FPCB. Joining of high voltage cables, metal fittings onto ceramic insulators and swaging of copper tubes to coaxial cables are recent examples of use of MPW in electrical industry.

For dissimilar welding applications that are difficult to realise with conventional impact and fusion welding processes, MPW offers cleaner and more energy efficient solution. The MPW operation is economic because of fast and repeatable operation without any need of post cleaning or processing. However, a precise control on process parameters is essential for successful MPW operation. The current limitations of MPW are mainly related with design and process considerations. The discussion in the previous sections clearly states that MPW is an encouraging welding technology with wide opportunities for further investigation and this fact has been the prime motivator behind the present work. The applicability of the MPW process in industries can further be enhanced if the end user is provided with some predictive models that can be utilized at the shop floor. The subsequent section provides the overview of the thesis.

1.2 Overview of thesis

The present thesis has been divided into six chapters and the major work presented in each chapter is as follows:

Chapter 1: Introduction

This chapter begins by introducing the MPW process, its development over the years and its usefulness in joining various similar and dissimilar materials. The process principle, the parameters affecting the process, the welding mechanism, advantages and limitations and applications of the process is then discussed. In addition, this chapter also gives overview of the thesis.

Chapter 2: Current State of Art

This chapter presents a critical and detailed review of the MPW process based on previous investigations carried out by researchers since the inception of the process

and identifies the potential areas of research in MPW. Based on the various gaps and opportunities established during the critical review, the problem has been defined and the work plan has been presented. The major objectives and scope of investigation related with the present work have also been given.

Chapter 3: Numerical Modelling and Simulation Work

This chapter presents the numerical modelling and simulation work carried out as a part of the present investigation. Development of the finite element model along with its validation is discussed followed by development of various weldability windows based on the developed model. Development of predictive models based on weld validation criteria i.e. impact velocity using statistical regression analysis and artificial neural network is then described. The results of modelling have been discussed. The chapter also presents a case study based on the developed predictive models.

Chapter 4: Experimental Work

This chapter describes the experimental work carried out as a part of the present investigation. The chapter discusses the materials and process parameters selected, the selected experimental procedures and set-up and methodology. Mechanical and Metallurgical tests carried out to validate the results from chapter 3 have been presented and discussed in detail.

Chapter 5: Conclusions

This chapter discusses the major outcomes of the investigation carried out.

Chapter 6: Future research directions

This discusses the possibilities ahead for research in MPW. The chapter also addresses some of the open questions and unsolved problems together with future research directions.

Chapter 2

Current State of Art

The present chapter reviews the available literature in MPW. The chapter is divided in four sections; the first section discusses the past studies related to MPW conducted by various researchers over the years. Most of the work carried out is experimental and very few studies have been reported for numerical modelling and simulation work for MPW. The first section discusses a wide variety of topics on MPW including state-of-art on process physics, interface phenomenon, metallurgical studies, weld quality and integrity evaluation, numerical and simulation studies, and weldability window development. Based on the outcome of the detailed stated review, various gaps and opportunities have been discussed in the second section. The third section of this chapter describes the formulation of the problem and the work plan. In the last section objectives and scope of the present work is discussed.

2.1 Past studies in MPW

The literature on MPW can be broadly classified into two major categories viz. experimental and modelling and simulation. Almost 60% of the published work constitutes experimental studies [59]. The experimental and modelling work done can be further classified into sub-categories as shown in Fig. 24. Some researchers have done experimental studies and combined them with simulation work in order to better understand the physics of the problem. The literature on numerical modelling and simulation of MPW is very limited and the same focusses on understanding the process and related science with it, formulate ways to have better process control techniques, develop optimum process parameters suitable for product development and to ascertain process feasibility.

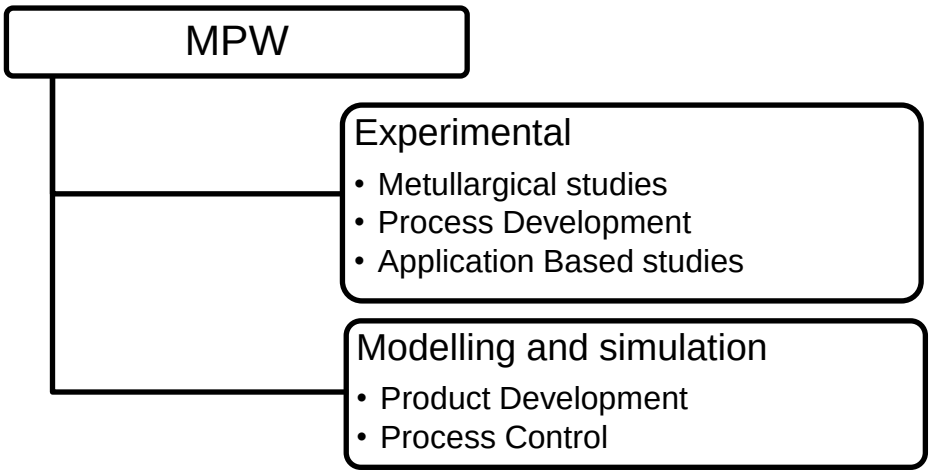

Fig. 24 Areas of research in MPW

The MPW has been applied to both tubes and sheet metals. The use of magnetic forces to join tubes and sheets was first patented by Lysenko et al. [60]. With the recent advancement in the process, welding of the cylindrically symmetrical workpiece has been made possible. The welding of axi-symmetric structures, i.e., tubes has been established by many researchers [4, 61-64]. Successful application of MPW of flat sheets has been proved by many researchers [65-67]. The feasibility of MPW of flat sheets has been proved for various material combinations viz. Al-Al, Al-Cu, Al-SS, Cu-SS, Cu-Cu, Mg-Al and Al-Al-Li alloy [68]. However, it has been reported that difficulty in controlling the magnetic field makes MPW of flat sheets a bit difficult [49].

2.1.1 Process physics, Interface phenomenon and Metallurgical studies

Experimental work on MPW has been mainly driven towards understanding the physics of the process and the phenomenon occurring at the interface of the joint. Brown et al. [69] suggested that the temperature at the interface was well below the melting temperature of the mating members even after the members collided at very high pressures and velocities. The formation of intermetallic compounds during MPW was very unlikely as the process was governed by magnetic pressure and not by heat [70]. Brown et al. [69] suggested that high strain rates and severe plastic deformation might yield a solid-state weld. This theory was validated by Hisashi et al. [71] who performed experiments and combined them with a numerical model for electromagnetic welding of aluminium and steel. The temperature increase at the weld

interface was not high enough to melt any of the mating members. The studies conducted by Uhlmann and Ziefle [72] also supported the analogy given by Brown et al. [69]. Experimental studies by Kore et al. [73] found that no eutectic microstructure and no intermetallic compounds were formed when aluminium and magnesium were welded using MPW. Some researchers found evidence of melting and solidification at the interface. Aizawa and Okagawa [65] suggested that a high temperature is generated at the interface but the temperature rise was not high enough to heat up the workpieces largely. The welding is caused due to combination of magnetic pressure and joule heating at the interface. Gobel et al. [74] performed metallographic investigations on MPW of aluminum tubes to copper cylinders. The welds were free of diffusion layers. The melting was found primarily responsible for the phase formation and the bonding process. Wu and Shang [75] performed MPW of Al and Cu tubes and concluded that the weld interface was subjected to a rapid temperature rise. They stated that surface topology had an important role to play in the mechanical mixing and formation of wavy pattern at the weld interface. Existence of intermetallic compounds involving mass transportation and interdiffusion of Cu and Al atoms in solid phase or liquid phase was found. It was concluded that a solid state reaction at the weld interface can lead to the formation of IP; however, localised interface melting was not usually observed in MPW and was not a prerequisite for intermetallic formation.

Investigators have also tried to understand the interface morphology of the MPW joint. Brown et al. [69] stated that formation of a wavy or rippled pattern was a characteristic feature of impact bonding. Nassiri et al. [76] and Cui et al. [77] cited shear instability as the source behind the formation of a wavy interface. A sound and high strength weld is guaranteed by the presence of a wavy pattern at the interface of the mating members [78, 79]. The presence of a wavy pattern at the interface was also proved by Aizawa et al. [5]. They performed experiments on several aluminium and steel sheets whereas Watanabe et al. [80] performed MPW of aluminum to iron, nickel and copper. Gobel et al. [74] and Groche et al. [81] however suggested that presence of a wavy pattern at the interface was not a necessity to conduct a successful weld. The geometry of the specimen is the most substantial parameter with regard to weld morphology. Shribman [3] also suggested that material properties and process parameters affect the weld morphology. Investigations show that the wave parameters viz. wavelength and amplitude are related to the discharge energy and the impact velocity [78]. Elsen et al. [82] performed numerical simulations and showed the

dependency of wavelength and amplitude of the wavy interface on impact velocity. This observation was supported by findings of Nassiri et al. [76]. They also stated that the presence of a wavy interface directly depends on the velocity of impact of the mating members. The typical weld interfaces obtained for MPW of similar and dissimilar metals are shown in Figs. 25 (a) to (d). The photomicrographs of the welded interfaces illustrate the dependency of the interface morphology on the material combination employed during the process of welding. The formation of a wavy pattern at the interface of the welded members can be seen in case aluminium-aluminium (Fig. 25 (a)) and copper brass welds (Fig. 25 (b)) whereas in case of aluminium-steel (Fig. 25 (c)) and aluminium-copper (Fig. 25 (d)) welds the interface displayed a flat interlayer.

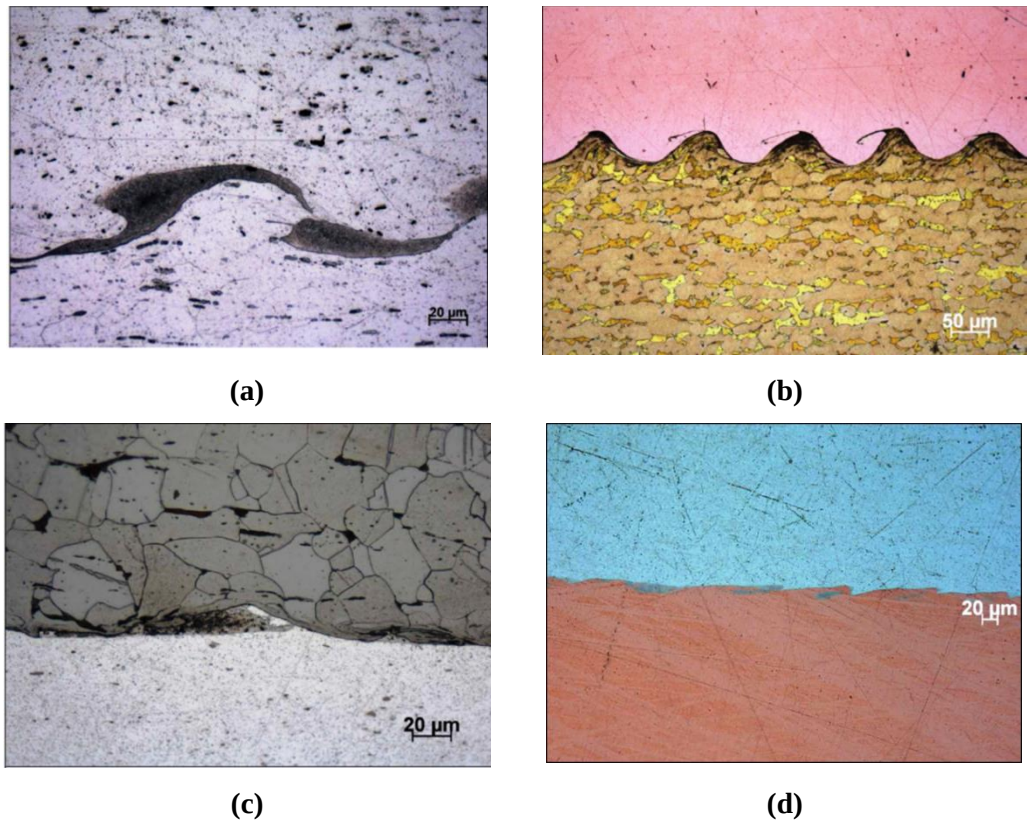

(a) **(b)**

(c) **(d)**

Fig.25 Photomicrograph of weld interfaces (a) aluminium-aluminium, (b) copper-brass, (c) aluminium-steel (d) aluminium-copper [22]

Lee et al. [33] performed MPW for steel and aluminium as mating members and found out the existence of an intermediate layer (IML) between the mating members. Similarly, the existence of an inhomogeneous layer at the weld interface was found by other researchers [5, 83]. In contrary to popular belief that intermetallic compounds

formation could be avoided in electromagnetic welding, it was proved by Gobel et al. [74] that intermetallic formation are inevitable. They suggested the existence of "melt pockets" in which IP are concentrated in case of a wavy interface; however, in case of a waveless interface the IP form a film of wavering thickness. The findings of Gobel et al. [74] were in good agreement with published results of Zhang et al. [1] who found the existence of IP in MPW in the corner of wave vortex. Gobel et al. [74] related the formation of IP with discharge energy. A reasonably thin phase of intermetallics is generated at low discharge energies whereas at higher energies the thickness of the intermetallic phase increases resulting in generation of cracks, voids and pores. The findings of Gobel et al. [74] were further supported by the findings of Psyk et al. [83] where it was proved that microfractures occurs if the discharge energy chosen is excessively high. Faes et al. [84] performed MPW of copper tubes to brass mandrels and showed occurrence of melting and formation of an intermetallic phase if the process parameters chosen were not optimum. This led to cracking in and around the weld zone that deteriorated the weld quality. Haiping et al. [85, 86] conducted MPW experiments on Steel-Al tubular members. It was found that a minimum input voltage was essential to obtain a metallurgical joint between the considered members. The weld interface was subjected to mutual diffusion of Fe and Al elements. They found out the existence of two interfaces viz. transition zone and two basic metals. There was a variation of microhardness along the transition zone. Presence of micro cracks and apertures was evident in the transition zone. Stern et al. [87] conducted studies on the interfaces of pulse welded Al-1050/Al-1050 and Al-1050/Mg-AZ31 MP members. The weld interface had a wavy appearance and underwent localised melting and rapid solidification. Presence of relatively coarse intermetallic precipitates was detected in certain pockets. They concluded that the interface of the dissimilar members welded through MPW was heterogeneous. Raoelison et al. [88] studied the interface properties of MPW of dissimilar materials by conducting experiments on Al-Cu tubular members and compared the results with MPW of Al-Al tubular members. An amorphous intermetallic IML was observed in case of Al-Cu joint whereas the Al-Al joint was bonded with a metal continuity. The intermetallic layer was characterised by a porous media with a random allocation of pores and cracks in cracks in multiple direction. They cited cavitation phenomenon as the source of pores. During push out tests the dissimilar metal joint had a brittle failure due to the presence of the intermetallic layer whereas the similar metal joint had a ductile failure.

2.1.2 Structural studies

Almost all published literature suggests that the ensuing weld is of high structural strength [78]. When MPW joints were subjected to mechanical strength tests, failure occurred in the parent metal instead of the weld zone. Aizawa and Okagawa [65] however stated that the weld zone attains a high strength only if the standoff distance selected between the mating members was optimum. The standoff distance must be high enough to allow the flyer workpiece to attain sufficient impact velocity and kinetic energy before it made an impact with the target workpiece. The current flowing in the weld zone even after the impact occurs, influences the quality of the weld in a positive way as this current supplies energy to the weld in the form of joule heat. The standoff distance and the discharge voltage must be chosen very carefully to ensure that weld has high strength. The analogy given by Aizawa and Okagawa [65] was supported by the findings of Kore et al. [13]. The experimental study conducted by Kore et al. [13] suggested that with a surge in the capacitor bank energy, the shearing strength of the welded joint improved considerably on condition that the standoff distance in the initial condition was kept constant. The joint strength could be improved by altering the coil dimensions. These facts were proved to be correct for aluminium- steel welds by Kore et al. [11] when MPW of stainless steel on aluminium was tried with stainless steel plate as the flyer plate. Stainless steel being less conductive than the aluminium target plate; they employed aluminium driver plates to provide the necessary acceleration to create the weld. Kore et al. [89] employed aluminium driver sheet to accelerate copper flyer sheet onto copper base sheet. Inspite of copper being highly conductive the use of driver sheet was because of the limitation provided by the skin depth and thickness of the sheet. Due to the same limitation, Kore et al. [73] used aluminum drivers to perform MPW of magnesium to aluminium and proved the feasibility of the process using additional driver sheets. Berlin et al. [90] also conducted MPW of AZ31 magnesium alloy. They concluded that with an increase in discharge energy the strength of the joints improved considerably. The bond had high shear strength values and in some cases, it was approximately equal to the strength of the base metal. Kumar et al. [91] conducted MPW of flat sheets and came to a conclusion that collision velocity decides the strength of the welded joint.

Researchers have also tried to investigate the weld geometry and the continuity of the weld. Faes et al. [84] conducted experiments on tubular components and found out the existence of three distinct zones in the weld. The actual weld occurred in the

middle where a typical wavy pattern was present. The wavelength of the wavy pattern increased towards the end of the welds. Watanabe et al. [80] considered the cross section of electromagnetically welded lap joint of sheet metals. No welding occurred at the centre of the seam while at the sides two bulging sections could be seen. The bonding of the mating members took place in these regions. As the discharge energy was increased the width of these regions increased. The findings of Watanabe et al. [80] were supported by the findings of Kore et al. [13] and Lee et al. [33]. Kore et al. [13] cited entrapped oxides, rebound due to Lorentz forces acting perpendicularly and the intricate deformation at the interface of the joint as the possible reasons for no welding occurring at the centre of the seam. During the impact, the Lorentz forces acting on the mating members were perpendicular to the sheet at the centre and had a shear component elsewhere (Fig. 26).

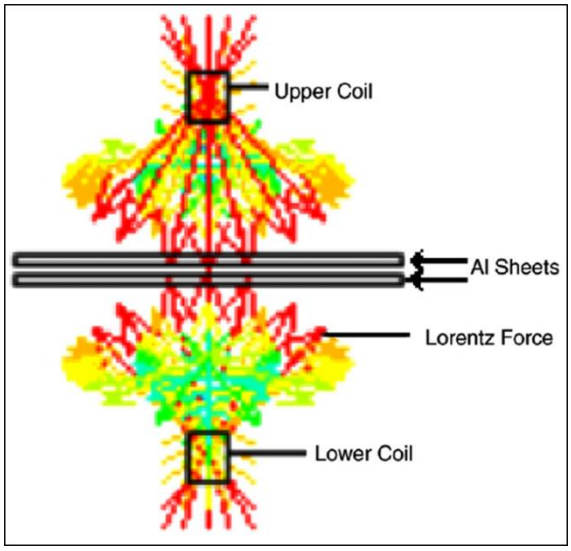

Fig. 26 Mating members at the time of impact [13]

There was no indication of rebound effect at a considerable distance from the centre and thus the mating members remained in contact leading to formation of welded zones. Kore et al. [11] suggested the use of driver sheets to obtain continuous weld without no-weld areas at the centre. Kore et al. [49] performed numerical simulations to validate their own findings [11]. For welding of aluminium-to-aluminium no-weld regions occurred at the centre of the weld. The numerical simulations suggested that Lorentz forces and the rebound effect caused by these forces were the main reasons for the no weld regions occurring at the centre of the

weld. The simulations proved the analogy that by using driver sheets no weld regions could be avoided to be correct.

The experimental studies conducted by Berlin et al. [90] further proved the existence of distinct bond zones in MPW joint. Fig. 27 shows the photomicrograph of a cross section of pulse welded members. Along the impact zone, there are three distinct zones viz. one unbonded zone at the centre, two bonded zones and two unbonded outer zones. It is evident from Fig. 27 that bonding did not occur at the centre, while the same occurred on each side of the centre zone. At a considerable distance from the centre unbonded zones reappeared. Fig. 28 shows the photomicrograph of the unbonded centre zone. Berlin et al. [90] cited low collision angle as the possible reason behind no bonding occurring at the centre of the weld. Due to low collision angles at the centre zone the jetting of the oxide layer and the contaminants did not take place, and hence no bonding occurred while in two bond zones the oxide layer removal was successful.

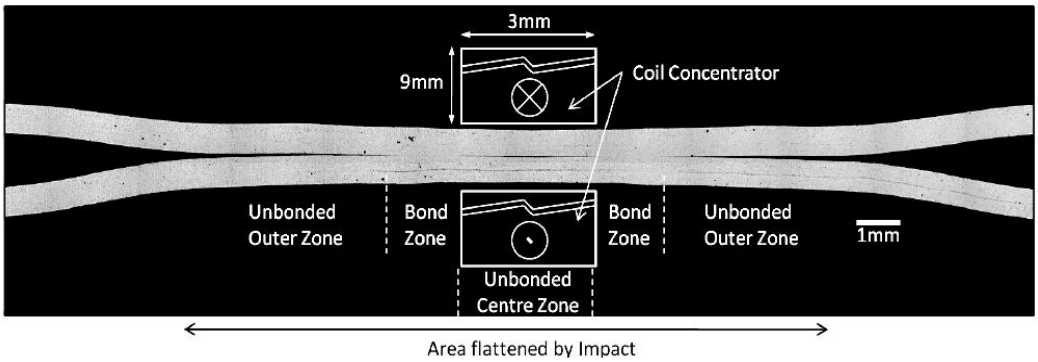

Fig. 27 Photomicrograph showing cross section of a MPW joint [90]

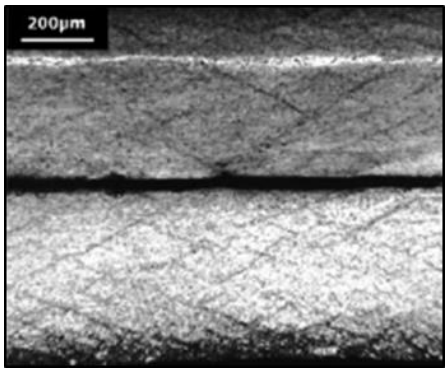

Fig. 28 Photomicrograph showing unbonded centre zone [90]

The findings of Berlin et al. [90] were further supported by the experimental findings of Aizawa et al. [92]. They conducted parallel seam welding using MPW

technique of Al sheets and found out the existence of no bond zone at the centre of the sheets after impact. Fig. 29 shows photomicrographs of centre of weld interface for Al-Al welded sheets.

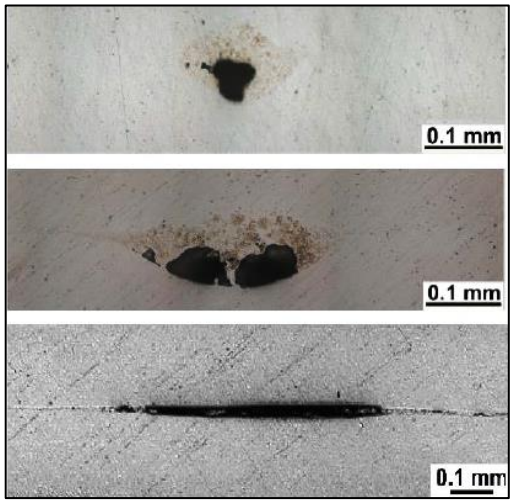

Fig. 29 Photomicrograph showing unbonded centre zone [92]

2.1.3 Numerical and simulation studies

The success of MPW depends mainly upon the process parameters being set to their accurate values. An electromagnetic field analysis can help in predicting and optimising accurate values of the essential process parameters viz. current, inductance, frequency and dimensions of the coil and work-piece. Selection of optimum process parameters and an optimum coil design can be effectively done through a Finite element model (FEM). The MPW process is a multiphysics problem where the FEM requires coupling between electromagnetic and structural models. The literature available on numerical modelling of MPW is very limited. A FEM for electromagnetic welding process was developed by Casalino and Ludovico [9] in order to estimate the profile of temperature distribution, workpiece displacement and the effects of varying input parameters on the weld. A FEM to investigate the weld characteristics according to the distribution of an electromagnetic force on the weldment in order to find the optimal process parameters such as input current and frequency was developed by Shim et al. [93]. Haiping et al. [94] formulated a numerical model to investigate the influence of the geometry of the field concentrator on welding quality as well as other main controllable input parameters such as feeding size, standoff distance and voltage. Aizawa and Kashani [95] conducted numerical studies to garner more insight about the

MPW processes. They successfully developed a numerical model that could predict electromagnetic force distribution that helps in reducing coil deformation and improve its lifetime. Zaitov and Kolchuzhin [96] build an analytical model and a FEM to measure coil parameters. The developed model could predict geometric, thermal and load carrying boundaries of the coil. Based on the model a new bitter coil design was implemented. Shim and Kang [97] developed a 3-dimensional FEM to analyze the distribution of electromagnetic force in MPW for a square working coil. It was found out that the electromagnetic force was greatest at the centre of the coil and decreased along the edges. A comprehensive study to predict the impact velocities of the impact points of aluminium–Iron pipefitting was conducted by Zhidan et al. [98]. Zhang et al. [99] tried a simulation-based approach to design a system that could predict impact velocities and temperatures along the weld interface for MPW using the electromagnetic module in FEM software LS- DYNA. The finding of their study concluded that no melting occurred along the weld interface that was also proven experimentally. Uhlmann et al. [100] developed FEM for symmetrical as well as nonsymmetrical sheet metal deformation processes. They concluded that the pressure and the plastic work calculated by their model could be used as welding criterion. Miyazaki et al. [101] performed a numerical analysis of the dynamic deformation process in magnetic pressure seam welding process using a FEM. They studied the behaviour of collision velocity and collision angle as a function of standoff distance or gap length. Initially the collision velocity was high but its value reduced as time progressed. With decrease in gap length, the collision velocity decreased early while the collision angle increased early. The deformation behaviour as predicted by their model is shown in Fig. 30. The flyer plate collided with the target plate at a time of 8μs (Fig. 30 (c)). The collision of (c) is called the initial collision point. The collision point moved outside during the welding process at (d), (e), and (f).

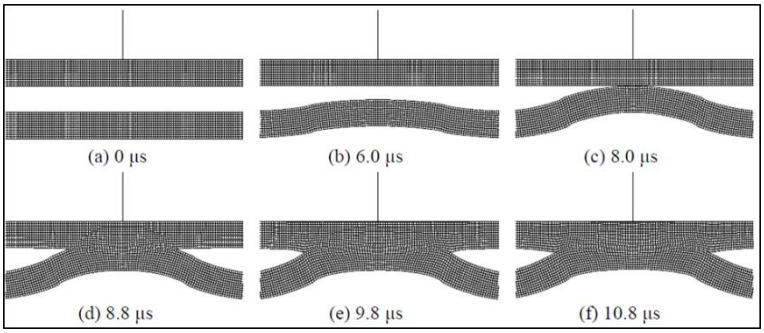

Fig. 30 Deformation behaviour as predicted by FEM model at various time steps [101]

Elsen et al. [82] performed experiments together with numerical simulations to identify process parameters that govern the development of a solid-state cold weld in impact welding processes. The impact angle and impact velocity along the impact zone were identified as important parameters for the formation of a welded joint. Metallographic examinations showed the presence of a characteristic wavy interface that suggested that the material behaviour of the surface layers involved is similar to the Kelvin-Helmholtz instability mechanism in fluid dynamics. The material behavior was included in the finite element simulations by use of the Johnson- Cook plasticity model. Fig. 31 compares the numerical simulation of a spatial Kelvin-Helmholtz-instability to a microsection of a weld interface. Elsen et al. [82] observed periodic sequences of sinusoidal waves and turbulent vortices in both the numerical simulation and the microsection of the specimen and thus concluded that the theory of wave formation being an effect similar to the turbulent flow in fluids moving at different speeds is plausible.

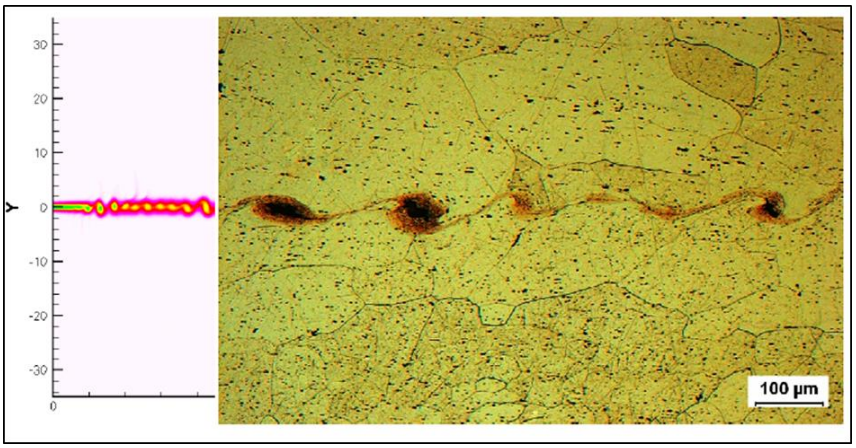

Fig. 31 Numerical simulation of a spatial Kelvin-Helmholtz-instability (left) compared to a microsection of a weld interface of Al-Al (right) [82]

2.1.4 Process feasibility and development of weldability windows

The feasibility of the MPW process depends upon various criteria. The criteria that decide the feasibility of the MPW process and are available in literature are namely impact velocity, effective plastic strain and shear stress. To adopt the criteria that give an insight into the success of the process, it is very much necessary to recognize the dissimilarities in the physical attributes for the bonded and non-bonded samples [2]. Available literature shows the use of a combination of different criteria to evaluate the

feasibility of the process by researchers and subsequent development of weldability windows as given in Table 1.

Table 1 Summary of Bonding criteria and weldability windows available in literature

SL. No.	Author(s)	Welding Technique	Criteria used	Geometry	Welding Window
1.	Vivek et al. [102]	Impact welding	Impact velocity	Flat plates	Developed
2.	Raoelison et al. [103]	MPW	Plastic deformation and Wavy shape interface	Tube	Developed
3.	Deng et al. [104]	EXW	Plastic strain	Tube	Not developed
4.	Zhidan et al. [98]	MPW	Impact velocity	Tube	Not developed
5.	Ghomi et al. [105]	EXW	Plastic strain, Shear stress	Flat plates	Not developed
6.	Raoelison et al. [10]	MPW	Air gap and charging voltage	Tube	Developed
7.	Alipour and Najarian [106]	EXW	Plastic Strain	Flat plates	Not developed
8.	Uhlmann and Ziefle [72]	MPW	Deformation, Collision velocity	Tube	Developed
9.	Kore et al. [49]	Electromagnetic welding	Impact velocity, Spatial pressure variation	Flat plates	Not developed
10.	Chizari et al. [107]	EXW	Equivalent plastic strain (PEEQ) and Shear stress	Flat plates	Not developed

11.	Hisashi et al [71]	Magnetic pressure seam welding	Plastic strain	Flat plates	Not developed
12.	Akbari et al. [108]	EXW	Plastic strain, Shear stress	Flat plates	Developed
13.	Akbari [109]	EXW	Plastic strain, Shear stress	Tube	Developed
14.	Akbari and Al-Hassani [110]	EXW	Plastic strain, Shear stress and Impact velocity	Flat plates	Developed
15.	Chizari et al. [111]	Impact welding	Plastic strain and Shear stress	Flat plates	Not developed
16.	Akbari and Al-Hassani [112]	EXW	Plastic strain, Shear stress and Impact velocity	Flat plates	Not developed
17.	Akbari et. al. [113]	EXW	Plastic strain, Shear stress and Impact velocity	Flat plates	Not developed
18.	Krishnan and Kakodkar [114]	EXW	Tube Velocity/ Impact energy	Tube	Not developed

Impact velocity is one of the major factors that decide the occurrence of weld and/or formation of a wavy interface in the welded zone. Zhidan et al. [98] used impact velocity of the flyer as a criterion to determine the feasibility of the process. Thibaudeau and Kinsey [115] developed a simplified, loosely coupled solution to determine the workpiece velocity. They stated that an analytical model reduces time and cost of calculation compared to FEM that are fully coupled and the environment is multiphysics. Groche et al. [116] designed and performed experiments on a novel test rig to determine impact velocity and impact angle for MPW of flat sheets. They simultaneously performed numerical simulations and validated them with experimental values. Althoff et al. [117] developed analytical relations to determine

impact velocity during compression welding process. They compared the analytically calculated values with experimentally determined values. A Photon Doppler Velocimetry (PDV) set up was used to determine the velocity experimentally. Kore et al. [49] suggested analytical relations to calculate the minimum velocity of impact required for the weld occurrence for similar and dissimilar material combination. The relations are given as [49]:

- **Velocity calculations for similar metals**

$$U_T = \left(\frac{\sigma_{TU}}{S}\right)^{1/2} \tag{6}$$

where U_T is the minimum impact velocity required for successful welding to occur (m/s), σ_{TU} is the ultimate tensile stress (MPa) and S is the bulk sound velocity (m/s).

- **Velocity calculations for welding of dissimilar metals**

Kore et al. [49] suggested that relations available for EXW could also be applied to MPW. EXW takes three main factors for weldability viz. the critical angle for jet formation (Φ), the critical impact pressure for jet formation in the subsonic state (P_c), and the critical impact velocity (U_T). The impact pressure for any impact state (Φ, V); can be deduced from equation stated below Kore et al. [49]:

$$P_c = \frac{1}{2} Z_{eq} U_T \cos \Phi \tag{7}$$

where Z_{eq} is the equivalent acoustic impedance of the colliding sheets/tubes and is given by the relation Kore et al. [49]:

$$Z_{eq} = \frac{2}{1/Z_1 + 1/Z_2} \tag{8}$$

where $Z_1 = \rho_1 S_1$ is the flyer sheet/tube acoustic impedance, $Z_2 = \rho_2 S_2$ is the base sheet/tube acoustic impedance, S_1 and S_2 are the speeds of sound in the flyer and base sheet/tube materials respectively, and ρ_1, ρ_2 are the material densities of the two sheets/tubes.

To conduct a successful weld through MPW a threshold value of pressure must be exceeded. This pressure is given by the relation Kore et al. [49]:

$$P = 5 \times Hugoniot\ elastic\ limit\ (HEL) \tag{9}$$

where *HEL* is given by the relation:

$$HEL = \frac{1}{2}\left(\frac{K}{G} + \frac{4}{3}\right) Y_0 \quad (10)$$

where K is the bulk modulus, G is the shear modulus and Y_0 is the tensile yield stress.

Table 1 shows the use of impact velocity alone as the deciding parameter for formation of bond by some researchers. Vivek et al. [102] and Akbari and Al-Hassani [112], however, suggested that a high value of impact velocity does not always lead to a successful weld. They suggested that the use of impact velocity as a sole parameter to decide upon the feasibility of the process might result in inaccurate predictions. The findings of Vivek et al. [102] and Akbari and Al-Hassani [112] paved the way for researchers to rely upon multi-criterion study to determine the feasibility of the MPW [118, 119]. Two other criteria viz. effective plastic strain and shear stress have been used by researchers to determine the feasibility of MPW. Table 1 shows the use of these two criteria by researchers to determine the process feasibility and reach upon weldability windows. Some researchers used effective plastic strain and shear stress together as the deciding criteria for formation of the bond, whereas some used all the three available criteria together to determine the feasibility of MPW process as summarised in Table 1.

Since the inception of the EXW process, an extensive study has been done in order to understand the process and its underlying principles and has led to the development of a number of weldability windows. Available information in the literature and experimental data on EXW has helped and guided researchers to work upon MPW. In both EXW and MPW processes, the same process parameters have influenced the resultant bond irrespective of whether a good weld is produced or otherwise. Researchers have thus relied upon the weldability windows developed for EXW to develop weldability windows specific to MPW. However, these weldability windows are specific to a general set of materials and geometries and can only be used to make a rough approximation of the parameter settings for MPW. Thus, development of a practical weldability window specific to MPW that can define accurate process parameters for producing a successful weld is the need of the hour.

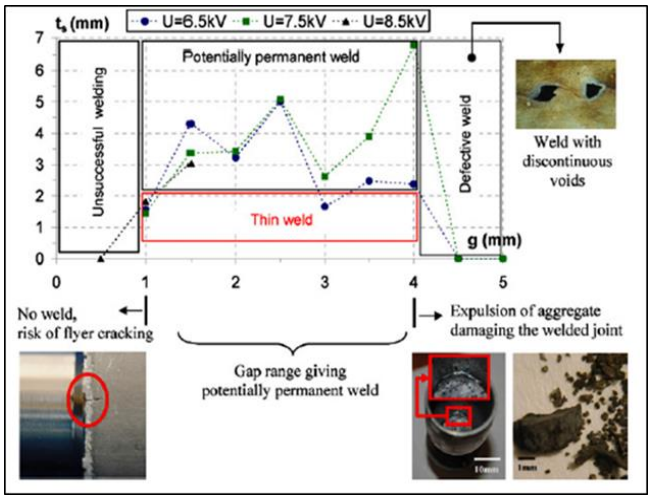

Fig. 32 Graphical abstract showing both welding conditions and found welded joint kinds [10]

Fig. 32 shows the weldability window developed by Raoelison et al. [10]. The window defined particular values of input voltage and standoff distance for achieving a successful weld for MPW of AA6060T6 tubular assembly. They defined a lower boundary below which welding was unsuccessful and a higher boundary above which defective welds were produced. Based on the window they concluded that low standoff distances as well as high standoff distances are unfavourable conditions for welding. It is seen from the Fig. 32 that at intermediate gaps successful welds were created. Raoelison et al. [10] also developed two more weldability windows for assembly of AA6060T6 (Fig. 33 (a)) and AA6060T6/Cu (Fig. 33 (b)) tubes. They presented the weld variance in a chart defined by controllable process parameters viz. input voltage and standoff distance. At lower values of standoff distance bad welds were produced. They cited low impact velocities and lower collision angles for the same. These values of input voltage and standoff distance for which bad welds were produced formed the lower boundary of the weldability window. At very high values of standoff distance weld with discontinuous voids were produced. This condition was chosen to define the higher boundary for window. It can be seen from the Fig. 33 that the range of good weld is wider for the case of similar aluminium AA6060T6 assembly than for AA6060T6/Cu assembly.

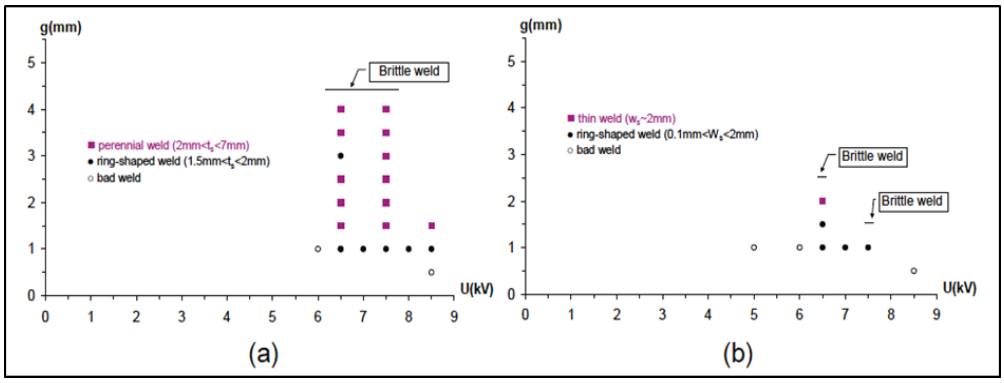

Fig. 33 Operational welding range (a) AA6060T6 pair assembly, (b) AA6060T6/Cu assembly [53]

Zhang et al. [120] developed a weldability window for plate-to-plate welding of 0.254mm thick Cu110 plates (Fig. 34). They conducted several experiments and subsequently measured the impact velocities. An analytical relation was developed to determine the corresponding impact angle. The window developed by Zhang et al. [120] gave a welding range based on the values of impact velocities and impact angles for all the cases where a successful weld was produced which was determined experimentally. It can be seen from the figure that an impact velocity of 250m/s was the bare minimum to conduct a successful weld. The suitable values of impact angle to conduct a successful weld were between 2^0 to 7^0.

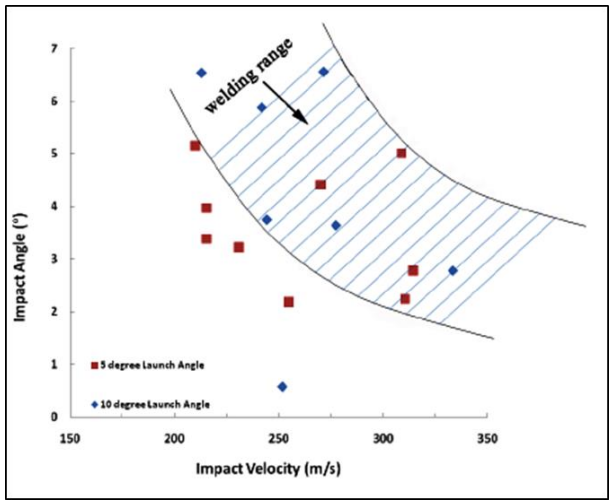

Fig. 34 Weldability window for Cu110 joints of 0.254mm thick plates [120]

2.1.5 Weld Quality and Integrity Evaluation

The welds produced by MPW must be characterised objectively in order to evaluate its integrity and quality. At present there are no tests which are specifically

designed for MPW but the MPW welds usually satisfies the standards set for conventional welding tests [36]. Available literature suggests use of two types of tests viz. non-destructive testing (NDT) and destructive testing to evaluate weld integrity [18]. The available tests are classified in Fig. 35.

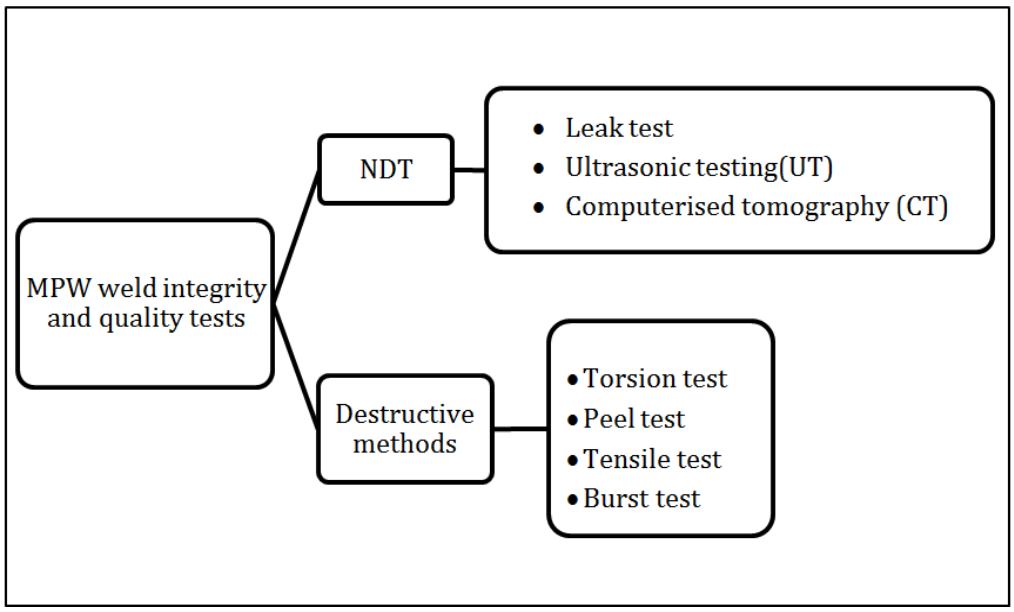

Fig. 35 Available tests for weld integrity assessment of MPW joints

NDT tests have been carried out on MPW welded specimens to identify bonding defects in the weld in order to provide an indication of the weld quality. One of the main features of NDT tests is that it does not destroy the welded specimen and can thus be applied to ready to be sold products. Leak test gives a good understanding of the presence of any weld defect very quickly but does not allow the user to quantify the defects accurately. Water leak tests and Helium leak tests have shown that MPW is able to produce hermetic seals [36]. Ultrasonic testing (UT) allows one to search flaws and cracks and determine joints with deficient bonding. UT detects flaws and discontinuity by capturing high energy reflected sound waves from the defects and transforming it into an electrical signal. However this method has not gained much popularity to find flaws in pulse welded joints due to the associated problems [18, 121]. Fig. 36 shows the operating principle of UT and detection of flaws.

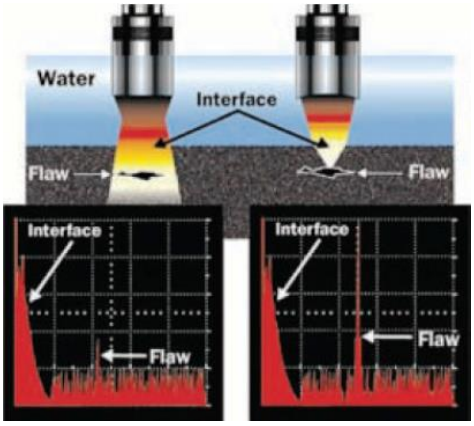

Fig. 36 Operating principle of UT [18]

Computerised Tomography (CT) is an advanced radiographic technique useful in detecting internal defects and internal structures of the object under consideration. CT has already been successfully used to study the wavy pattern of explosive welded joints. Fig. 37 shows a pulse welded joint put under CT test.

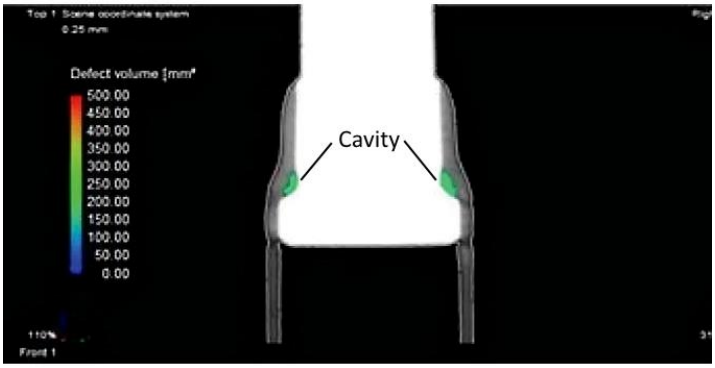

Fig. 37 CT image of a MPW specimen [121]

Destructive methods also give a measure of the weld quality but in doing so destroy the specimen. One of the most important and common tests for MPW welded specimens is microscopic examination followed by fracture tests viz. tensile, shear, bending. These tests help researchers evaluate the bond strength under actual shop floor applicable load conditions. Determination of intermetallic layers which are brittle and hard is generally done through hardness tests. Peel test gives an idea of the adhesive strength of the bond whereas a chisel test examines the ductility and strength of the bond. Tubular MPW joints are mostly subjected to torsion tests to determine strength of the weld by comparing it to the strength of the tube [121]. Researchers have concluded that if the fracture occurs at the tube and not at the weld zone, the weld is sound. In most of the pulse welded joints the welded zone is stronger than the

weaker of the base metals causing the failure to occur outside the weld zone [13, 23]. Fig. 38 shows the direct lap sample joints of AA6061 and Cu110 subjected to mechanical tests. For both AA6061 and Cu110, the fracture of was out of the welded region and broke at base metals [82].

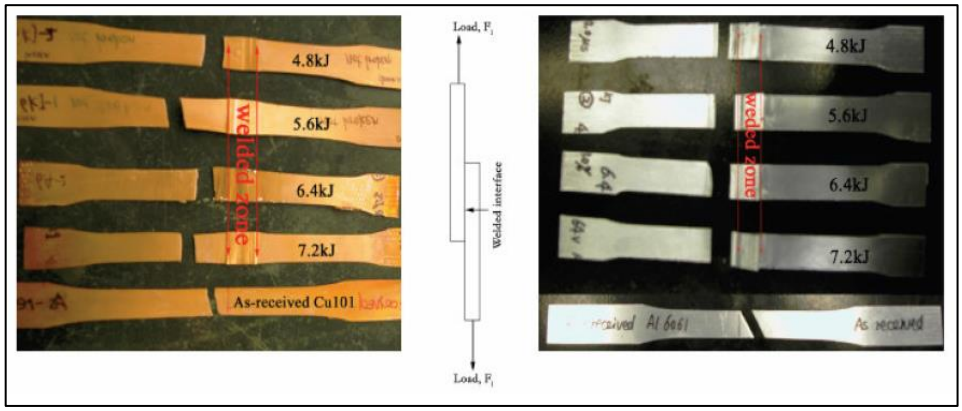

Fig. 38 Mechanical tests showing failure outside the welded zone [82]

Fig. 39 (a) shows an Al-Steel tubular joint welded by MPW after it was subjected to peel test. Haiping et al. [86] found that at a preset angle of 3^0 the Al strips along circular directions could not be peeled from the steel member which confirmed the presence of a metallurgical joint between the two members. Fig. 39 (b) shows the burst test result on an Al-Al weld. It was found that the failure occurred at the base metal suggesting that the weld was not the weak link [36]. Researchers have also carried out torsion tests for various pulse welded similar and dissimilar members. Figs. 39 (c) and (d) show the torsion test results Al-Al and Al-Steel joints respectively. In both the cases it was found that the weak point was the base tube metal and not the weld confirming the strength and integrity of the weld. Kore et al. [73] conducted tensile shear tests on Al-Mg sheets welded through MPW. They found that beyond certain discharge energy all the samples either failed at the base metal or at the plastically deformed zone suggesting that the MPW weld strength was higher than the base metal (Fig. 39 (e)). Similar results were reported by Shribman [36] when MPW was performed on a tubular steel member. Fig. 39 (f) depicts the same and suggests that the failure occurring remote from the weld is a sign of MPW weld being stronger than the base metal.

(a)

(b)

(c)

(d)

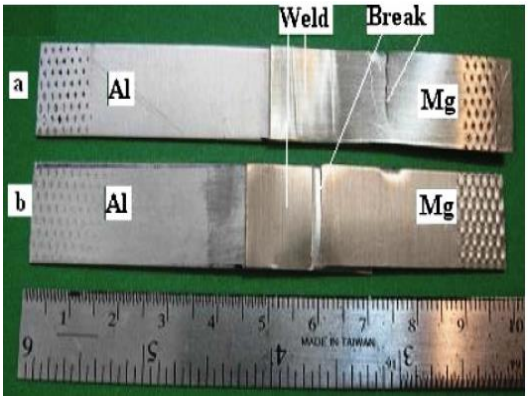

(e)

(f)

Fig. 39 (a) peeling test result of MPW joint [86], (b) burst test for Al6061-T6 capsule [36], (c) torsion tested Al/Al 6061-T6 members [36], (d) torsion tested Al/steel drive [36], (e) shear tested samples of Mg to Al welds with failure in a base metal and b plastically deformed zone [73] (f) tensile Test of welded 1020 steel tube [36]

2.2 Gaps and opportunities

Based upon the extensive review presented in the previous section some gaps have been identified. These gaps give opportunities to carry out research in the numerical and experimental analysis of the process. Table 2 lists the various available gaps and opportunities in MPW.

Table 2 Gaps and Opportunities available for research in MPW

Gaps	Opportunities
1. Very limited literature is available on finite element modelling of MPW process for tubular geometry.	1. FEM models for tubular geometry can be developed for compression and expansion joining for both similar and dissimilar materials.
2. Weldability criteria have been identified by researchers but available literature suggests the use of one or at most two criteria to develop weldability windows.	2. Multi-criterion weldability windows can be developed for similar and dissimilar materials which will be practical and shop floor applicable.
3. People have carried out modelling of burst pressure as a function of MPW parameters while very limited literature talks about modelling of weldability criteria.	3. Modelling of weldability criteria in MPW can be carried out. Statistical and mathematical models can be developed. Weldability criterion based predictive models van be developed

In addition to the above stated opportunities the developed models can further be used to optimize the process. Based on the identified gaps and opportunities, the problem for the present investigation has been formulated. The following section presents the problem formulation of the problem.

2.3 Problem definition and workplan

Problem definition:

Feasibility study of the MPW process for joining of similar and dissimilar materials through numerical modelling and experimental analysis.

Problem formulation:

Based on the literature review, the problem considered for the present investigation is formulated in the following two stages:

Stage 1: Numerical analysis of MPW through development of a FEM.

Stage 2: Experimental study of the MPW process to validate the findings of stage 1.

2.4 Objectives and Scope of investigation

Stage 1 (Numerical modelling)

Objectives:

- Perform coupled magnetic-structural finite element analysis (FEA) of the MPW process for tubular geometry for similar and dissimilar materials for both the cases of compression and expansion joining.
- Investigate various weldability criteria, namely, impact velocity, effective plastic strain and the direction and magnitude of the shear stress at the impact zone during magnetic pulse welding.
- Understand the effect of varying process parameters, i.e., input voltage and the gap between the two mating members on the above mentioned weldability criteria.
- Determine the feasibility of the MPW process based upon the available weldability criteria and subsequently develop optimal weldability windows.
- To understand and the process mechanism and its relationship with the process parameters.
- To develop predictive model for impact velocity in MPW using regression analysis and Artificial neural network (ANN).

Scope:

The scope of the present investigation (Stage 1) in terms of material, process parameters, process outcomes and computational techniques is presented Table 3:

Table 3 Scope of investigation in Stage 1

Features to be investigated	• **Weldability criteria:** Impact velocity, Effective plastic strain, Shear stress • **Process parameters:** Voltage, Coil turns, Coil length, Coil c/s area, Capacitance, Frequency, Air gap, Inductance, Resistance
Material	• The investigation is planned to cover both similar and dissimilar material combinations
Computational Techniques	• **Predictive Modelling :** Regression analysis and ANN • **Finite element solver:** COMSOL Multiphysics
Operational areas and working environment	• Compression and expansion joining of tubular members. • Model developed with temperature independent properties

Stage 2 (Experimental work)

Objectives:

- Perform experiments to validate the findings of stage 1.
- Develop the technology for joining of similar and dissimilar materials.
- To understand the effect of welding parameters on the joint strength and weld quality and correlate the process mechanism with process parameters.

Scope:

The various experimental tests planned to be carried out to validate the FEM developed in stage 1 is listed in Table 4.

Table 4 Validating tests

Mechanical Investigation	Metallurgical Investigation
• **Lap shear test:** Failure should occur in the weaker metal and outside the weld zone. • **Hardness Profile:** An increase in the hardness across the interface relative to the base metal should be observed.	• **Optical Microstructures and SEM:** A wavy pattern at the weld interface should be seen to ascertain weldability.

Apart from this, sensitivity analysis technique would be used at different places as per requirement of the subject. A detailed discussion regarding numerical modelling and simulation work, material and parameters selection, development of FEM and its validation, range of parameters and design of experiments, predictive model development, have been given in following chapter.

Chapter 3

Numerical Modelling and Simulation Work

This chapter describes the numerical modelling and simulation work conducted for the MPW process and material pairs selected for the present investigation. Firstly the materials along with their geometries and process parameters selected are discussed. The development of the FEM along with its assumptions and governing equations have been described then followed by validation of the same. The development of different weldability windows based on the FEM is then described. Development of impact velocity based predictive models through statistical regression modelling and ANN is discussed thereafter. Models have been validated and confirmed for their predictability. The results of the modelling exercise has been analysed and discussed.

3.1 Materials, geometry and process parameters

In order to examine the process of MPW, two different material pair's i.e. pure Al and SS 304 grade tubes and AA 2219-SS 321were simulated as a 2D axisymmetric problem in the FEM. The investigated welding tests were typically composed of a hollow flyer and a hollow cylindrical base tube for both pairs. The arrangement of the flyer and the base tubes along with specific dimensions for the two metal pairs are shown in Fig. 40 and Fig. 41. The air gap between the tubes has been denoted by G. Table 5 shows the chemical composition of the materials used in the model.

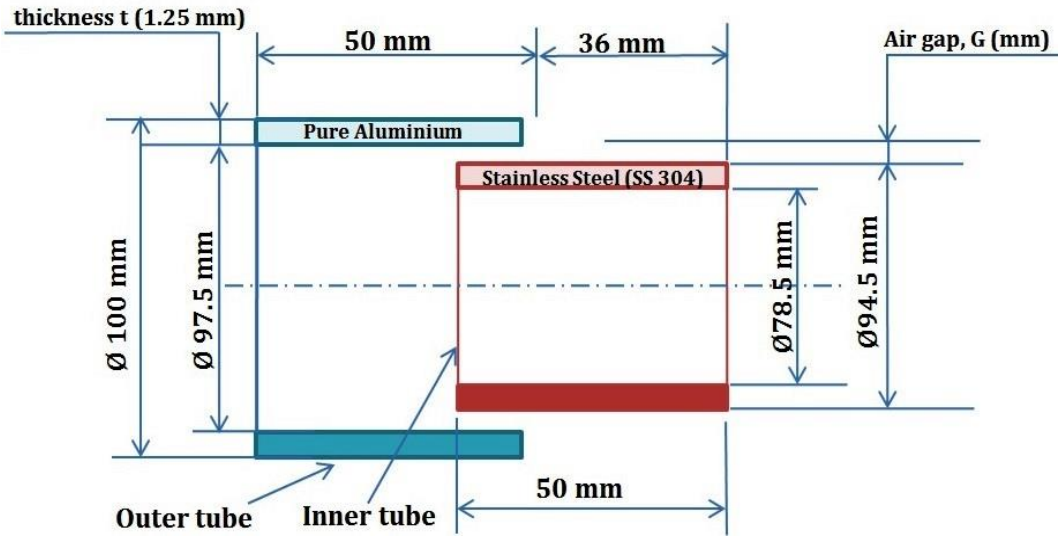

Fig. 40 Configuration of flyer and base tubes (Al-SS 304) for different air gaps

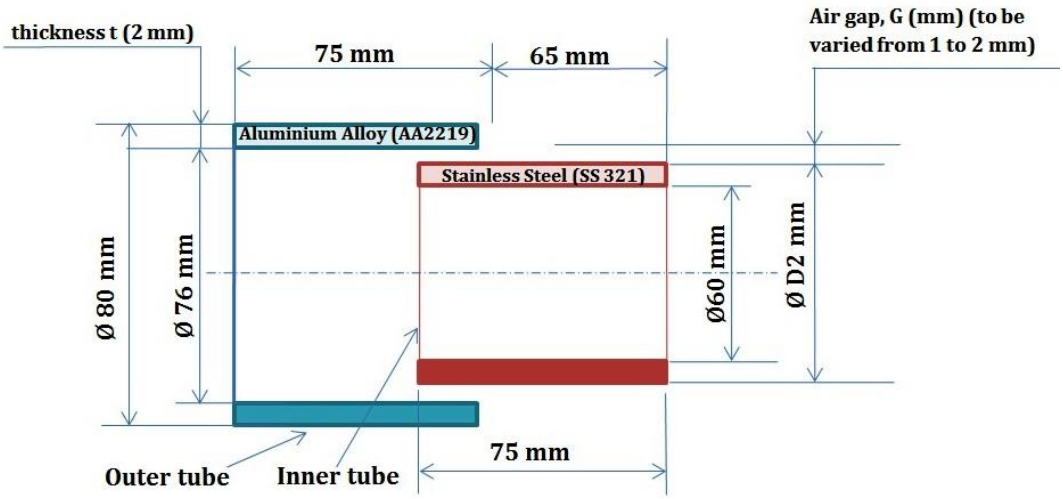

Fig. 41 Configuration of flyer and base tubes (AA 2219-SS 321) for different air gaps

Table 5 Chemical composition of flyer and base tubes

Base tube (SS 304)	Element	C	Mn	Si	P	S	Cr	Ni	N
	Composition %	0.08	2	0.75	0.045	0.03	19.0	10.0	0.10
Base tube (Pure Al)	Element	Fe	Cu	Mn	Si	Mg	Zn	Ti	Al
	Composition %	0.40	0.05	0.05	0.25	0.05	0.07	0.05	99.5
Base tube	Element	C	Mn	Si	P	S	Cr	Ni	N

(SS 321)	Composition %	0.08	2	0.75	0.045	0.03	20.0	10.5	0.10
Flyer tube	Element	Fe	Cu	Mn	Si	Mg	Zn	Ti	Al
(AA 2219)	Composition %	0.3	6.3	0.3	0.2	0.02	0.1	0.06	92.65

The numerical simulations were carried out with varying process parameters in order to understand their effect on the process. The process parameters which were varied for performing the simulations were input voltage, coil turns, coil length, coil cross sectional area, air gap, capacitance, frequency of operation, inductance and resistance. The simulations were performed with a multi turn copper coil. Properties of the copper coil are listed in Table 6. Table 6 also lists the material properties of the flyer and base tubes for the material pairs selected for the present study.

Table 6 Material properties and dimensions

Properties of flyer tube (pure Al)	Density (Kg/m^3)	2700
	Modulus of elasticity (GPa)	70
	Bulk modulus (GPa)	76
	Shear modulus (GPa)	26.2
	Poisson's ratio	0.33
	Speed of sound (m/s)	5305
Properties of flyer tube (AA 2219)	Density (Kg/m^3)	2700
	Modulus of elasticity (GPa)	73
	Bulk modulus (GPa)	76
	Shear modulus (GPa)	26
	Poisson's ratio	0.33
	Speed of sound (m/s)	5100
Properties of base tube (SS 304)	Density (Kg/m^3)	8033
	Modulus of elasticity (GPa)	193
	Bulk modulus (GPa)	142.5
	Shear modulus (GPa)	77.5
	Poisson's ratio	0.29
	Speed of sound (m/s)	4211
Properties of base tube (SS 321)	Density (Kg/m^3)	8027
	Modulus of elasticity (GPa)	193
	Bulk modulus (GPa)	120

	Shear modulus (GPa)	90
	Poisson's ratio	0.29
	Speed of sound (m/s)	5130
Properties of electromagnetic coil (Copper)	Relative permeability	1
	Resistivity (ohm m)	3.4×10^{-8}
	Inductance (nH)	10^{-7}
Weld validation criteria	Threshold value of impact velocity (m/s) (see Eqs.7-10) for Al- SS 304	161.03
	Threshold value of impact velocity (m/s) (see Eqs.7-10) for AA 2219- SS 321	139.36
Process employed	Compression joining of tubular parts	

3.2 FEM development

The flowchart for a sequentially coupled Electromagnetic–Structural analysis is illustrated in Fig. 42. The physical environments viz. Electromagnetic and Structural (electromagnetic coil, and flyer and base tubes, respectively) were established at first. The electromagnetic environment was then solved, which calculated the transient magnetic forces, i.e. Lorentz forces. These forces were fed as input load in the structural module to calculate the flyer tube's deformation at subsequent time steps. Based on the updated geometry of the tube, the time dependent magnetic forces were found out at subsequent time steps. The electromagnetic module consisted of the flyer and target tubes, the electromagnetic coil and a surrounding air region, whereas the structural module was related to the flyer, the target tubes, and the coil. The structural module took into consideration the inertial effects because of time dependent stress.

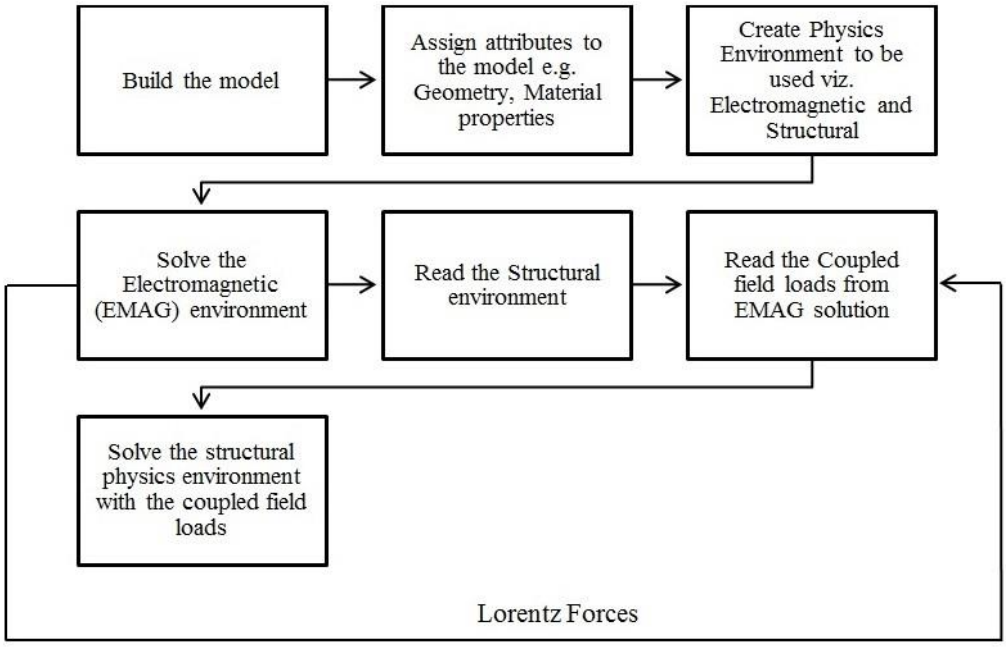

Fig. 42 Simulation flow chart for a sequentially coupled Electromagnetic – Structural analysis

3.2.1 Model assumptions

The FEM has been developed with the following considerations for simplification of the problem considered:

- Cracking and the heat generated by friction, deformation and the joule heating has been neglected.
- Use of temperature independent elasto-plastic properties.
- Resistance offered by air inside the flyer tube was neglected in the model.
- Field shaper has not been employed.

3.2.2 Governing Equations

In the tube region, Eq. (11) stated below is reached upon by substituting the constitutive equations into the equations given by Maxwell [122]:

$$\nabla \times \left(\frac{1}{\mu} \nabla \times \vec{A}\right) = -\Upsilon \frac{\partial \vec{A}}{\partial t} \tag{11}$$

where μ represents the permeability of the medium (H/m), Υ represents the conductivity of the medium (S/m), $-\Upsilon(\partial \vec{A}/\partial t)$ represents the current density (A/m^2) and $\vec{A}$ represents the magnetic vector potential.

The magnetic force $\vec{f}$ in unit volume of medium, i.e., the magnetic force density is given by Maxwell's equation as follows [122]:

$$\vec{f} = \vec{J} \times \vec{B} = \frac{1}{\mu}\left(\nabla \times \vec{B}\right) \times \vec{B} \tag{12}$$

where $\vec{J}$ represents the coil current density (A/m^2) and $\vec{B}$ represents magnetic flux density (T).

The forces applied on the tube due to the generated magnetic fields can thus be calculated by substituting $\nabla \times \vec{A} = \vec{B}$ and Eq. (1) into Eq. (2) and the input body load in the structural module.

The load in the electromagnetic module is the current which passes through the electromagnetic coil and this current is approximately expressed as [122]:

$$I = U\sqrt{\left\{\frac{C}{L} exp(-\beta t)\sin(\omega t)\right\}} \tag{13}$$

where U represents the input voltage, C represents the capacitance, L represents the inductance, β represents the damping exponent and ω is the angular frequency.

The constitutive behaviour of the tube material is described by the default constitutive relation built in COMSOL i.e. the Cowper-Symonds constitutive model [122].

$$\sigma = \sigma_y\left[1 + \left(\frac{\dot{\varepsilon}}{P}\right)^m\right] \tag{14}$$

where $\sigma_y$represents the quasi-static flow stress, $\dot{\varepsilon}$ represents the plastic strain rate (s^{-1}), P and m are specific material parameters.

3.3 Weld validation criteria

Three different criteria are available in literature which helps the user to ascertain the weldability of the joint namely:

a) Impact velocity
b) Effective plastic strain
c) Shear stress

a. Impact velocity

The determination of impact velocity is a very essential step during MPW. Impact velocity determines the success of the weld. Available literature suggests analytical relations that give threshold values of impact velocity [49]. The weld occurs when the threshold limit is crossed. Researchers have carried out extensive studies regarding the effect of impact velocity on the occurrence of weld. Separate relations have been suggested for similar and dissimilar material combinations. The present study uses the relations given by Eqs. (7-10) to determine the minimum impact velocity required to conduct a successful weld between the dissimilar mating members.

In MPW higher impact velocity leads to an increase in the impact pressure which causes severe plastic deformation at the interface of the mating members. One of the major requirements of conducting a successful weld through MPW is that the surfaces of the mating members are free of any oxide layers and contaminations. The impact velocity is the main parameter that causes variations in the bonding. If the impact velocity is excessively high, intermetallic compounds might be formed at the interface of the mating members or brittle damage might occur whereas on the other hand if the velocity is too low the jet formed is not sufficient to remove the contaminants and oxide layer from the surface of the workpiece which does not allow successful weld to occur. The impact velocity is directly related to input voltage which in turn is related to discharge energy. With increase in charging voltage the discharge energy also increases and with this increase the shearing strength of the metals also increases.

b. Effective plastic strain

Available literature [110] suggests the use of effective plastic strain by researchers to ascertain weldability in MPW of similar and dissimilar material combinations. The literature states that a MPW weld can be classified as successful if the threshold value of plastic strain is crossed at the impact zone. The threshold value changes with change in mating members.

c. Shear stress

Available literature [109] suggests that shear stresses in the base and flyer tubes at the impact zone should be of opposite sign for successful welding. If the shear stresses in the weld interface were of the identical sign in the two mating members welding was doubtful.

3.4 FEM validation

The developed FEM was validated by comparing the numerically computed impact velocity with the experimental values available in literature. The numerical simulations to assess the impact velocity of the MPW process for various considered cases was performed under a wide range of input parameter, material combination and dimension of the flyer and base tubes. The influence of these parameters on impact velocity of the flyer tube was investigated. Figs. 43 (a) and (b) show the deformation (3D plot) and the variation of impact velocity along the impact zone for the Al-SS 304 material combination at 14 kV and an air gap of 2 mm. It can be observed that the deformation of the tube is different for every point along the arc length. The arc length is the distance along the edge of the tube. The velocity of the flyer tube in MPW is maximum at the centre of the impact zone and it shows a decrease along the edges. This is caused due to the location of the maximum magnetic field in the axial centre of the air region between the coil and the flyer tube [49]. The flyer tube attains maximum velocity just at the time of impact and the same starts to decrease as the process progresses [49]. The workpiece (flyer tube) starts moving as soon as the magnetic pressure generated by the electromagnetic coil exceeds the plasticization pressure for the workpiece [117].

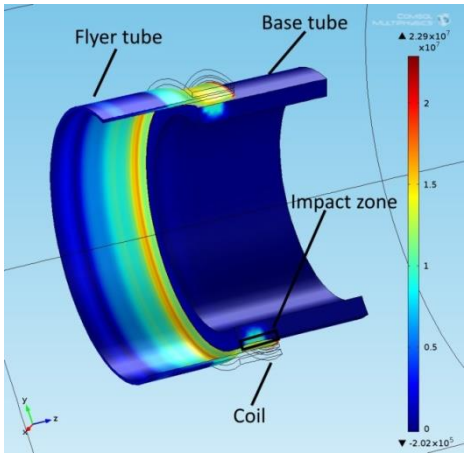

(a)

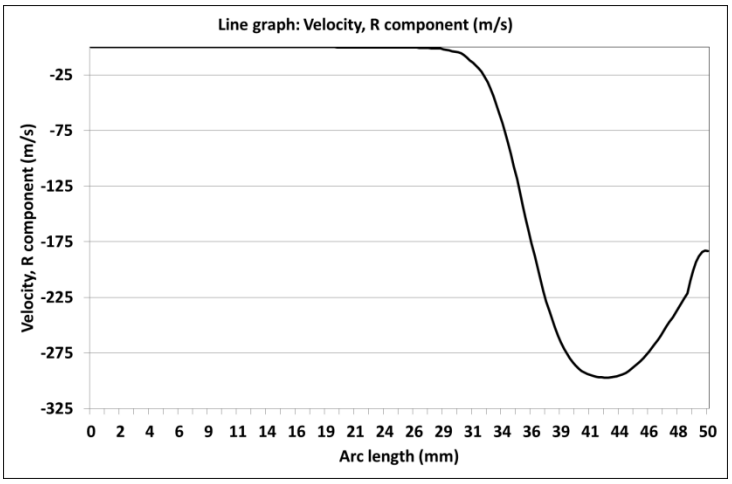

(b)

Fig. 43 (a) surface deformation 3D plot and (b) impact velocity along arc length (14 kV, 2 mm air gap)

Figs. 44 (a) and (b) show the comparison of experimental and simulated values of workpiece velocity computed by the FEM for dissimilar metal joining through electromagnetic compression. It can be seen that there was a close agreement between the simulated and experimental values within a range of ±10% variation. Fig. 44 (a) shows the velocity of the flyer tube for a displacement of 1 mm whereas Fig. 44 (b) shows the workpiece velocity after 2 mm displacement of the same. The velocity was computed for different energy levels and varying process parameters viz. capacitance, inductance and resistance of the MPW set up [117]. Figs. 44 (a) and (b) give useful insight into the influence of process parameters on the workpiece velocity. It can be observed that the velocity increases with an increase in charging energy or in other words the input voltage. The influence of capacitance on the velocity is also seen clearly in the said figures. The highest workpiece velocity was recorded for the case with lowest value of capacitance even if the charging energy supplied was not highest. The velocities predicted after 2 mm displacement (Fig. 44 (b)) of the flyer tube are higher than those after 1 mm displacement of the flyer. This is due to the increased magnetic pressure acting on the workpiece leading to higher acceleration and higher velocities.

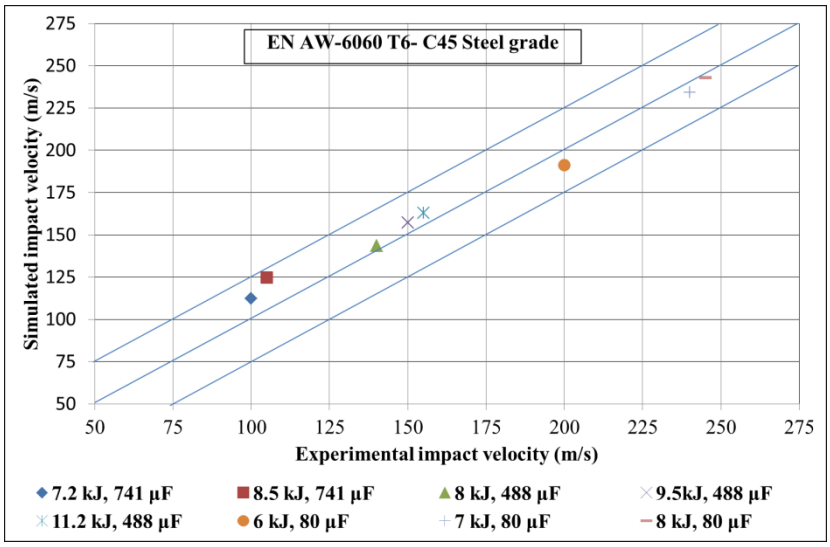

(a)

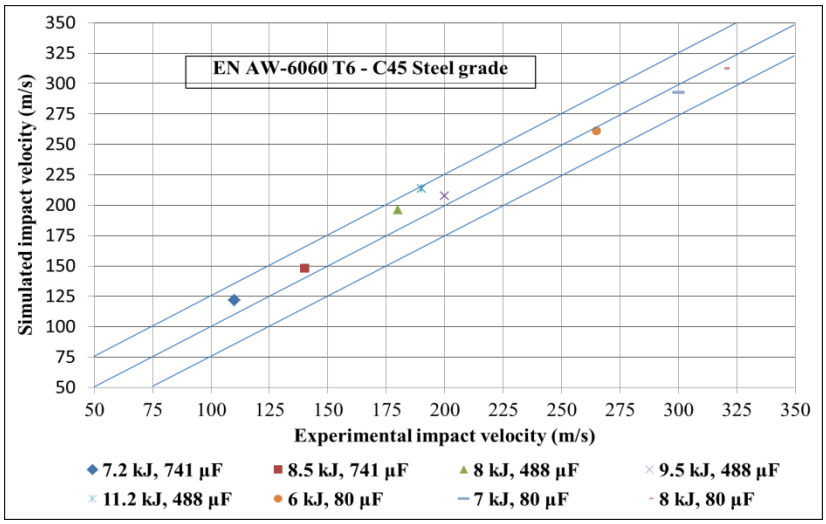

(b)

Fig. 44 Comparison of experimental and simulated values of workpiece velocity for compression joining of dissimilar materials (a) after 1 mm displacement of flyer tube (b) after 2 mm displacement of flyer tube [117]

Fig. 45 also shows the comparison of impact velocity computed through the FEM with the experimental values available in literature [14, 98]. In this case also the numerically computed impact velocities were within the within a range of ±10% variation.

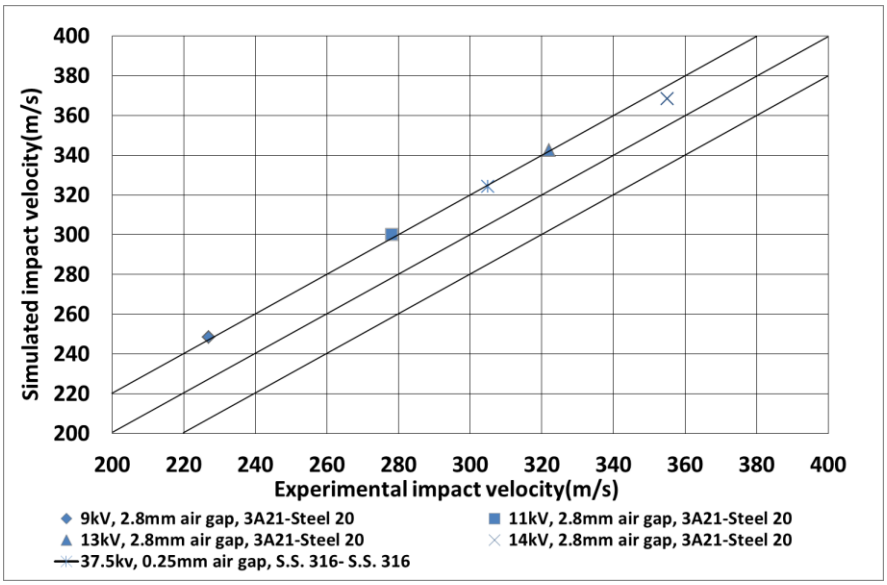

Fig. 45 Comparison of experimental and simulated values of impact velocities for compression joining of similar and dissimilar material [14, 98]

A magnetic pulse welded tubular joint can be divided into three zones, as shown in Fig. 46 (a). The actual welding of the mating members occurs only in the middle part of the working/impact zone. As the flyer tube impacts the solid workpiece (base tube), two no weld zones are formed on either side of the middle part. The zone on the left without weld is called the run-in zone and the right zone is called the run-out zone [84]. The available literature has not suggested any clear correlation between the lengths of the run-in and run-out zones and the settings of the process parameters. At the end of the run-out zone, the flyer tube makes a certain angle with the base tube. In general, the base tube is severely deformed during the impact. The most pronounced deformation occurs at the run-in zone, where the base tube is compressed in a narrow zone. From there on, the deformation of the base tube declines gradually towards the end of the weld (from left to right in Fig. 46 (a)). For the “no bond” zones the flyer tube would rebound, and there would literally be a gap between the two plates at the end of the simulation (Figs. 46 (a) and (b)). Sufficient plastic deformation was required in order for the two plates to join.

Similar results were observed when pure Al-SS 304 material combination (the material pair selected for the present investigation) were made to undergo pulsed welding in the developed FEM. The presence of distinct bond and no-bond zones is clearly visible in the numerically computed results shown in Fig. 46 (b). The similarity in the experimental and numerically computed results gives the user confidence over the developed FEM and also validates the same.

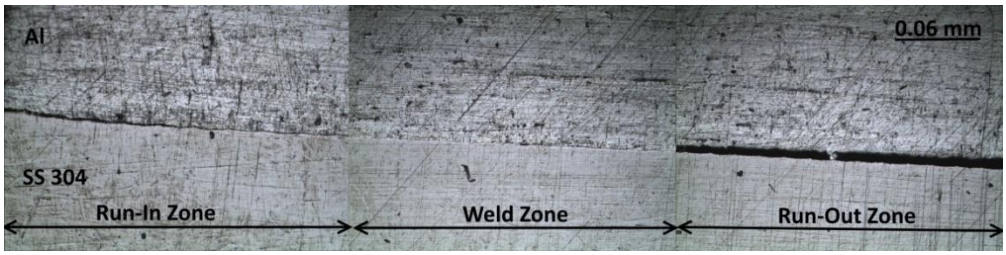

(a)

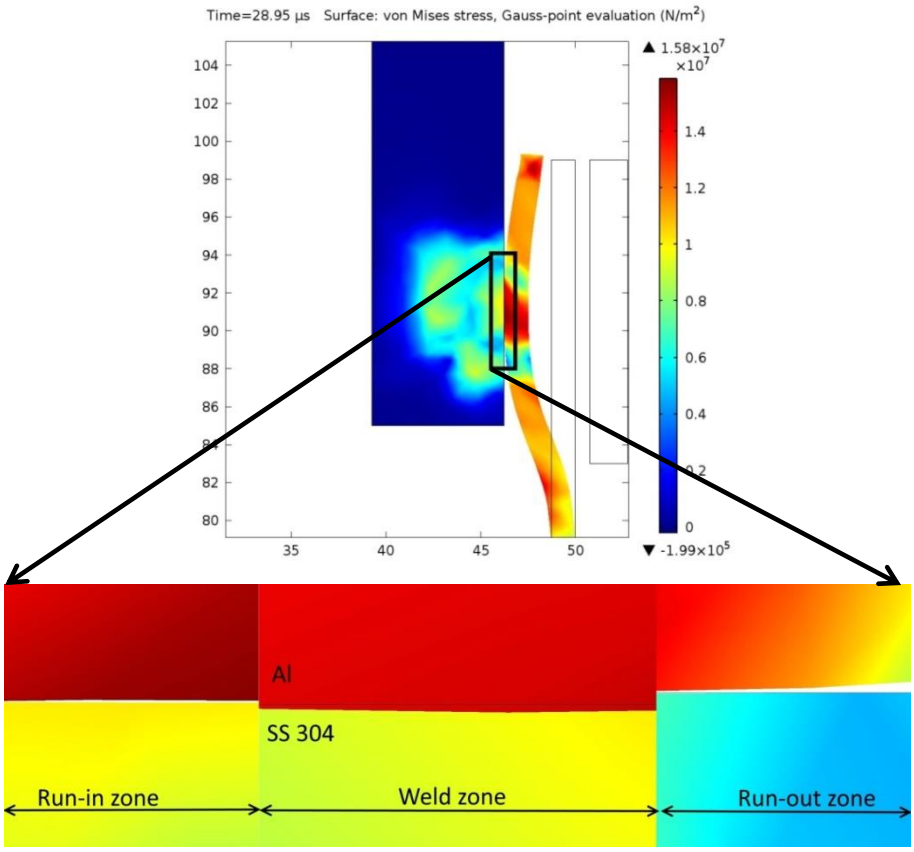

(b)

Fig. 46 (a) optical micrograph of a pulse welded Al-SS 304 member showing distinct zones at 10X magnification and (b) impact zone predicted by the FEM

Figs. 47 (a) and (b) show the distribution of shear stress and effective plastic strain along the length of the interface of mating members. It is known from literature that the shear stress and effective plastic strain must cross a threshold value to obtain a successful bond. As explained previously, a MPW welded tubular specimen consists of two unbonded zones with the presence of a welded centre zone. Thus the stress and strain distribution is bound to vary along the weld interface. This fact is depicted in Figs. 47 (a) and (b) where variation of the stress and strain is seen at the various zones

of the welded specimen. At the bonded centre zone a higher value of stress and strain were generated compared to the unbonded zones i.e. run-in zone and run-out zone as shown in Figs. 47 (a) and (b) which led to a bond at the centre of the interface. The stress values generated at the unbonded zones is due to the rebound action of the mating members upon impact. By conducting a large set of experiments and simultaneous numerical simulations the end user can predict the threshold values of stress and strain required to obtain a bond for a particular material. This exercise has not been conducted in the present study and is considered as a scope in future work.

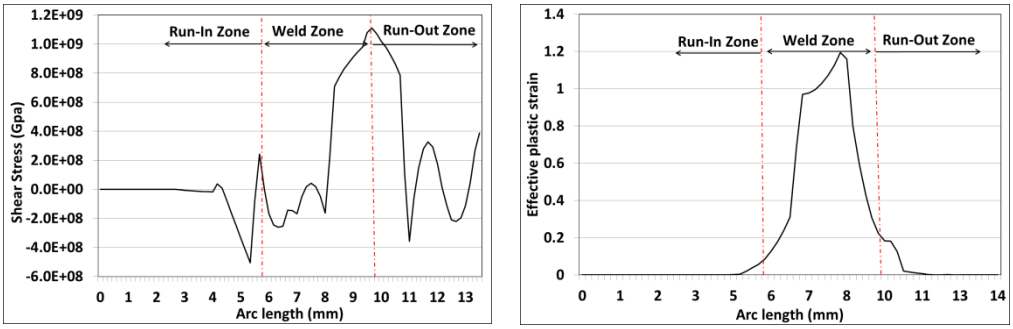

(a) **(b)**

Fig. 47 (a) and (b) weld validation criteria along arc length in different zones of the interface of pulse welded Al-SS 304 members

A typical MPW weld shows a wavy pattern at the impact zone. The Al-SS 304 metal pair pulse welded in this study also shows a similar wavy nature at the welded zone. Fig. 48 (a) shows the bonded interface with wavy nature for the Al-SS 304 steel members. The FEM developed for the present study also predicts similar results as shown in Fig. 48 (b). The numerical simulations clearly show a wavy morphology at the interface of the two mating members. Fig. 48 (b) shows the region where a wavy morphology was observed in the numerical simulations as a function of impact velocity.

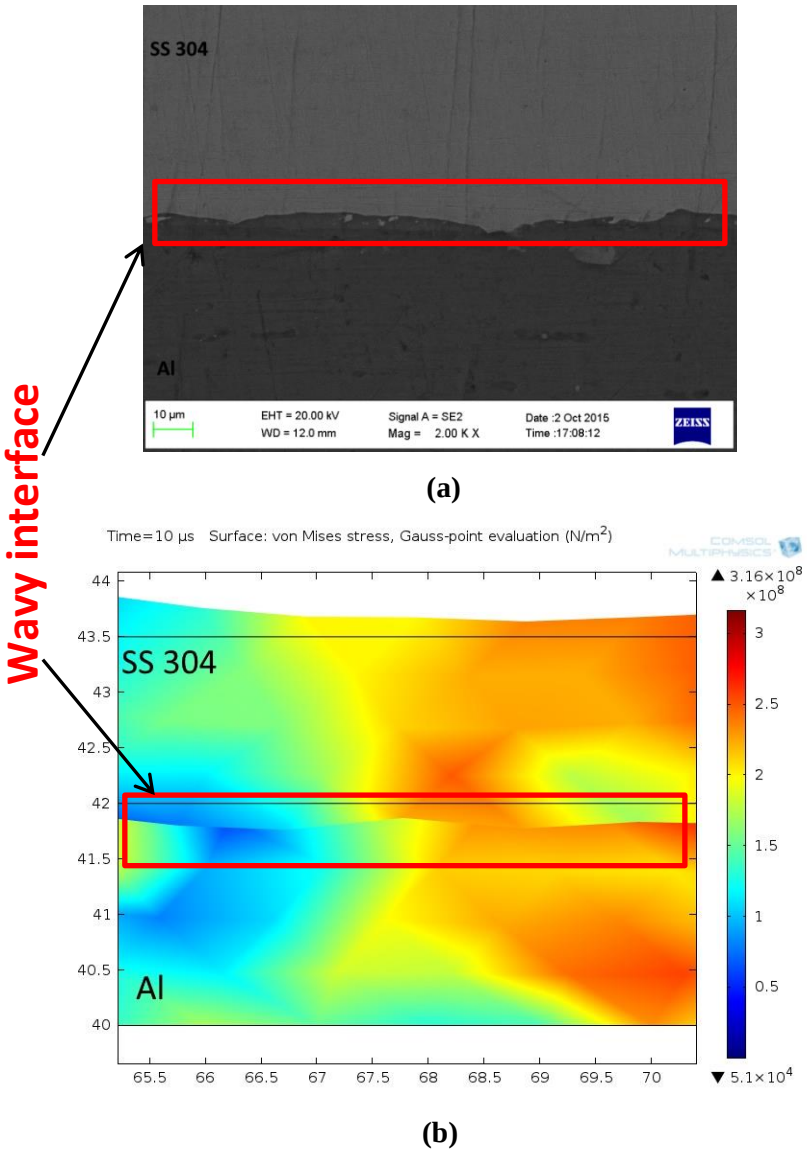

Fig. 48 Comparison of interface morphology between (a) experimental test and (b) FEM model

3.5 Weldability window development

The MPW process is influenced by several parameters that are inherent to the process: parameters regarding the electrical circuit (discharge energy, capacitance, operating frequency etc.), parameters regarding the material characteristics (electrical conductivity, density, yield strength, etc.) and parameters regarding the geometry of the workpieces (diameter, thickness, standoff distance). This wide variety of parameters makes it very complicated to find the conditions for an optimal weld for a given workpiece. Also it is difficult to find the optimal range for each parameter using analytical calculations This makes the process and development of a product through experimentation and analytical calculations very time consuming and costly.

One of the ways to reduce the cost and time spent in developing a product and producing a successful weld is by development of suitable weldability windows by FEA. The objective of the work presented in this section is to develop weldability windows for welding of the desired material combinations through a FEM which can be used as a tool when welding with MPW. A large number of numerical simulations with different parameter combinations were conducted and weldability windows were established for each material combination. Two different types of windows were developed based on the available weld validation criteria, the first type incorporating only one criterion i.e. impact velocity whereas the second type used all the three available criteria. The material, geometry, process type and development of the weldability windows is discussed in the following sub section.

3.5.1 Impact velocity based weldability window

The work presented in the present section focusses on development of impact velocity based weldability windows for the material combination chosen. The present study deals with the determination of impact velocity of the workpiece (flyer tube) during MPW of similar and dissimilar metallic tubular assembly via numerical simulations. The numerical simulations were conducted for a wide range of process parameters viz. charging voltage and air gap. The flyer and the target tubes were simulated as a 2D axisymmetric problem using the finite element model (FEM) software COMSOL Multiphysics. The process parameters, material chosen and respective threshold velocities are mentioned in Table 7.

Table 7 Material properties, process parameters and threshold velocities

Material	• EN AW 6060 and SS 316
Process parameters	• **Voltage(kV)**: 5, 5.5, 6, 6.5, 7, 7.5, 8, 8.5, 9, 9.5, 10, 10.5, 11, 11.5, 12 • **Air gap(mm)**: 0.5, 1, 1.5, 2, 2.5, 3, • **Capacitance(µF):** 250 • **Inductance(nH):** 7.5 • **Resistance(micro ohm):** 6.8 • **Frequency (rad/s):** 50000
Threshold velocities (similar materials, Eq. 6)	• Compression and Expansion joining (EN AW 6060-EN AW 6060) = **204 m/s**

	• Compression and Expansion joining (SS 316-SS 316) = **297.7 m/s**
Threshold velocities (dissimilar materials Eqs. 7-10)	• Compression and Expansion joining (EN AW 6060-SS 316)= **230.27m/s**

Numerical simulations have been performed for compression and expansion joining of similar and dissimilar materials and expansion. A number of practical and shop floor applicable weldability window based on impact velocity weldability criterion have been developed for compression and expansion joining of different material combination. Figs. 49 (a) to (e) show different weldability windows developed for compression and expansion joining of EN AW 6060 and SS 316. The plots shows the points at particular levels of input voltage and air gap where the impact velocity crossed the threshold required to ascertain the weldability of the joint. Fig. 49 (a) shows the comparison of expansion and compression welded EN AW 6060 flyer and base tube members while Fig. 49 (b) compares the pulse welded SS 316 members through compression and expansion joining. It is quite evident from the figures that compression welded members dominated the range of values crossing the threshold over the expansion welded members indicating a higher possibility of occurrence of a successful weld in the compression welded members. In the expansion joining process the electromagnetic coil needs to be place inside the two tubes unlike compression joining where the coil is placed outside the outer mating member. This placement of coil restricts the user to explore the coil parameter options like coil diameter, coil turns etc. The application of field shaper in expansion joining is also very difficult due to the space constraints. However, in the case of compression joining the user does not have to limit his options due to space constraint and can have a larger variation in coil parameters. The application of field shaper is also more widespread in compression joining. These facts definitely aid the compression joining process in a positive way and allows for a greater range of velocities crossing the threshold to be achieved. Fig. 49 (d) depicts the comparison of compression welded EN AW 6060 members with expansion welded SS 316 members. In this case also compression welded members dominated the expansion welded in terms of data points crossing the threshold velocity. One more factor apart from the above stated reasons led to this phenomenon. As stated in chapter 2 of this thesis the MPW process is also material dependent. It is seen from the Figs. 49 (d) and (c) that the range of values

exceeding the threshold value is greater in case of EN AW 6060 than SS 316. This is due to the fact that the yield strength of EN AW 6060 is much lower than that of SS 316 which aids in its deformation and subsequent acceleration to higher velocities. One of the basic requirements of the MPW process is that the flyer workpiece should be highly conductive which leads to better magnetic field distribution together with high magnetic pressure generation. In this case EN AW 6060 is a superior conductor when compared to SS 316 and thus the velocities reached in EN AW 6060 exceed those of SS 316. Fig. 49 (e) compares pulse welded (EN AW 6060 flyer tube with SS 316 base tube) members for both compression and expansion joining processes. The geometrical constraint material parameter constraint together effected this dissimilar material combination and process type. In this case also the compression welded members dominated the expansion welded ones. The developed weldability windows help us to pick particular process parameters suitable for the type of process chosen viz. compression joining or expansion joining and the material combination chosen.

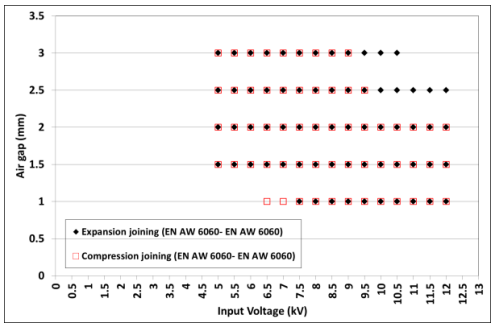

(a)

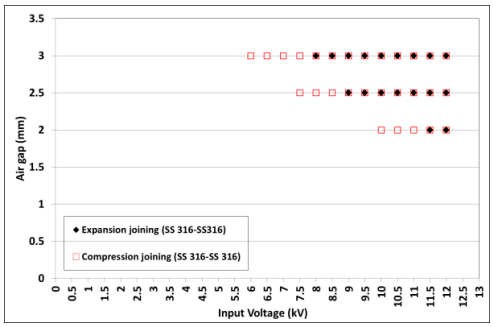

(b)

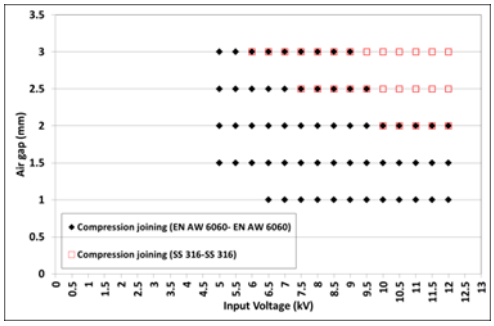

(c)

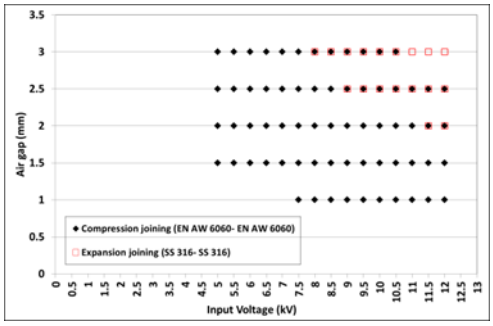

(d)

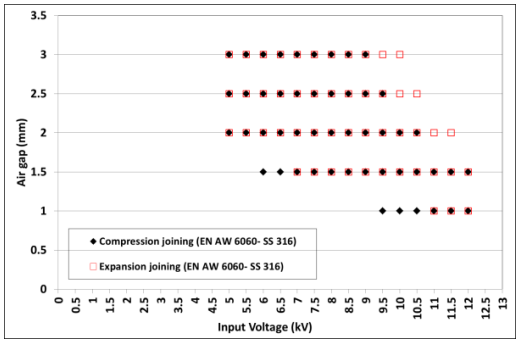

(e)

Fig. 49 (a) to (e) weldability windows for compression and expansion joining of similar and dissimilar material combination

3.5.2 Multi-criteria weldability window

In order to develop the multi-criteria weldability window, Structural steel ASTM A36 tubes were simulated as a 2D axisymmetric problem in the FEM. Table 8 shows the chemical composition of the material used in the model.

Table 8 Chemical composition of Structural steel ASTM A36

Structural steel ASTM A36	Element	C	Cu	Fe	P	S	Mn	Si
	Composition %	0.25-0.29	0.2	98	0.040	0.05	1.03	0.28

The investigated welding tests were typically composed of a hollow flyer and a hollow cylindrical base tube. The outer and inner diameters of the flyer tube were adjusted to calibrate the required air gap and are denoted as D2 and D1 respectively. The air gap between the tubes has been denoted by G. The arrangement of the flyer and the base tubes along with specific dimensions is shown in Fig. 50.

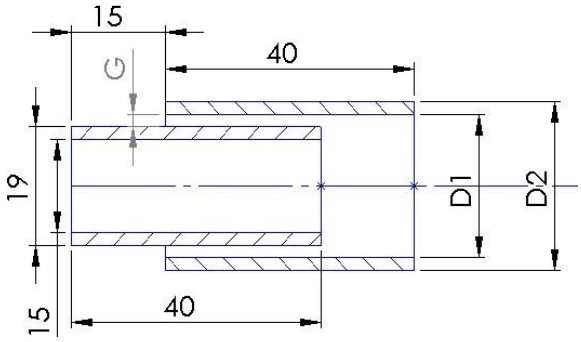

Fig. 50 Configuration of flyer and base tubes for different air gaps

The outer and inner diameters of the base tube were kept fixed at 19 mm and 15 mm respectively for each of the test cases. The simulations were carried out at varying process parameters. The process parameters which were varied for performing the simulations were air gap and input voltage. The input voltage was varied in steps of 0.5 kV from 6 kV to 9.5 kV, the air gap being varied from 0.5 mm to 2.5 mm in steps of 0.5 mm. The simulations were performed with a multi turn copper coil. Properties of the copper coil are listed in Table 9. Table 9 also lists the material properties and dimensions of the flyer tube.

Table 9 Material properties and dimensions for Structural steel ASTM A36

Properties of flyer tube and target tube	Density (Kg/m^3)		7850
	Tensile yield strength, (MPa)		250
	Modulus of elasticity (GPa)		200
	Bulk modulus (GPa)		140
	Shear modulus (GPa)		79.3
	Poisson's ratio		0.26
	Speed of sound (m/s)		4512
	Threshold value of impact velocity (m/s) (see Eq. 6)		297.7
	Threshold value of plastic strain [110]		0.35
	Threshold value of shear stress (GPa) [112]		0.5
Properties of electromagnetic coil-Copper	Relative permeability		1
	Resistivity (ohm m)		3.4×10^{-8}
	Inductance (H)		10^{-7}
Dimensions -flyer tube	Air Gap (mm)	Outer diameter (mm)	Inner diameter (mm)
	0.5	24	20
	1	25	21
	1.5	26	22
	2	27	23
	2.5	28	24

The numerical simulations to assess the weldability of the structural steel ASTM A36 tubular assembly was carried out at various process parameters as mentioned in

the preceding section. The flyer tube was affected by both radial and axial forces at a time and thus it suffered complicated stresses. The surface Von Mises stress developed in the flyer tube increased continuously with time (Figs. 51 (a) to (d)) and reached the maximum value when the flyer tube collided with the target tube Fig. 51 (e). A wavy interface at the impact zone can be seen at the time of impact. The impact velocities, effective plastic strain, and the shear stress at the time of impact were recorded for the 40 cases. The resulting weldability window and process mechanism are discussed in the succeeding section.

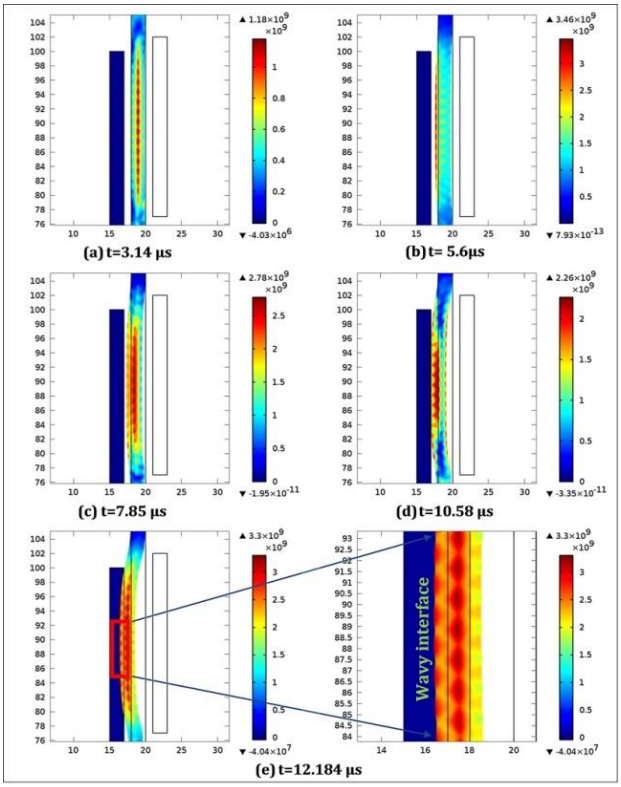

Fig. 51 Surface Von Mises stress at different times (input voltage- 8.5 kV, air gap- 1 mm)

Figs. 52 (a), (b) and (c) show the comparison of three weldability criteria along the arc length at varying input voltages and a constant air gap of 1 mm. The arc length is the distance along the edge of the flyer plate at the impact zone. It can be observed that the impact velocity criterion could not be satisfied at 8 kV (Fig. 52 (a)); whereas the effective plastic strain crossed the threshold at all the three input voltages (Fig. 52 (b)). On the contrary, the shear stress criterion crossed the threshold at 8 kV but failed to do the same at 9 kV (Fig. 52 (c)). The input voltage of 8.5 kV satisfied all the three

criteria. Thus, the existence of process parameters which can satisfy all the three criteria in the MPW process was non-trivial.

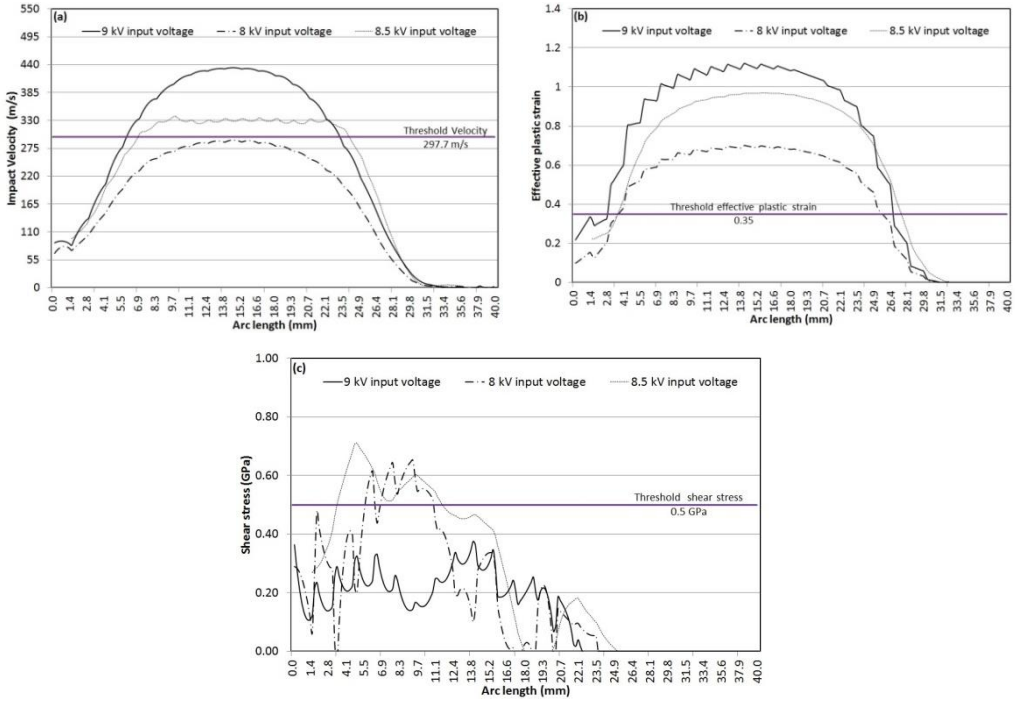

Fig. 52 Comparison of weldability criteria (a) impact velocity, (b) effective plastic strain and (c) shear stress (air gap = 1 mm)

The foregoing description was further extended to the remaining test cases and consolidated in Fig. 53. The pairs of the input voltage and the air gap are marked for the cases when an individual weldability criterion crossed the respective threshold value. It is seen that the plastic strain was the most versatile criteria that crossed the threshold limit followed by the impact velocity and the shear stress. The impact velocity crossed the threshold value at moderate and higher values of the investigated input voltage; whereas the same happened at moderate and lower values for the shear stress. The moderate input voltage except the minimal air gap of 0.5 mm was successful in crossing the threshold of the three criteria. Based on the above discussion a weldability window was reached upon, as shown in Fig. 53. This window encompassed only those values of process parameters, where the impact velocity, effective plastic strain and shear stress together crossed their respective threshold values. The window identified the particular process parameters suitable for conducting a successful weld.

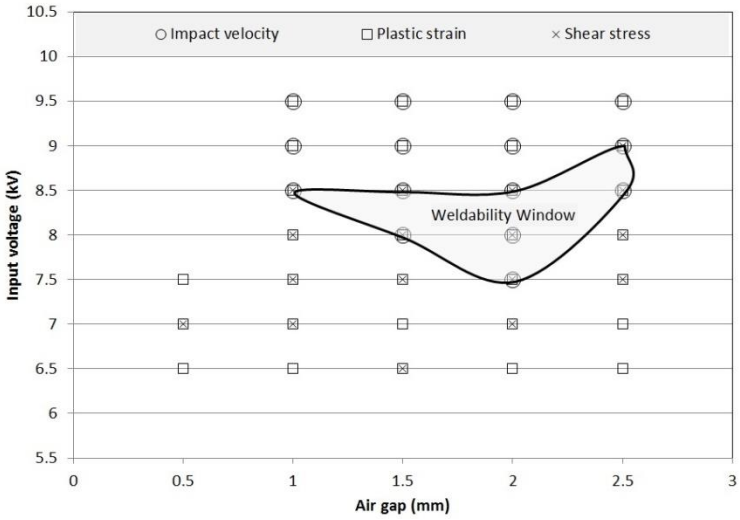

Fig. 53 Weldability window for MPW of structural steel ASTM A36

The process parameters that characterized the three weldability criteria were interrelated. The interrelation is explained through Figs. 54 (a), (b) and (c) that depict the influence of process parameters on the impact velocity, the effective plastic strain, and the shear stress, respectively.

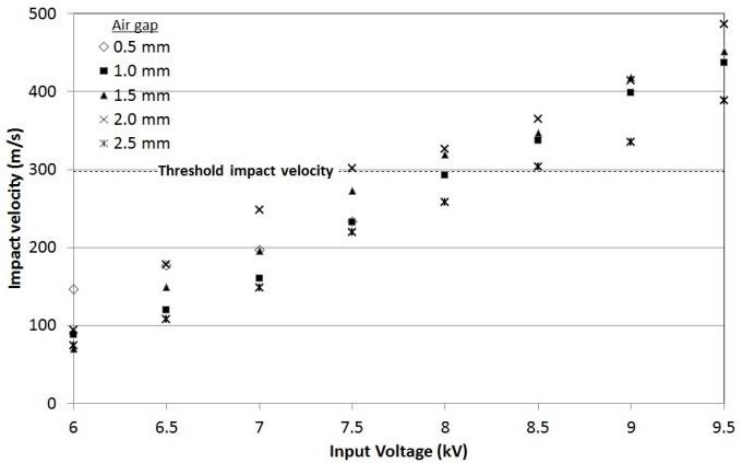

(a)

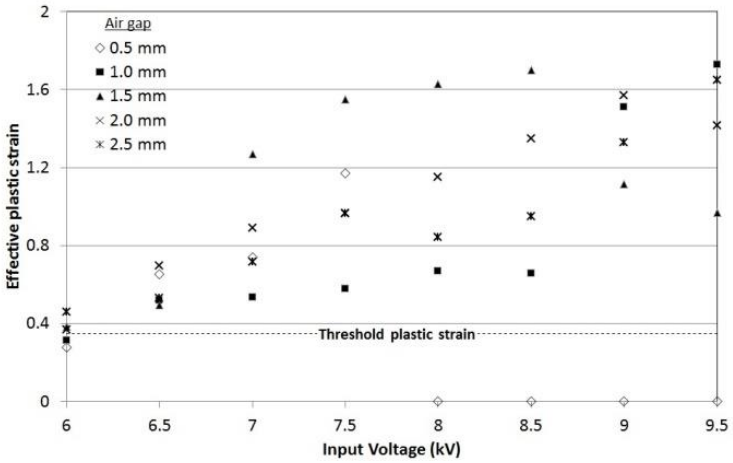

(b)

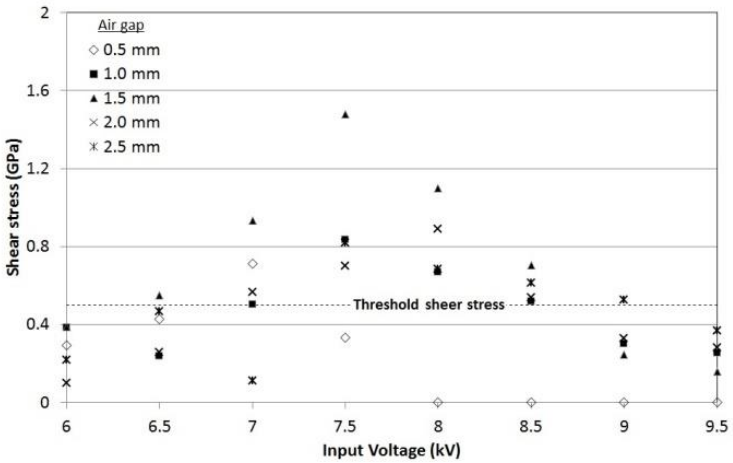

(c)

Fig. 54 Weldability criteria at different air gaps and input voltages (a) impact velocity, (b) effective plastic strain, (c) shear stress

From Fig. 54 (a) it is seen that the impact velocity increased with an increase in the input voltage. However, a minimum input voltage of 7.5 kV was essential to cross the threshold impact velocity. This is in agreement with the previously published observations [98] that one of the simplest ways to increase the quality of MPW is to increase the input voltage. At lower input voltages like 6 kV and 6.5 kV, maximum impact velocity was obtained with the lowest air gap of 0.5 mm. A further increase in the input voltage at 0.5 mm air gap did not result in a significant amount of change in the impact velocity and eventually the flyer plate damaged at voltages ranging from 8 kV to 9.5 kV. The damage might be a result of low strain rate and high stress level that occurred at the time of discharge leading to crack initiation and propagation in the

flyer [103]. At a particular value of the air gap, the velocity and kinetic energy of the tubes reached a maximum value. Below this particular value the tubes were unable to attain the maximum possible velocity. At lower values of the air gap, e.g. 0.5 mm in the present case, the tubes collided well before the flyer attained the maximum velocity; whereas in case of larger air gaps the velocity reached a value lower than the maximum at the time of the impact. The previously published experimental results [13] are in agreement with the observed numerical results in the present study.

As the input voltage was increased, the plastic strain induced in the members as well as the shear stress, increased up to an extent as shown in Figs. 54 (b) and (c), respectively. The increase of the input voltage led to an increase in the pressure acting upon the flyer tube. The pressure in the impact zone was mainly due to two phenomena: pressure induced due to the magnetic field and a pressure due to the impact intensity [10]. High impact velocities produced high plastic deformation which subsequently resulted in higher levels of effective plastic strain at the impact zone. The numerically computed results suggest the existence of a plastic strain band, as well as a severely deformed impact zone with high values of plastic strain. The values of plastic strain crossed the threshold value for input voltages ranging from 6.5 kV to 9.5 kV suggesting that below 6.5 kV the bonding would not take place (Fig. 54 (b)). As the air gap was increased, the plastic strain values showed an increasing trend up to a certain value of input voltage and subsequently the value decreased. This confirms the presence of an optimum air gap (around 1.5 mm in the present case) between the members to achieve a good weld. At the lower air gap, it would not be possible to create a weld due to pressure deficiency, whereas at higher gaps the impact would not take place.

The foregoing observation was also supported by the shear stress distribution shown in Fig. 54 (c). The shear stress values had opposite signs for the flyer and target tubes, respectively, for the cases where it crossed the threshold value of 0.5 GPa. At an input voltage of 6 kV the shear stress value was below the threshold value for all the air gaps. From Fig. 54 (c) it can be observed that the shear stress crossed the threshold value for almost all air gaps at voltages ranging from 7 kV to 8.5 kV. Beyond this value of input voltage, the shear stress started to decrease and was unable to cross the threshold value. This would limit the allowable range of input voltage in a manner the velocity and the effective plastic strain would limit the allowable air gap as mentioned earlier.

The results of the present investigation emphasise on the need for an all-inclusive approach towards weldability criteria for MPW. Considering all the three criteria would provide a more reliable range of process parameters to work with. Furthermore, use of FEM simulation would save the cost and the time spent in development of a product.

3.6 Predictive Model Development

As discussed in the previous section impact velocity is one of the essential criterions to ascertain the weldability of the magnetic pulse welded joint. The current section discusses the development of an impact velocity based predictive model which can predict the impact velocity for any combination of process parameters. ANN has been utilized to develop the model. The model is shop floor applicable as it gives the end user and idea of MPW process parameters at which welding might occur. The development of the model is explained in the succeeding subsections.

3.6.1 Design of Experiments

Many factors/variables must be taken into consideration when making a predictive model. Design of experiments (DOE) is an important tool for designing processes and products. DOE is a method for quantitatively identifying the right inputs and parameter levels for making a high quality product or service. The present focusses on developing a predictive model which could predict values of impact velocity for different combinations of the parameters selected according to the DOE. DOE allows studying the influence of several process parameters on one or more responses simultaneously. Furthermore, DOE can create mathematical models for the responses, optimizing the selected factors that exhibit the highest influence on the system [123, 124]. Generally, the aim of DOE is to determine the optimal experimental conditions using a minimum number of experiments, whereas a major advantage is its inherent ability to predict interactions between the various experimental factors.

A DOE scheme was employed to develop the impact velocity based predictive models. The MPW process is dependent on a large number of parameters, as such prior to fixing the upper and lower limits of the process parameters, trial runs were done for varying process parameters in finite element based software COMSOL multiphysics. A total of nine parameters were chosen and the trial runs were conducted for the two material pairs chosen. The parameters for the selected material pairs and

their values chosen are listed in Tables 10 and 11. The geometry, material properties and pulse welding process chosen for the investigation are mentioned in Figs. 40 and 41 and Table 6 respectively.

Table 10 Parameters and values for the trial runs (Al–SS 304 material pair)

Parameter	Values
Voltage (kV)	6, 8, 11, 14, 17, 20, 25
Coil turn	3, 4, 6, 8, 12, 14, 16
Coil length (mm)	15, 20, 25, 30, 40
Coil c/s area (mm^2)	9, 16, 25, 36, 49
Capacitance (μF)	250, 300, 400, 500, 650, 800
Frequency (rad/s)	30000, 40000, 50000, 60000, 70000 80000
Air gap (mm)	0.5, 1, 1.5, 2, 2.5, 3, 3.5
Inductance (nH)	1.5, 3, 4.5, 6, 7.5, 9
Resistance (μohm)	6.8, 25, 50, 100, 200, 320

Table 11 Parameters and values for the trial runs (AA 2219–SS 321 material pair)

Parameter	Values
Voltage (kV)	5, 8, 11, 14, 17, 20, 25
Coil turn	4, 6, 8, 12, 14, 16
Coil length (mm)	15, 20, 25, 30, 40, 50
Coil c/s area (mm^2)	9, 16, 25, 36, 49, 64
Capacitance (μF)	150, 250, 300, 400, 500, 650, 750
Frequency (rad/s)	30000, 40000, 50000, 60000, 70000 80000
Air gap (mm)	0.5, 1, 1.5, 2, 2.5, 3, 3.5
Inductance (nH)	1.5, 3, 4.5, 6, 7.5, 9
Resistance (μohm)	6.8, 25, 50, 100, 200, 300

The trail runs were conducted in order to obtain the higher and lower limits of operating parameters. One parameter was varied at a time whereas all other parameters were kept at their mid values. Based on the runs, parameter values were identified where considerable damage was seen to the members under impact. Damage was

observed at the parameters listed in Tables 12 and 13. Damage was caused either due to very high speed impact of the members or due to impact at very low air gaps. However there is no clear indication of the particular parameter causing the damage as the MPW process itself is governed by a host of electrical, geometrical and material parameters as mentioned in chapter 1. The FEM was significantly affected due to the above phenomena and the same caused non-linear solver iterations to stop. The particular process parameters for which the iterations stopped and the simulation ended abruptly were noted down and are mentioned in Tables 12 and 13.

Table 12 Parameters causing damage to the members in the trial run (Al–SS 304 material pair)

Voltage (kV)	Coil turn	Coil length (mm)	Coil c/s area (mm^2)	Capacitance (μF)	Frequency (rad/s)	Air gap (mm)	Inductance (nH)	Resistance (μohm)
25	6	30	25	250	50000	1.5	7.5	6.8
14	16	30	25	250	50000	1.5	7.5	6.8
14	6	30	25	750	50000	1.5	7.5	6.8
14	6	30	25	250	80000	1.5	7.5	6.8
14	6	30	25	250	50000	0.5	7.5	6.8
14	6	30	25	250	50000	3.5	7.5	6.8

Table 13 Parameters causing damage to the members in the trial run (AA 2219–SS 321 material pair)

Voltage (kV)	Coil turn	Coil length (mm)	Coil c/s area (mm^2)	Capacitance (μF)	Frequency (rad/s)	Air gap (mm)	Inductance (nH)	Resistance (μohm)
25	6	30	25	250	50000	1.5	7.5	6.8
16	16	30	25	250	50000	1.5	7.5	6.8
16	6	30	25	750	50000	1.5	7.5	6.8

16	6	30	25	250	80000	1.5	7.5	6.8
16	6	30	25	250	50000	0.5	7.5	6.8
16	6	30	25	250	50000	3.5	7.5	6.8

After identification of parameters causing damage to the pulse welding members additional five test runs were conducted at highest values of all the parameters to check for further damage if any to the members. The results of the additional five test runs conducted for both the material pairs are listed in Tables 14 and 15.

Table 14 Additional test runs (Al–SS 304 material pair)

Voltage (kV)	**Coil turn**	**Coil length (mm)**	**Coil *c*/s area (mm^2)**	**Capacitance (µF)**	**Frequency (rad/s)**	**Air gap (mm)**	**Inductance (nH)**	**Resistance (µohm)**	**Velocity**
20	15	40	9	800	70000	3	1.5	6.8	Damage
19	15	40	9	800	70000	3	1.5	6.8	Damage
18	15	40	9	800	70000	3	1.5	6.8	Damage
18	15	40	9	800	70000	3	2.5	6.8	484.184
18	15	40	9	800	70000	1	2.5	6.8	244.1

Table 15 Additional test runs (AA 2219–SS 321 material pair)

Voltage (kV)	**Coil turn**	**Coil length (mm)**	**Coil *c*/s area (mm^2)**	**Capacitance (µF)**	**Frequency (rad/s)**	**Air gap (mm)**	**Inductance (nH)**	**Resistance (µohm)**	**Velocity**
20	15	50	9	700	70000	3	1.5	6.8	Damage
18	15	50	9	700	70000	3	1.5	6.8	Damage
17	15	50	9	700	70000	3	1.5	6.8	Damage
17	15	50	9	700	70000	3	2.5	6.8	505.95

17	15	50	9	700	70000	1	2.5	6.8	244.1

Based on the outcome of the additional five tests conducted the higher and lower values of the parameters for the DOE were fixed as shown in Tables 16 and 17.

Table 16 Parameter range for the orthogonal array (Al–SS 304 material pair)

Parameters	Minimum value	Maximum Value
Voltage (kV)	6	18
Coil turns	3	15
Coil length(mm)	16	32
Coil c/s area(mm^2)	9	49
Capacitance(μF)	250	750
Frequency(rad/s)	30000	70000
Air gap(mm)	1	3
Inductance(nH)	2	10
Resistance(μohm)	10	310

Table 17 Parameter range for the orthogonal array (AA 2219–SS 321 material pair)

Parameters	Minimum value	Maximum Value
Voltage (kV)	5	17
Coil turns	3	15
Coil length(mm)	16	48
Coil c/s area(mm^2)	9	64
Capacitance(μF)	160	700
Frequency(rad/s)	30000	70000
Air gap(mm)	1	3
Inductance(nH)	2	10
Resistance(μohm)	10	310

Based on the selected maximum and minimum values of the process parameters for the DOE two 9 parameter, 5 level and 75 run orthogonal arrays were designed and the impact velocities were calculated for each run. The orthogonal array and the numerically computed impact velocities are shown in Tables 18 and 19.

Table 18 Orthogonal array (Al–SS 304 material pair)

Exp. No	Voltage (kV)	Coil turn	Coil length (mm)	Coil c/s area (mm^2)	Capacitance (μF)	Frequency (rad/s)	Air gap (mm)	Inductance (nH)	Resistance (μohm)	Velocity (m/s)
1	6	3	16	36	250	30000	1	4	85	***22.72***
2	6	6	20	25	750	60000	3	2	310	***103.85***
3	6	9	24	16	625	40000	2	10	10	***189.36***
4	6	12	32	49	500	50000	1.5	8	235	***88.86***
5	6	15	28	9	375	70000	2.5	6	160	***464.57***
6	9	3	20	49	625	70000	3	10	235	***40.25***
7	9	6	24	9	500	30000	2	8	160	***205.91***
8	9	9	32	36	375	60000	1.5	6	85	***153.85***
9	9	12	28	25	250	40000	2.5	4	310	***168.74***
10	9	15	16	16	750	50000	1	2	10	***237.28***
11	12	3	24	25	375	50000	2.5	2	235	***69.64***
12	12	6	32	16	250	70000	1	10	160	***145.07***
13	12	9	28	49	750	30000	3	8	85	***196.71***
14	12	12	16	9	625	60000	2	6	310	***220.25***
15	12	15	20	36	500	40000	1.5	4	10	***201.52***
16	15	3	32	9	750	40000	2.5	10	85	***326.4***
17	15	6	28	36	625	50000	1	8	310	***102.16***
18	15	9	16	25	500	70000	3	6	10	***257.51***
19	15	12	20	16	375	30000	2	4	235	***259.31***
20	15	15	24	49	250	60000	1.5	2	160	***204.18***
21	18	3	28	16	500	60000	3	4	160	***367.58***
22	18	6	16	49	375	40000	2	2	85	***134.87***
23	18	9	20	9	250	50000	1.5	10	310	***263.55***
24	18	12	24	36	750	70000	2.5	8	10	***411.24***
25	18	15	32	25	625	30000	1	6	235	***217.78***
26	6	3	20	9	375	60000	1	8	10	***85.54***
27	6	6	24	36	250	40000	3	6	235	***52.31***

28	6	9	32	25	750	50000	2	4	160	***206.41***
29	6	12	28	16	625	70000	1.5	2	85	***342.97***
30	6	15	16	49	500	30000	2.5	10	310	***80.09***
31	9	3	24	16	750	30000	1.5	6	310	***73.73***
32	9	6	32	49	625	60000	2.5	4	10	***193.15***
33	9	9	28	9	500	40000	1	2	235	***226.95***
34	9	12	16	36	375	50000	3	10	160	***188.57***
35	9	15	20	25	250	70000	2	8	85	***226.84***
36	12	3	32	36	500	70000	2	2	310	***29.49***
37	12	6	28	25	375	30000	1.5	10	10	***116.78***
38	12	9	16	16	250	60000	2.5	8	235	***257.64***
39	12	12	20	49	750	40000	1	6	160	***104.79***
40	12	15	24	9	625	50000	3	4	85	***501.27***
41	15	3	28	49	250	50000	2	6	10	***75.54***
42	15	6	16	9	750	70000	1.5	4	235	***249.53***
43	15	9	20	36	625	30000	2.5	2	160	***208.86***
44	15	12	24	25	500	60000	1	10	85	***190.07***
45	15	15	32	16	375	40000	3	8	310	***535.84***
46	18	3	16	25	625	40000	1.5	8	160	***93.18***
47	18	6	20	16	500	50000	2.5	6	85	***332.68***
48	18	9	24	49	375	70000	1	4	310	***125.46***
49	18	12	32	9	250	30000	3	2	10	***584.61***
50	18	15	28	36	750	60000	2	10	235	***367.22***
51	6	3	16	9	250	30000	1	2	10	***70.96***
52	6	6	20	16	375	40000	1.5	4	85	***112.15***
53	6	9	24	25	500	50000	2	6	160	***150.71***
54	6	12	28	49	625	60000	2.5	8	235	***136.38***
55	6	15	32	36	750	70000	3	10	310	***258.81***
56	9	3	20	25	625	70000	1	4	160	***74.02***
57	9	6	24	36	750	30000	1.5	6	235	***75.73***
58	9	9	28	49	250	40000	2	8	310	***63.73***
59	9	12	32	9	375	50000	2.5	10	10	***489.09***
60	9	15	16	16	500	60000	3	2	85	***315.24***

61	12	3	24	49	375	60000	2.5	2	160	***45.81***
62	12	6	28	9	500	70000	3	4	235	***487.21***
63	12	9	32	16	625	30000	1	6	310	***158.68***
64	12	12	16	36	750	40000	1.5	8	10	***147.91***
65	12	15	20	25	250	50000	2	10	85	***216.73***
66	15	3	28	16	750	50000	3	6	10	***362.07***
67	15	6	32	36	250	60000	1	8	85	***102.14***
68	15	9	20	25	375	70000	1.5	10	160	***90.85***
69	15	12	16	49	500	30000	2	2	235	***123.63***
70	15	15	24	9	625	40000	2.5	4	310	***452.59***
71	18	3	32	36	500	40000	2.5	6	85	***149.94***
72	18	6	16	49	625	50000	3	8	160	***241.48***
73	18	9	20	9	750	60000	1	10	235	***283.81***
74	18	12	24	16	250	70000	1.5	2	310	***365.24***
75	18	15	28	25	375	30000	2	4	10	***321.45***

Table 19 Orthogonal array (AA 2219–SS 321 material pair)

Exp. No	**Voltage (kV)**	**Coil turn**	**Coil length (mm)**	**Coil c/s area (mm^2)**	**Capacitance (µF)**	**Frequency (rad/s)**	**Air gap (mm)**	**Inductance (nH)**	**Resistance (µohm)**	**Velocity (m/s)**
1	8	9	48	36	295	60000	1.5	6	85	***102.06***
2	14	15	32	49	160	60000	1.5	2	160	***119.45***
3	17	6	24	16	430	50000	2.5	6	85	***279.46***
4	8	6	48	49	565	60000	2.5	4	10	***97.93***
5	5	3	16	9	160	30000	1	2	10	***65.36***
6	14	3	40	16	700	50000	3	6	10	***305.11***
7	8	15	24	25	160	70000	2	8	85	***164.69***
8	17	3	48	36	430	40000	2.5	6	85	***105.18***
9	11	9	16	16	160	60000	2.5	8	235	***75.15***
10	8	12	40	25	160	40000	2.5	4	310	***134.61***
11	14	12	24	16	295	30000	2	4	235	***209.69***

12	14	9	16	25	430	70000	3	6	10	***239.06***
13	8	12	16	36	295	50000	3	10	160	***112.42***
14	14	3	40	49	160	50000	2	6	10	***55.17***
15	17	6	16	49	295	40000	2	2	85	***96.34***
16	11	9	40	49	700	30000	3	8	85	***165.25***
17	8	6	32	36	700	30000	1.5	6	235	***49.2***
18	5	6	24	16	295	40000	1.5	4	85	***79.66***
19	5	6	24	25	700	60000	3	2	310	***37.51***
20	11	6	40	9	430	70000	3	4	235	***491.25***
21	17	15	48	25	565	30000	1	6	235	***208.89***
22	14	6	40	36	565	50000	1	8	310	***82.22***
23	8	12	48	9	295	50000	2.5	10	10	***442.97***
24	5	3	16	36	160	30000	1	4	85	***17.51***
25	14	9	24	36	565	30000	2.5	2	160	***160.24***
26	17	12	32	36	700	70000	2.5	8	10	***394.49***
27	14	6	48	25	160	60000	1	8	85	***95.01***
28	17	3	40	16	430	60000	3	4	160	***269.07***
29	5	15	16	49	430	30000	2.5	10	310	***48.15***
30	14	12	16	49	430	30000	2	2	235	***124.12***
31	8	15	16	16	700	50000	1	2	10	***331.29***
32	5	12	40	16	565	70000	1.5	2	85	***301.96***
33	17	12	48	9	160	30000	3	2	10	***741.5***
34	11	6	40	25	295	30000	1.5	10	10	***97.57***
35	11	12	16	25	700	40000	1.5	8	10	***139.72***
36	14	6	16	9	700	70000	1.5	4	235	***266.29***
37	14	3	48	9	700	40000	2.5	10	85	***305.63***
38	14	15	32	9	565	40000	2.5	4	310	***611.23***
39	14	15	48	16	295	40000	3	8	310	***444.44***
40	14	9	24	36	295	70000	1.5	10	160	***122.27***
41	11	3	48	36	430	70000	2	2	310	***271.58***
42	11	3	32	25	295	50000	2.5	2	235	***63.92***
43	17	12	32	16	160	70000	1.5	2	310	***292.82***
44	17	15	40	36	700	60000	2	10	235	***349.65***

45	11	6	48	16	160	70000	1	10	160	***104.28***
46	8	6	32	9	430	30000	2	8	160	***175.89***
47	14	12	32	25	430	60000	1	10	85	***172.31***
48	17	9	24	9	160	50000	1.5	10	310	***213.86***
49	11	3	32	49	295	60000	2.5	2	160	***34.19***
50	5	9	32	25	430	50000	2	6	160	***104.63***
51	11	15	24	36	160	50000	2	10	85	***130.25***
52	17	9	32	49	295	70000	1	4	310	***96.59***
53	5	12	40	36	565	60000	2.5	8	235	***102.45***
54	8	15	16	16	430	60000	3	2	85	***433.25***
55	11	15	24	36	430	40000	1.5	4	10	***172.08***
56	8	9	40	49	160	40000	2	8	310	***35.27***
57	11	9	48	16	565	30000	1	6	310	***97.6***
58	17	6	16	49	565	50000	3	8	160	***124.65***
59	17	3	16	25	565	40000	1.5	8	160	***70.05***
60	17	15	40	25	295	30000	2	4	10	***337.73***
61	5	15	48	49	700	70000	3	10	160	***90.43***
62	8	9	40	9	430	40000	1	2	235	***192.31***
63	5	9	48	25	700	50000	2	4	160	***146.89***
64	5	6	32	36	160	40000	3	6	235	***37.42***
65	17	9	24	9	700	60000	1	10	235	***267.73***
66	5	15	40	9	295	70000	2.5	6	160	***424.28***
67	8	3	24	25	565	70000	1	4	160	***32.71***
68	11	15	32	9	565	50000	3	4	85	***600.3***
69	5	9	32	16	565	40000	2	10	10	***156.89***
70	5	3	24	9	295	60000	1	8	10	***61.13***
71	11	12	24	49	700	40000	1	6	160	***87.37***
72	11	12	16	9	565	60000	2	6	310	***333.51***
73	8	3	24	49	565	70000	3	10	235	***47.24***
74	8	3	32	16	700	30000	1.5	6	310	***43.98***
75	8	9	48	36	295	60000	1.5	6	85	***102.06***

3.6.2 Regression analysis

Regression analysis is a statistical computational tool that predicts continuous output variables from a number of independent input variables, by approximating their complex inner relationship. For a given number of samples where each one is characterised by certain input and output variables, regression analysis aims to approximate their functional relationship. The estimated functional relationship can then be used to predict the level of output variable for newer samples. In general regression analysis comes out to be useful under two circumstances [125]:

a) When there is limited knowledge of the underlying mechanism of the system. In this case, regression analysis can accurately predict the output variables from the relevant input variables without requiring details of the however complicated inner mechanism.
b) When the detailed simulation model relating input variables to output variables, usually via some other intermediate variables, is known, yet is too complex and expensive to be evaluated comprehensively in feasible computational time. In this case, regression analysis is capable of approximating the overall system behaviour with much simpler functions while preserving a desired level of accuracy, and can then be more cheaply evaluated.

Literature [125] suggest the existence of a large number of regression analysis methodologies including: linear regression, support vector regression (SVR), kriging, radial basis function (RBF), multiple regression, multivariate adaptive regression splines, multi-layer perceptron (MLP), random forest, K-nearest neighbour (KNN) and piecewise regressions.

The present study utilizes best subset selection in multiple regression as a basis for development of the model. The main objective of conducting the regression analysis is to develop an impact velocity based regression model which could predict accurate values of impact velocity that would enable the user to ascertain weldability of the pulse welded members. The development of the models for the selected material combinations is discussed in the next subsection.

3.6.2.1 Model development for impact velocity

Multiple regression is a technique that allows additional factors to enter the analysis separately so that the effect of each can be estimated and is quite valuable for

quantifying the impact of various simultaneous influences upon a single dependent variable. Further, because of omitted variables bias with simple regression, multiple regression is often essential even when the investigator is only interested in the effects of one of the independent variables. Subset selection refers to the task of finding a small subset of the available independent variables that does a good job of predicting the dependent variable. It recognizes the best possible grouping of model terms among the total possible number of terms. In this method total numbers of terms are defined at the beginning together with the subset size. The process begins with no term and then the iterations go on until the term producing the largest R^2 value i.e. the coefficient of determination is identified. R^2 is probably the most popular statistical measure of how well the regression model fits the data. Coefficient of determination (R^2) is defined as the proportion of the variability in the data explained by the model. R^2 can be defined either as a ratio or a percentage and its values range from zero to one. A value of R^2 near zero indicates no linear relationship between the dependent and independent variables, while a value near one indicates a perfect linear fit. R^2 is defined as follows [126]:

$$R^2 = \frac{SQ_{model}}{SQ_{Total}} \tag{15}$$

where SQ_{model} is sum of squares of predicated values of the model and SQ_{Total} is sum square of actual process outcome.

The process then continues by addition of terms one by one and with each addition of a new term the covariates are activated one at a time and a check for increase in R^2 is conducted. If an increase in the value of R^2 is observed the switching continues with the left over covariates. When the R^2 value shows very little improvement another term is added and switching process continues once again. The designed algorithm stops once the predefined subset size is reached and its switching is completed and the user obtains the best subset of defined size. This method is termed as Forward selection with switching and the algorithm is represented in Fig. 55. The algorithm is started by defining the total covariates in the full model and an index c initialised to zero. The index c represents the number of model covariates which are to be identified with the subset selection method. The algorithm used in the study helps identify the best combination of covariates (c) to represent the model.

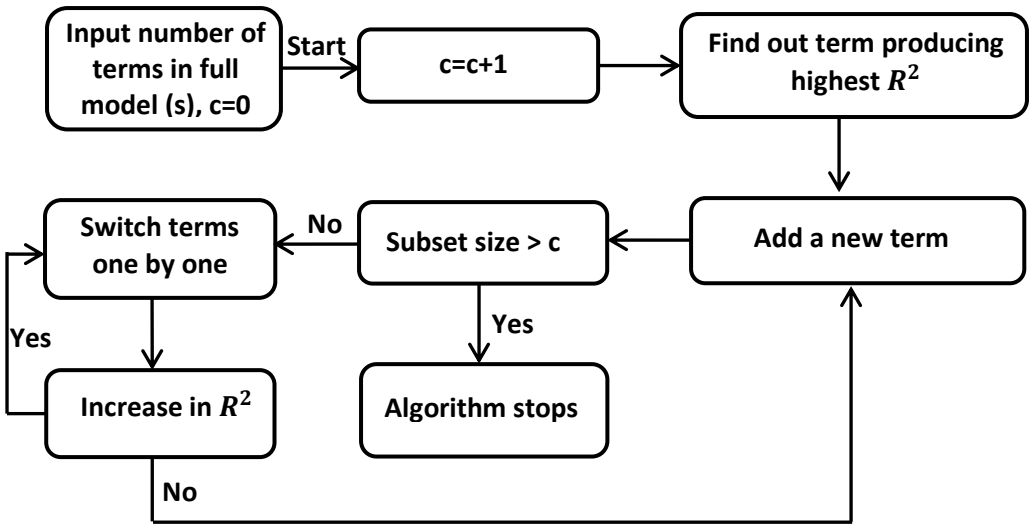

Fig. 55 Algorithm for regression modelling (forward selection with switching)

Based on the algorithm described above, regression analysis was carried out for the two different material pairs selected for the present investigation. The ranges of the independent input variables and dependent output variables for the two material pairs have been listed in Tables 18 and 19. The data for the analysis consisted of total of nine input variables and a single dependent output variable. The output variable for the present study was the weld validation criteria i.e. impact velocity. NCSS software was used to conduct the regression analysis. Two-way regression models consisting of all individual variables, two-way interactions, and squares of numeric variables were developed. In general researchers neglect the constant term or intercept in their models, however the models developed in this study included the constant term or the intercept as it is known that deleting the intercept distorts most of the diagnostic statistics including R^2. Non-hierarchical forward selection with switching with best subset selection algorithm was used to develop the models as explained earlier. The developed models and obtained results for the two material pairs are discussed below.

a) AA 2219-SS 321material pair

The orthogonal array developed in the previous section (Table 18) states the range of the dependent and independent variables for developing the regression model. The data was divided into two sets viz. model run data and validation data and three different datasets were generated and are shown in Table 20.

Table 20 Models and dataset for analysis

Model type	Model run data	Validation data
1	50	25
2	60	15
3	65	10

The model run data and validation data were selected randomly for all the three model types. Five sets of sub models each for the type 2 and 3 models were generated by randomizing the original data (Table 21). Sometimes the model developed by regression analysis becomes too much dependent on the DOE. Hence, in order to develop a robust model, randomly selected runs are taken such that the total data set contains sufficient runs to model the process behaviour accurately.

The analysis is started by defining the total terms in the full model, in this case this being 25. The iterations then continue as per the flowchart shown in Fig. 55. Once the subset size exceeds the predefined index c the iterations stop and the best subset model is saved. The R^2 value and the number of terms for the subset model are noted down. A significance level (alpha) value of 0.05 is used in conducting the hypothesis tests. An assumptions alpha value of 0.2 i.e. the significance level that must be achieved to reject a preliminary test of an assumption was used together with a confidence level of 95 %. The interpretation of confidence level is that if confidence intervals are constructed across many experiments at the same confidence level, the percentage of such intervals that surround the true value of the parameter is equal to the confidence level. Table 21 lists the R^2 values for all the developed models for AA 2219-SS 321material pair. It also lists the no of terms obtained for the best subset model.

Table 21 Coefficient of determination (R^2) and number of terms for developed models (AA 2219- SS 321 material pair)

Model type	Coefficient of determination (R^2)	No of terms
1	0.90	18
2	Random 1 = 0.94	11
	Random 2 = 0.81	5
	Random 3 = 0.60	16
	Random 4 = 0.94	10

	Random 5 = 0.90	12
3	Random 1 = 0.98	19
	Random 2 = 0.96	13
	Random 3 = 0.68	4
	Random 4 = 0.88	14
	Random 5 = 0.90	12

b) Al-SS 304 material pair

The same algorithm depicted in Fig. 55 and described previously is being used for the Al-SS 304 material pair also. For this material pair also three model types (listed in Table 21) were developed and analyzed. The R^2 values and the corresponding no of terms obtained for the best subset model for all the regression runs for AA 2219-SS 321material pair is listed in Table 22.

Table 22 Coefficient of determination (R^2) and number of terms for developed models (Al-SS 304 material pair)

Model type	Coefficient of determination (R^2)	No of terms
1	0.96	20
2	0.89	13
3	0.90	15

In general a model should contain the least possible number of covariates/terms as long as it can fit in the input data and accurately predict the new data. The models with higher number of covariates are subject to over-fit and may give poor predictions. From the developed models it is observed that maximum R^2 values of 0.98 and 0.96 were obtained for the two material combinations chosen for the study. In the present models the best R^2 values were obtained for a total number of 19 and 20 terms which indicate that the data was over-fitted. This limits the applicability of the developed models in shop floor applications. One more way the present algorithm was limited was that it required the user to make an assumption of the number of terms initially. The maximum absolute and percentage errors in impact velocity predicted by the models were then calculated in the next step. It was found that none of the models could predict data where error was in the ± 10% variation range. The absolute maximum percentage errors in prediction of impact velocity by the different models

are listed in Table 23. This fact also made the models developed by regression inadequate and inapplicable for use in real world applications. All these limitations of statistical modelling i.e. regression analysis faced by the user in the present investigation led to the use of ANN which is one of the modern day tools used for modelling of nonlinear features. The development of the ANN, its architecture, its validation along with sensitivity analysis and a case study based on the developed ANN is presented and discussed in the next subsection.

Table 23 Maximum absolute percentage errors in prediction of impact velocity by the different models

	Model type		**Absolute maximum percentage error (%)**
AA 2219-SS 321material pair	1		35.71
	2	Random 1	22.18
		Random 2	33.14
		Random 3	59.35
		Random 4	17.87
		Random 5	36.42
	3	Random 1	13.45
		Random 2	25.59
		Random 3	71.43
		Random 4	45.67
		Random 5	34.86
	Model type		**Maximum percentage error (%)**
Al-SS 304 material pair	1		51.37
	2		26.88
	3		35.76

3.6.3 Artificial Neural Network

In the recent years there has been a surge in numerical simulation based studies in which ANN has gained immense popularity as a tool capable of modelling the input–output relationships of complicated systems. It has found widespread recognition across various disciplines for modelling complex real world problems. ANN represents a type of computing that is based on the way that the brain performs computations. Neural networks are good at fitting non-linear functions and recognizing patterns.

Consequently, they are used in the aerospace, automotive, banking, defence, electronics, entertainment, financial, insurance, manufacturing, oil and gas, robotics, telecommunications, and transportation industries. ANN's have been also utilised in various manufacturing fields like casting [127], machining [128], surfacing [129], hot rolling [130], micro machining [131] etc. The use of ANN in the field of welding is also prevalent and has been used to investigate different issues related to welding like diffusible hydrogen content and cracking susceptibility [132], prediction of weld quality [133], modelling for automotive welding process [134] etc. ANN is a mathematical model or computational model imitating the structure and function of biological neural networks. The basic unit is artificial neuron. Each input of the neuron is connected to one or several outputs of other similar neurons, thus forming a network. Modern neural network is a non-linear statistical data modeling tool to reflect the relationship between inputs and outputs, or to explore the data pattern [135, 136], forecasting, mapping, optimisation, control, etc. ANN consists of a set of interconnected neurons (nodes) that can evaluate outputs from inputs by feeding information through the network and adjusting the weights. In each neuron, the sum of input values are weighted and added with a parameter called bias, and the sum is passed through a function which is called transfer function or activation function. The transfer function calculates the output of a neuron from its input. Some ANN includes several layers. Each layer includes several neurons and performs a simple process on data. The first layer is connected to the process inputs and hence known as input layer while the terminating layer generates the required output and is termed as the output layer. All the intermediate layers are called hidden layers. The input signal propagates forward from input layer to the output layer passing through hidden layers. There are several different types of ANN's namely, MLP, radial basis function network (RBF), adaptive linear network (ADALINE), modular neural network and more [137, 138]. Compared with conventional regression analysis, it has obvious advantages:

- Fault tolerance is good. The neural network can accommodate samples with great individual differences.
- Depending on the nature of the application and the strength of the internal data patterns one can generally expect a network to train quite well. This applies to problems where the relationships may be quite dynamic or non-linear. ANNs provide an analytical alternative to conventional techniques which are often limited by strict assumptions of normality, linearity, variable independence

etc. Because an ANN can capture many kinds of relationships it allows the user to quickly and relatively easily model phenomena which otherwise may have been very difficult or impossible to explain otherwise.

- Learning performance is great. Once meeting unconventional individuals, the network can acquire new learning and store this memory.
- Reasoning performance is excellent. Network may not need to learn and make a good prediction in some cases.

The development of an ANN for any particular application is a four prong process involving the below mentioned steps [139]:

(i) Identification of the various input and input variables.
(ii) Identification of optimum network architecture including number of hidden layers and nodes in each layer.
(iii) Identification of the optimum weight distribution.
(iv) Validation of the predictability of the developed network.

Steps (i) and (ii) are pre and post processing steps respectively while steps (ii) and (iii) come under the training module of the developed network. During the initial epoch, the predictability of a particular network for training and validation data increase. One phase of correction is called an epoch. However, at higher epochs the training error starts decreasing while an increase in the validation error is observed. This particular phenomenon is termed as overtraining or memorising. Hence it is very essential that the user stops the training of the network at the start of increase in validation error thereby making the validation data set a part of the training process. Thus the complete data set divided into three parts viz. training set, cross-validation set and testing set. The training and validation sets are used for model development while the testing set is used to test the model.

3.6.3.1 Network architecture

There are two categories of ANN's in terms of training approach: supervised networks and unsupervised networks [140]. The present study deals with a supervised network where the inputs and the outputs (targets) that are being used for training are known. The weights and biases are then being adjusted to compare the resulting outputs versus the desired outputs (targets). The developed orthogonal array and the numerically computed impact velocities in the previous subsection are fed as input to a multilayer modular neural network in this investigation. Modular feedforward

networks are a special class of MLPs. The modular neural network is a combination of many parallel neural networks. These networks process their input using several parallel MLPs, and then recombine the results. This tends to create some structure within the topology, which will foster specialization of function in each sub-module. In contrast to the MLP, modular networks do not have full interconnectivity between their layers. Therefore, a smaller number of weights are required for the same size network (i.e. the same number of processing elements). This tends to speed up training times and reduce the number of required training exemplars.

The present study deals with the development of predictive models for weld validation criteria i.e. impact velocity for two different material combinations with different geometries. In this study, the developed ANN for both the materia combinations, the input dataset is divided into 3 sets randomly: training data, validation data, and test data. 70% of data set is regarded as train data , 15% of dataset is regarded as validation, and 15% of data is regarded for test data. This selection has been randomly made in order to make the model robust. The training data set is used to adjust the weights on the neural network. The validation set is used to minimize possible overfitting by verifying that any increase in accuracy over the training data set yields an increase in accuracy over a data set that has not been introduced to the network yet. Finally, the testing set is used only for testing the final solution in order to confirm the actual predictive performance of the network. The test dataset shows how good the ANN is trained [140]. The trained network is then saved and used to predict the impact velocity for the pulse welded Al-SS 304 tubular members.

Multilayer modular networks with sigmoid axon transfer function for each of the layers were used in the present study to predict the impact velocity. The transfer is given by the equation [141]:

$$f(net_j) = o_j = \frac{1}{1+e^{-net_j}} \tag{16}$$

where o_j is the output of the *j*th neuron and net_j is the linear activation of the neuron and is obtained by the relation [141]:

$$net_j = \sum_{i=1}^{x} w_{ij} o_i \tag{17}$$

where x is the number of input connections, w_{ij} is a component of the weight vector, and o_i is the input activation of the *i*th neuron in the preceding layer.

The selected learning algorithm is LM. The LM algorithm is one of the most appropriate higher-order adaptive algorithms known for minimizing the mean squared error (MSE) of a neural network. It is a member of a class of learning algorithms called "pseudo second order methods". Levenberg–Marquardt algorithm is a combination of the steepest gradient descent method and the Gauss–Newton method, aimed at rapidly increasing the fitting accuracy at the beginning and reaching the target as soon as possible when the fitting error is close to the minimum point [142]. Standard gradient descent algorithms use only the local approximation of the slope of the performance surface (error versus weights) to determine the best direction to move the weights in order to lower the error. Second order methods use the Hessian or the matrix of second derivatives (the curvature instead of just the slope) of the performance surface to determine the weight update, while pseudo-second order methods approximate the Hessian. In particular the LM utilizes the so called Gauss-Newton approximation that keeps the Jacobian matrix and discards second order derivatives of the error. The Jacobian matrix and the weight update relations for LM algorithm is given as [142]:

- Jacobian matrix in the input layer

$$J_{i-h} = \begin{pmatrix} \frac{\partial(t_v - y)}{\partial w_{11}} & \cdots & \frac{\partial(t_v - y)}{\partial w_{nk}} \\ \vdots & \ddots & \vdots \\ \frac{\partial(t_v - y)}{\partial w_{1k}} & \cdots & \frac{\partial(t_v - y)}{\partial w_{nk}} \end{pmatrix} \tag{18}$$

- Jacobian matrix in the output layer

$$J_{i-h} = \begin{pmatrix} \frac{\partial(t_v - y)}{\partial w_{11}} & \cdots & \frac{\partial(t_v - y)}{\partial w_{nk}} \\ \vdots & \ddots & \vdots \\ \frac{\partial(t_v - y)}{\partial w_{1k}} & \cdots & \frac{\partial(t_v - y)}{\partial w_{nk}} \end{pmatrix} \tag{19}$$

- The updating process of the weights is given as [142]:

$$V \to V - \frac{1}{(J_{h-o}^T J_{h-o} + uI)} J_{h-o}^T (t_v - y) \tag{20}$$

$$W \to W - \frac{1}{(J_{i-h}^T J_{i-h} + uI)} J_{i-h}^T (t_v - y) \tag{21}$$

where u is a positive number and I is a unit matrix. The value of u determines the speed of training. t_v, y are the target value and the value predicted by the neural network. W is weights passed from input layer to hidden layer and V is weights passed from hidden layer to output layer and are given as [142]:

$$V = \begin{pmatrix} v_{11} & \cdots & v_{1q} \\ \vdots & \ddots & \vdots \\ v_{k1} & \cdots & v_{kq} \end{pmatrix} \quad (22)$$

$$W = \begin{pmatrix} w_{11} & \cdots & w_{1k} \\ \vdots & \ddots & \vdots \\ w_{p1} & \cdots & w_{pk} \end{pmatrix} \quad (23)$$

where p, k, q number of cells in the input, hidden and output layer.

In nonlinear systems like neural networks, the big issue is that the performance surface may be non-convex, and so quadratic approximations may require several steps for convergence, or more importantly they may diverge. A key advantage of the LM approach is that it defaults to the gradient search when the local curvature of the performance surface deviates from a parabola, which may happen often in neural computing. In this network, during learning process, maximum number of iterations/epochs is 10000; maximum number of fail in cross validation check is 100, and the performance of network is MSE. The value of MSE is calculated from Eq. (24) [143]:

$$MSE = \frac{\sum_{i=1}^{n_1}(t_i - a_i)^2}{n} \quad (24)$$

where n_1 is the number of data, t_i denotes *i*th target value and a_i is the predicted value

In many cases, ANN is not able to predict the output value precisely. In order to select the best architecture of ANN, different structures were used to obtain the optimal neural network which can predict data correctly and these different structures were made by permutation. The proposed network was reached upon after a number of iterations with different network topologies were tried. This optimum architecture was selected based on the smallest cross validation MSE between predicted values (outputs of ANN) and input dataset (impact velocity) obtained from the FEM. Cross validation is a highly recommended criterion for stopping the training of a network. Cross validation computes the error in a validation set at the same time that the network is being trained with the training set. It is known that the MSE will keep decreasing in the training set, but may start to increase in the validation set. This happens when the network starts "memorizing" the training patterns. The algorithm used in this study monitors the cross validation set error and automatically stop the network when it is not improving .The selected architecture was then run for many times with different randomly initialised weights and the best network weights were identified. The

proposed algorithm to find the optimal neural network is illustrated in Fig. 56. The algorithm begins with selection of a structure for the model and then the dataset is input. The network then calculates the cross validation MSE and checks if it below a predefined value. If the network finds that the value is less than the minimum value it outputs the training results. If any other dataset is not available the algorithm stops and the network (optimum) is saved. If the network after calculating cross validation MSE finds that the value is higher than the minimum it reiterates the entire process and trains the algorithms and updates the network weights until the cross MSE comes below the minimum. The neural network parameters reached upon for the optimum architecture for the selected material pairs are listed in Table 24 and 25. The network topologies are also shown in Figs. 57 and 58. The obtained network for the Al-SS 304 material pair is a 3 hidden layer modular feedforward network while for the AA2 2219-SS 321 material pair the optimum network obtained is a 5 hidden layer modular feedforward network.

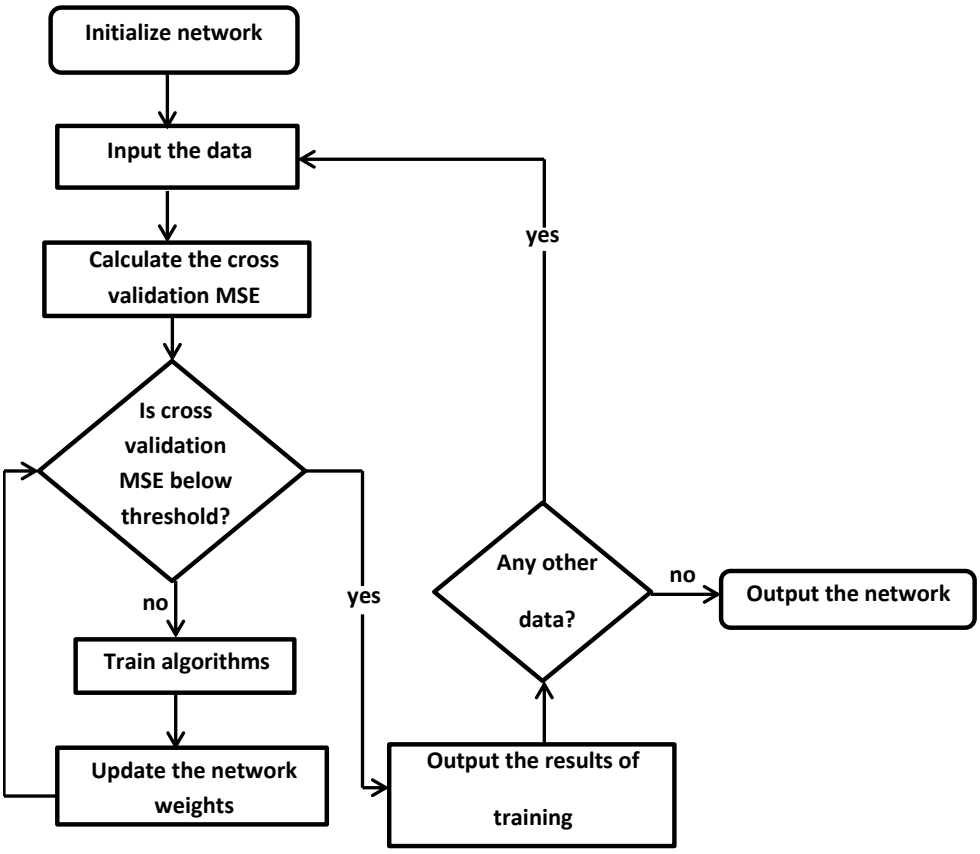

Fig. 56 Proposed algorithm to find the optimal neural network

Table 24 Neural network parameters for Al-SS 304 material pair

Type of network	Multilayer Modular Network		
Number of hidden layers	3		
Processing Elements	**Hidden layer**	**Upper processing elements**	**Lower processing elements**
	1	8	6
	2	6	4
	3	4	4
Transfer function used	Sigmoid Axon		
Learning algorithm	Levenberg–Marquardt (LM)		
Processing software used	Matlab		
Limit of nodes	Lower = 1, Upper = 10		
Data classification	Training data (%)	Validation data (%)	Test data (%)
	70	15	15

Table 25 Neural network parameters for AA 2219-SS 321 material pair

Type of network	Multilayer Modular Network		
Number of hidden layers	4		
Processing Elements	**Hidden layer**	**Upper processing elements**	**Lower processing elements**
	1	12	6
	2	8	5
	3	8	4
	4	6	4
Transfer function used	Sigmoid Axon		
Learning algorithm	Levenberg–Marquardt (LM)		
Processing software used	Matlab		
Limit of nodes	Lower = 1, Upper = 15		
Data classification	Training data (%)	Validation data (%)	Test data (%)
	70	15	15

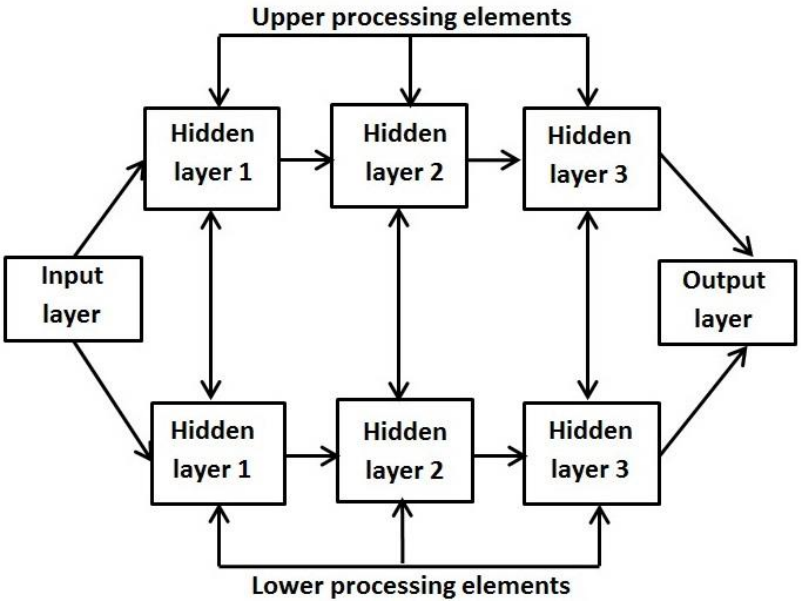

Fig. 57 Neural network topology for Al-SS 304 material pair

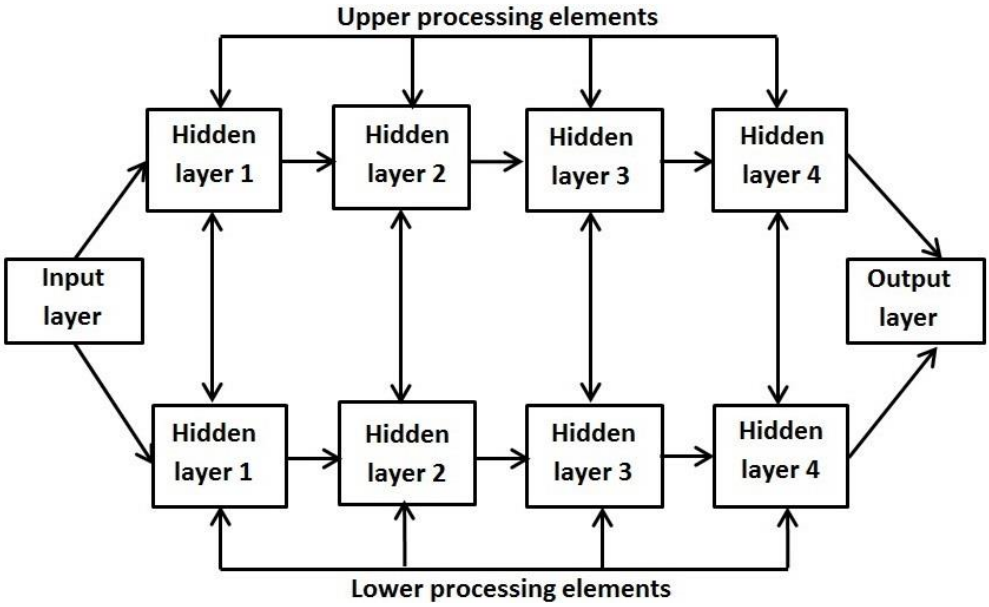

Fig. 58 Neural network topology for AA 2219-SS 321 material pair

Figs. 59 and 60 show the variation of MSE for training and cross validation data with number of iterations for the selected network topologies and material pairs. After the training error reaches a predefined value the iteration stops and the network checks for cross validation error. These variations of MSE are shown for the optimum network obtained after large number iterations were performed according to the algorithm explained previously and shown in Fig. 56. The minimum and the final

values of MSE for the optimum network architecture are listed in Table 26. The algorithm then saves the best weights based on the error of the training set and the cross validation set. The weight distributions resulted in minimum cross-validation error for the developed models and have been given in Appendix 1.

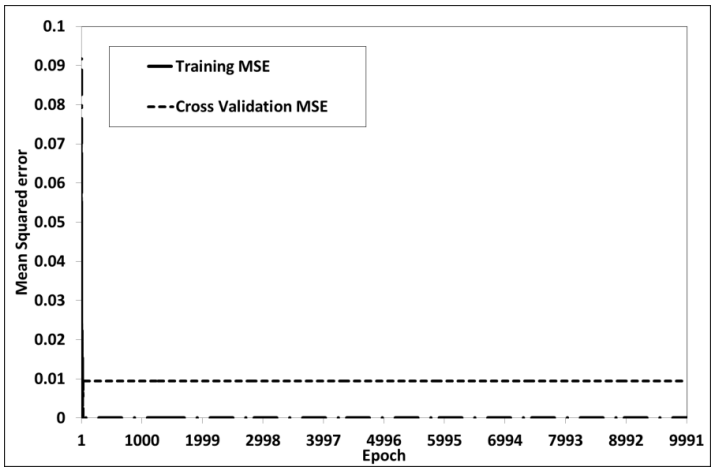

Fig. 59 Variation of MSE with number of iterations for network developed for Al–SS 304 material pair

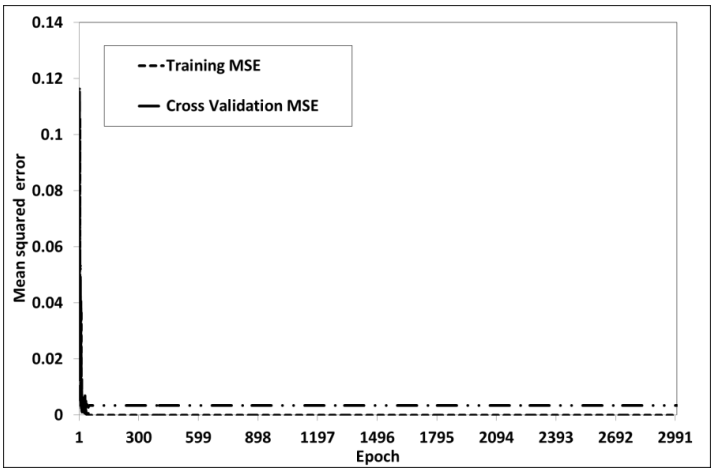

Fig. 60 Variation of MSE with number of iterations for network developed for AA 2219–SS 321 material pair

Table 26 Minimum and the final values of MSE for training and cross validation data

Material pair	MSE	Training	Cross validation
Al- SS 304	Minimum MSE	8.15478E-28	0.001040656
	Final MSE	8.15478E-28	0.009410198
AA 2219- SS 321	Minimum MSE	5.77552E-31	0.002716758
	Final MSE	5.77552E-31	0.003433675

3.6.3.2 Network validation

After the network is trained and cross validated, testing is done with data predefined as testing data. The network computed impact velocities are compared with velocities calculated by the FEM in order to confirm the developed model (Tables 27 and 28). The absolute and percentage errors between the impact velocities calculated numerically by the FEM and the neural network is then computed and plotted in Figs. 61 and 62.

Figs. 61 and 62 show correlation between impact velocity values predicted by the FEM and the ANN for the considered dataset for selected material pairs. It can be observed that most of the data are on the bisector or in its vicinity which presents a proper correlation between FEM data and outputs predicted the ANN. It is evident that predicted impact velocities by the ANN are in good agreement with the velocities predicted by the FEM. The percentage error for the network developed for Al-SS 304 material pair lies within ± 10% range with a maximum absolute error of 17.26. Almost similar results were obtained when testing was conducted on the network developed for AA 2219-SS 321material pair. The percentage error in this case was also within the ± 10% range with a maximum absolute error of 32.32.

Table 27 Comparison of predicted velocity by ANN with simulated velocities (Al-SS 304 material pair)

Test No	Voltage (kV)	Coil turn	Coil length (mm)	Coil c/s area (mm^2)	Capacitance (μF)	Frequency (rad/s)	Air gap (mm)	Inductance (nH)	Resistance (μohm)	Velocity (m/s)	Predicted Velocity(m/s)	Absolute error	Percentage error (%)
1	6	3	16	36	250	30000	1	4	85	33.72	34.06	0.34	1.00
2	6	6	20	25	750	60000	3	2	310	137.85	131.20	6.65	5.07
3	6	9	24	16	625	40000	2	10	10	189.36	197.95	8.59	4.34
4	6	12	32	49	500	50000	1.5	8	235	82.86	76.42	6.44	8.42
5	6	15	28	9	375	70000	2.5	6	160	387.57	375.97	11.60	3.09
6	9	3	20	49	625	70000	3	10	235	68.25	62.54	5.71	9.13
7	9	6	24	9	500	30000	2	8	160	174.91	168.64	6.27	3.72
8	9	9	32	36	375	60000	1.5	6	85	126.85	116.73	10.12	8.67

9	9	12	28	25	250	40000	2.5	4	310	190.74	174.72	16.02	9.17
10	9	15	16	16	750	50000	1	2	10	237.28	220.02	17.26	7.85
11	12	3	24	25	375	50000	2.5	2	235	125.64	114.10	11.54	10.11

Table 28 Comparison of predicted velocity by ANN with simulated velocities (AA 2219-SS 321material pair)

Test No	Voltage (kV)	Coil turn	Coil length (mm)	Coil c/s area (mm^2)	Capacitance (μF)	Frequency (rad/s)	Air gap (mm)	Inductance (nH)	Resistance (µohm)	Velocity (m/s)	Predicted Velocity(m/s)	Absolute error	Percentage error (%)
1	8	9	48	36	295	60000	1.5	6	85	102.06	96.28	5.77	6.00
2	14	15	32	49	160	60000	1.5	2	160	119.45	113.12	6.32	5.58
3	17	6	24	16	430	50000	2.5	6	85	279.46	273.09	6.36	2.33
4	8	6	48	49	565	60000	2.5	4	10	97.93	90.98	6.94	7.62
5	5	3	16	9	160	30000	1	2	10	65.36	72.58	7.22	9.95
6	14	3	40	16	700	50000	3	6	10	305.11	337.4	32.32	9.57
7	8	15	24	25	160	70000	2	8	85	164.69	174.59	9.90	5.67
8	17	3	48	36	430	40000	2.5	6	85	105.18	116.24	11.06	9.51
9	11	9	16	16	160	60000	2.5	8	235	75.15	70.03	5.11	7.30
10	8	12	40	25	160	40000	2.5	4	310	134.6	146.9	12.35	8.40

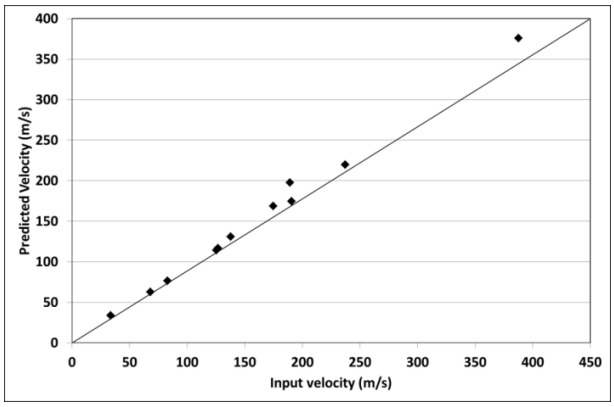

Fig. 61 Comparison of impact velocity predicted by the FEM and the ANN for testing data (Al-SS 304 material pair)

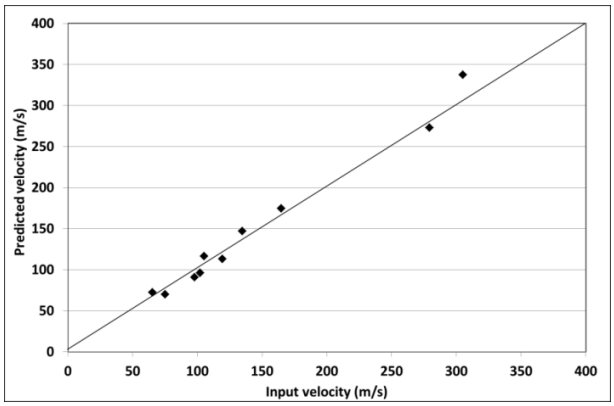

Fig. 62 Comparison of impact velocity predicted by the FEM and the ANN for testing data (AA 2219-SS 321material pair)

Figs. 63 (a) to (i) and 64 (a) to (i) show the general trend of impact velocity with process parameters. The velocity is calculated by the developed neural networks for random values of selected process parameters generated by the software, the random values being generated within the range given in Tables 16 and 17. The calculation is done with the best weights obtained during training step of the network development. The variation of the velocity with each parameter is done by generating random values of the considered parameter and keeping all the other parameters at their mid values.

Impact velocity is one of the most important criteria that decides the weldability of the MPW joint and is influenced by many parameters in some way or the other. The impact velocity is of crucial importance in the coalescence of the mating members, as it is this kinetic energy that is transformed to the energy used for bonding of the two materials. The impact velocity is directly related to the pressure that is required to move the flyer, and hence to the energy level used when conducting the weld. The voltage level of the pulse welding equipment is directly related to the energy level in the system as seen from Eq. (2). The voltage level is a crucial parameter in the forming of the weld, as it is this parameter that determines the impact velocity for a given geometry and given materials of the workpieces. If a good weld is not obtained in a chosen experimental setup and the cause is believed to be an insufficient impact velocity, then one simple way to achieve the weld is to increase the chosen voltage level. An increase in the voltage level results in an increase of the magnetic pressure on the flyer leading to a change in the deformation pattern of the same and to an increase in the impact velocity. This fact is corroborated in Figs. 63 (a) and 64 (a). The effect of coil parameters i.e. coil turns, coil length and coil c/s area on impact velocity is shown in Figs. 63 (b, c, d) and 64 (b, c, d). The intensity of magnetic field and hence

the generated magnetic pressure increases with increase in number of coil turns. The increase in coil turns also decreases the inductance of the system. These two factors in combine help in to increase the velocity of the flyer (Figs. 63 (b) and 64 (b)). The coil length has a major influence on the velocity attained by the flyer. With an increase in coil length the current amplitude i.e. peak current and the operating frequency of the current decrease. This decrease in peak current value and frequency decreases the magnetic pressure generated leading to reduced impact velocity (Figs. 63 (c) and 64 (c). Also the peak value of magnetic pressure is inversely proportional to coil length (Eq. (3)). A shorter coil results in maximum deformation and thus increased velocity of the flyer as seen in (Figs. 63 (c) and 64 (c)).

The coil cross sectional area is proportional to the inductance and is given by the relation:

$$L = \frac{\mu_0 N^2 A}{l_w} \tag{25}$$

where A is the cross sectional area.

The increase in area of the coil increases the inductance value which decays the amplitude of the current pulse and prolongs it period. This in turn decreases the magnetic pressure and the impact velocity. This is also observed in the obtained results (Figs. 63 (d) and 64 (d)).

Figs. 63 (e) and 64 (e) show the variation of impact velocity with capacitance. In MPW the energy stored at the capacitor bank is discharged in the coil and it is this energy that accelerates and deforms the workpiece. A higher capacitance value allows discharge of higher energy (Eq. (2)) which increases the pressure generated (Eq. (3)) and hence leads to an increase in impact velocity (Figs. 63 (e) and 64 (e)). The operating frequency plays an important role in deciding the space distribution of the magnetic field, the peak value and pulse width of the magnetic pressure. In order to get high-quality welds by MPW, the primary current pulse should be of high amplitude and high frequency, namely a narrow pulse with great amplitude. Higher frequencies increase this pulse width which in turn increases the time available for acceleration of the flyer workpiece. The higher the time available for acceleration higher is the velocity of the flyer as seen in Figs. 63 (f) and 64 (f). The air gap between the mating members directly affects the impact velocity. A lower gap does not allow the flyer enough time to attain high velocity. With increasing air gap the flyer gets the requisite time and space and thus attains higher velocity values Figs. 63 (g) and 64 (g). Lower

inductance values allow the capacitor to release the stored energy very quickly leading to a larger current pulse which aids in the increase of impact velocity, the same observation being seen in Figs. 63 (h) and 64 (h). On the other hand the increase of circuit resistance decreases the current peak values leading to a drop in the impact velocity as calculate by the network and shown in Figs. 63 (i) and 64 (i). All the variations are in agreement with the general trend observed in literature. This also confirms the validity of the network developed.

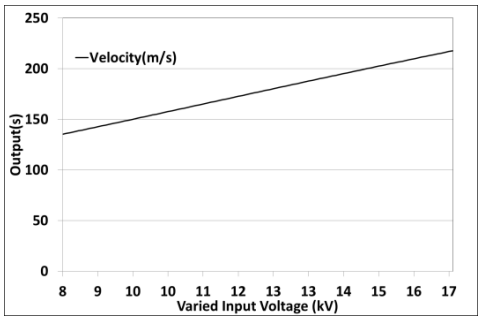

(a)

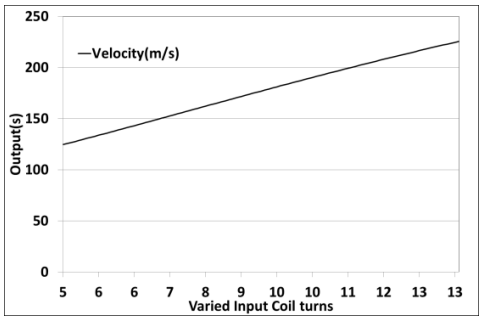

(b)

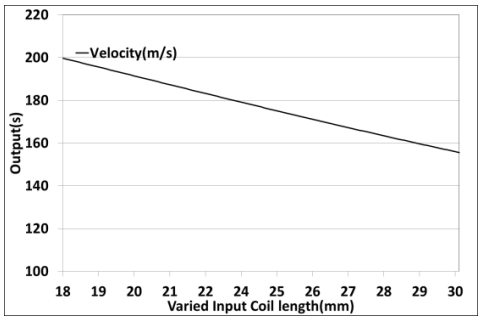

(c)

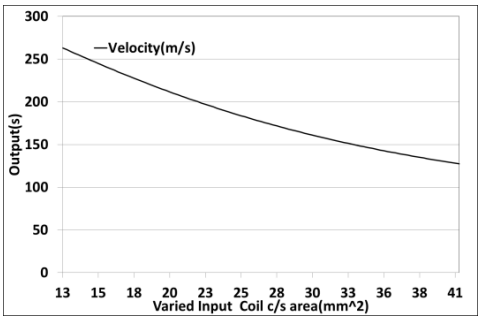

(d)

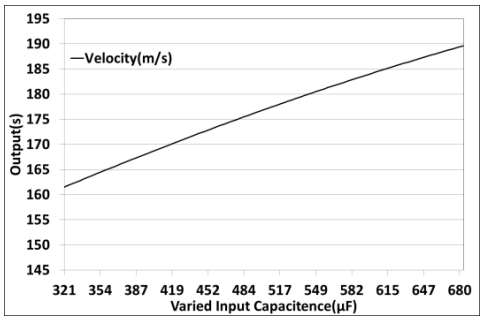

(e)

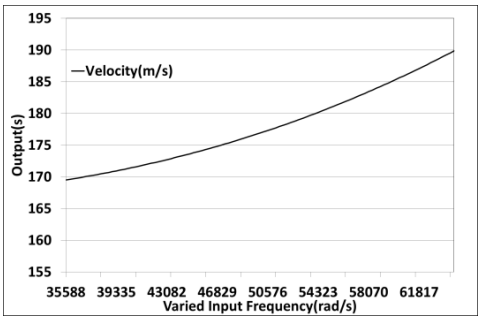

(f)

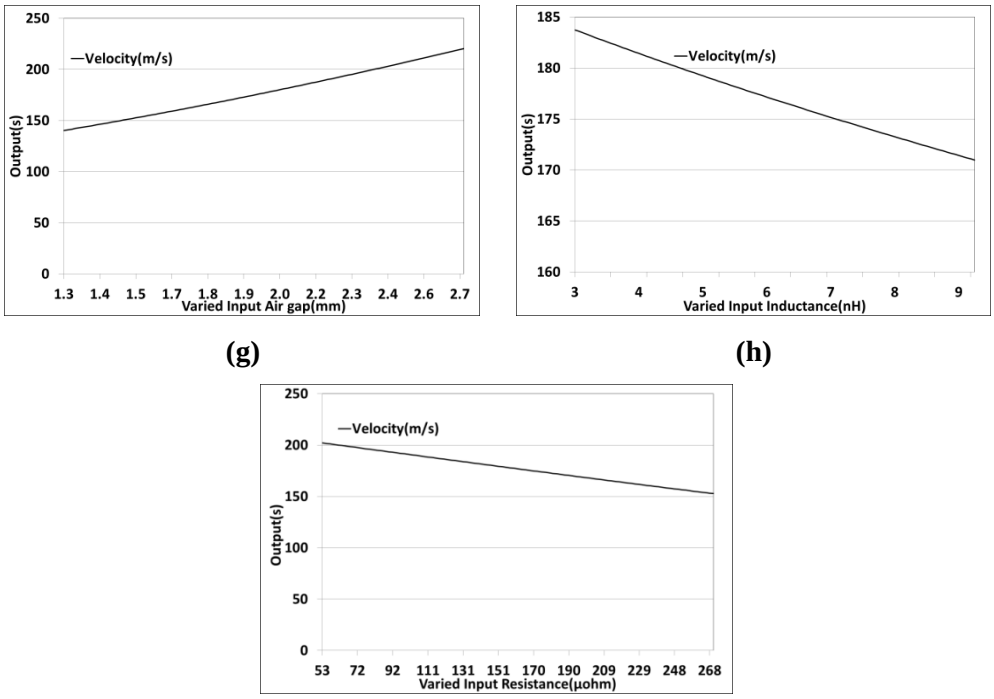

(g) **(h)**

(i)

Fig. 63 (a) to (i) General trend of velocity with process parameters predicted by the ANN (Al-SS 304 material pair)

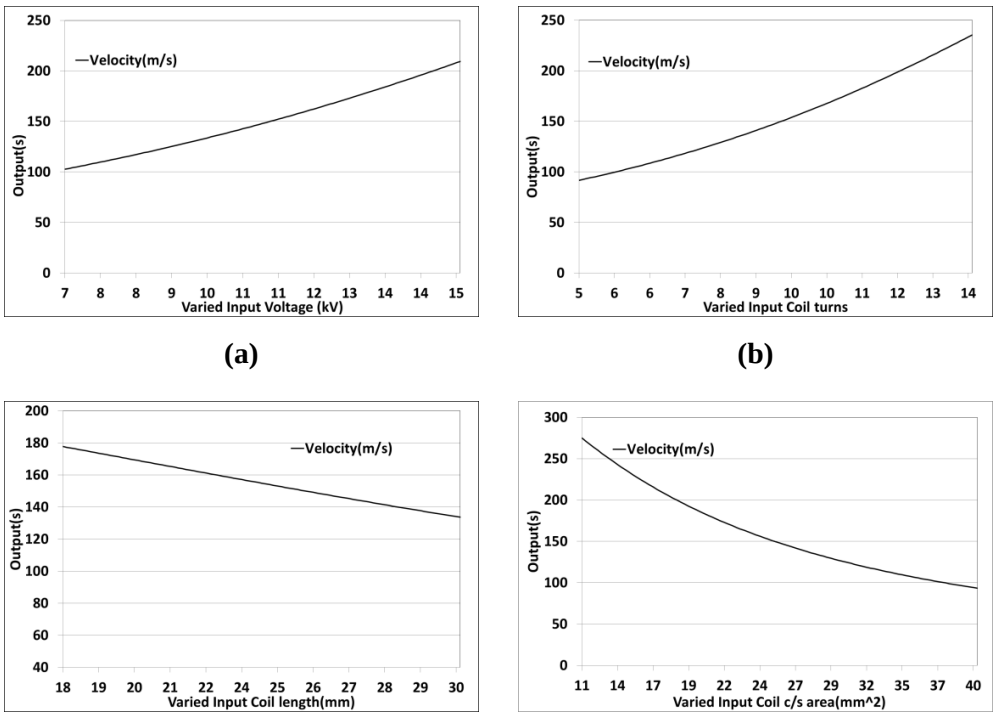

(a) **(b)**

(c) **(d)**

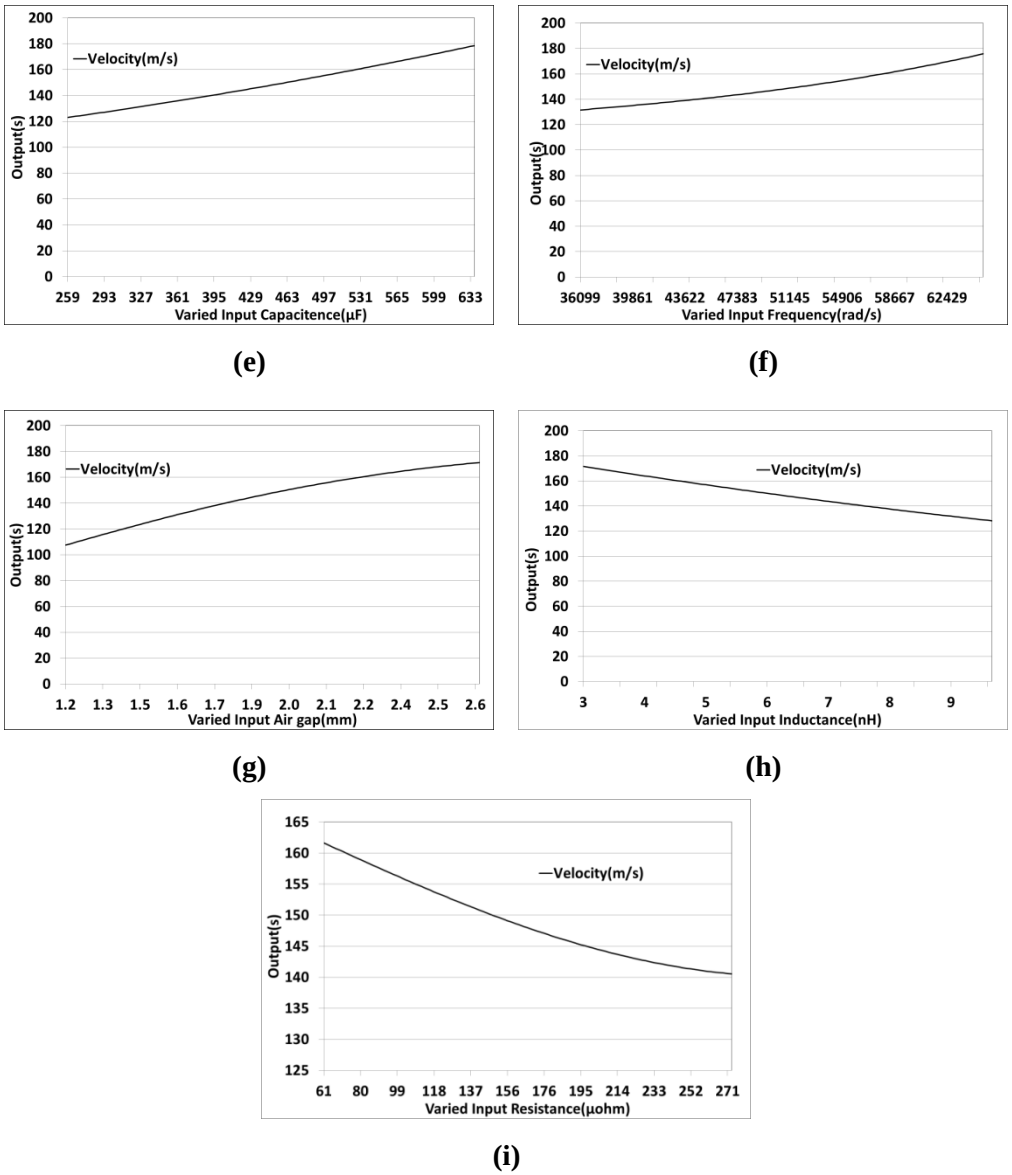

Fig. 64 (a) to (i) General trend of velocity with process parameters predicted by the ANN (AA 2219-SS 321material pair)

3.6.3.3 Sensitivity analysis

While training a network, it is very important to know the effect that each of the network inputs is having on the network output. This provides feedback as to which input channels are the most significant thereby helping the user to prune the input space by removing the insignificant channels. This will reduce the size of the network, which in turn reduces the complexity and the training times. Sensitivity analysis is a method for extracting the cause and effect relationship between the inputs and outputs of the network. The network learning is disabled during this operation such that the

network weights are not affected. The basic idea is that the inputs to the network are shifted slightly and the corresponding change in the output is reported either as a percentage or a raw difference.

The available literature and the developed models in the previous section clearly suggest that MPW is affected by a combination of process parameters. In the recent past researchers have tried to understand the effect of process parameters on the outcome of any process through graphical representation. This technique was however limited because of the fact that a single graph could show the effect of at most two parameters. Also when the parameters affect the process in interaction with other process parameters the graphical representation method does not seem feasible. In order to overcome the drawbacks of the earlier methods investigators have devised newer methods that can recognize the effect of parameters on a process output in a qualitative manner, sensitivity analysis being one of them. For given input (x) and output (y) sensitivity is defined as [144]:

$$Sensitivity = \frac{\partial y}{\partial x} \tag{26}$$

Sensitivity analysis helps express a group of parameters in terms of pattern in which each pattern represents a combination of process parameters with at least one process parameter having different value. Thus, for k^{th} pattern sensitivity due to i^{th} input is can be defined as [144]:

$$S_{i,k} = \frac{\partial y_k}{\partial x_i} \tag{27}$$

In other words sensitivity of an input is a vector of size *K*, where *K* is the total number of patterns.

Sensitivity analysis of the process parameters about the mean is also done in order to find out the parameters having major impact on the process. This testing process provides a measure of the relative importance among the inputs of the neural model and illustrates how the model output varies in response to variation of an input. The first input is varied between its mean +/- a user-defined number of standard deviations while all other inputs are fixed at their respective means. Fig. 65 shows the sensitivity of the various process parameters about the mean for the two neural networks developed for the selected material pairs i.e. Al-SS 304 and AA 2219- SS 321. It is clearly seen that in both material pairs the parameters viz. coil c/s area, coil turns, voltage and air gap affected the process in a major way. The effect of coil c/s area, coil

turns and voltage was more profound for AA 2219-SS 321material pair, while air gap affected the process more in Al-SS 304 pair. Two other parameters viz. coil length and resistance had a moderate effect on the process for Al–SS 304 pair while the same parameters had a negligible effect for AA 229- SS 321 material combination. All other parameters had a negligible effect on the MPW process. The sensitivity analysis of the MPW process reveals that the MPW process is controlled by a combination of parameters and the parameter effect is also dependent on the material combination chosen.

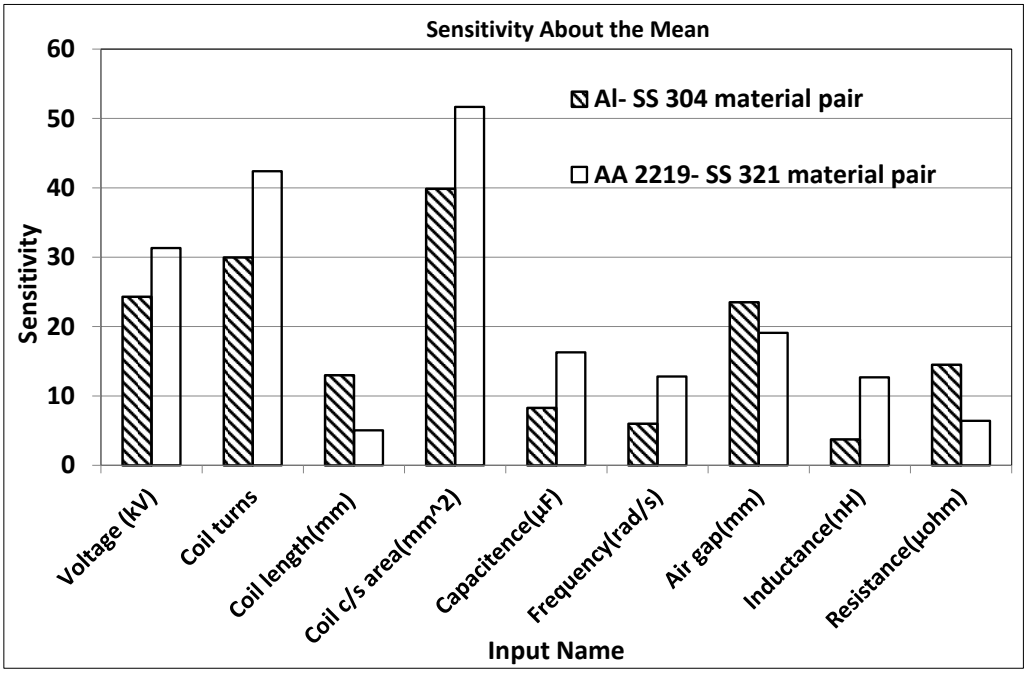

Fig. 65 Sensitivity of impact velocity with process parameters

3.6.3.4 Case study

To better understand the developed neural networks and to present its applicability in shop floor applications of MPW, the developed predictive models were used to conduct a case study where impact velocity was predicted with variation in process parameters. The input parameters considered in the developed neural networks were taken as variables in this study. The material chosen for the case study was Al-SS 304 metal pair. Random values were generated for the variable process parameters within the maximum and minimum values defined previously (Table 17) and subsequently used to calculate the respective impact velocities. The parameters were taken in the form of production data sets for the neural network developed in the preceding section (Table 24). Once the user has trained and tested a network and has determined that the

network adequately models the data, it is very necessary that new untrained data be put into that network and the network run with this new data. In this case the user only feeds the input data but no desired data. The data set to use for this case is the production data set. The parameter values for the case study are listed in Table 29. The case study for the selected material pair is discussed hereafter.

Table 29 Parameters for the case study

Parameter	**Value**
Voltage	Random values between 6 kV and 18 kV
Coil turns	Random values between 3 and 15
Coil length	Random values between 16 mm and 32 mm
Coil c/s area	Random values between 9 mm^2 and 49 mm^2
Air gap	Random values between 1 mm and 3 mm
Capacitance	Random values between 250 μF and 750 μF
Frequency	Random values between 30000 rad/s to 70000 rad/s
Inductance	Random values between 2 nH and 10nH
Resistance	Random values between 10 μohm and 310 μohm

For the considered case study a production data set of 2000 values (generated randomly) for each parameter was fed into the neural network and the corresponding impact velocities were calculated. From the 2000 values of impact velocities computed at different combinations of process parameters, the runs where the velocities satisfied a certain condition were sorted out. The condition for selecting the velocities is stated below:

$$1.2 * V_{threshold} < Impact\ velocity < 0.8 * V_{damage} \quad (28)$$

where, $V_{threshold}$ is the threshold impact velocity for the material combination chosen = **161.03 m/s** (Eqs. 7-10)

and V_{damage} is the velocity at which damage occurs to the impact members (observed from the FEA simulations) = **505.625 m/s**.

During the operation of MPW, the flyer tube produces high-speed diameter shrinkage deformation within a micro-second, and the air inside the tube is compressed severely, thus bringing an outward support to the outer tube in the radial direction. However in the present study, the impact of the air inside the tube was neglected during the simulation resulting in higher measured value compared with the

experimental values. This led to keeping the lower limit of the limiting condition (Eq.28) at 1.2 times the threshold calculated by the analytical relations (Eqs. 7-10). For producing a successful weld it is must that the velocity crosses the threshold and thus it became the criterion for choosing the lower limit of the condition. On the other hand for each material combination there exists a range of velocity at which the flyer and base workpieces get damaged. It is desirable that the peak velocities reached by the flyer at the time of impact must be well below the velocities inflicting damage to the flyer. This criterion led to the selection of the upper limit of the condition stated in Eq. (28). In the condition defined for the case study the upper limit is kept at 0.8 times the velocity at which damage was observed for the mating members in FEA simulation runs.

When the condition stated in Eq. (28) was applied to the 2000 production data set and the data computed by the ANN filtered, a total of 241 cases were found where the above condition was satisfied. In these 241 cases, a wide ranging combination of process parameters acted together such that impact velocity crossed the bare minimum to attain a successful weld and , at the same time the velocity at the impact did not reach a value which could damage either the flyer or the base tube.

Figs. 66 (a) to (i) show the scatter plots of velocity with variable process parameters selected in the present study. The plots show the points at which the impact velocity satisfied the criteria given in Eq. (28) at different combination of process parameters. The plots help us identify the particular values of process parameters at which the welding has certainty to occur. They also help us understand the relation between the process parameters and its relationship with the mechanism governing the same. Fig. 66 (a) shows the voltage levels at which the impact velocity satisfied the limiting condition (Eq. 28). It can be clearly seen that most of the data points are concentrated on the higher voltage level side (14 kV to 17 kV) which is in agreement with results available in literature. Analytical relations suggest that the energy varies as the square of the voltage (Eq. 28) and an increase in the voltage level increases the energy discharged by the MPW machine manifolds. This increase in energy generates higher magnetic pressure leading to high impact velocities. Figs. 66 (b-d) depict the various coil parameters at which the impact velocity condition was satisfied. Fig. 66 (b) suggests that at increased number of coil turns (12-15 in the present study) the velocity criterion is more likely to be satisfied which is in agreement with available results. The increase in coil turns increases the intensity of magnetic field and lowers

the inductance which aids in generation of higher velocities. On the other hand the velocity criterion could be satisfied only when the coil c/s area was on the lower side (around 9 mm^2 -16 mm^2) (Fig. 66 (d)). The increase in coil c/s area leads to a decay in the current pulse leading to lower peak velocities. The peak magnetic pressure has an inverse relationship with to the length of the coil employed. In the present case the moderate lengths in between 23 mm and 31 mm were found to be suitable (Fig. 66 (c)). However any further increase in length would lead to a decrease in the velocities and the velocity criterion will not be satisfied. The capacitance is another parameter influencing the MPW process and deciding the weldability of the joint. A higher capacitance value is always favourable for the success of the process as it increases the discharge energy and in turn the impact velocity. However capacitance works with a combination of lot of other parameters including coil parameters, voltage, operating frequency, inductance etc. It has been observed by researchers that a low to moderate capacitance value could produce a successful weld in many cases; on the other hand in some cases even a high capacitance value was not able to guarantee a successful weld. This particular observation was well captured by the neural network developed in this study and it is seen from Fig. 66 (e) that the velocity criterion was satisfied across the range of capacitance values selected. The operating frequency decides the depth of magnetic field penetration inside the flyer workpiece and in turn influences the magnetic pressure generated which deforms and accelerates the workpiece. The flyer workpiece selected for the present study had a thickness of 1.5 mm. The relation (Eq. 5) suggests the use of higher frequencies to obtain an ideal skin depth that would produce maximum magnetic pressure and in turn higher velocities. This fact is corroborated in Fig. 66 (f) where the data points (frequency values) satisfying the limiting velocity condition (Eq. (28)) were mostly on the higher side (50000 to 70000 rad/s). The geometric parameter i.e. air gap also influences the impact velocity. Lower gap restricts the rise of impact velocity and at higher gap the current pulse decays leading to drop in velocity at the time of impact. The results of effect of gap on velocity seem to a little erroneous in this study as suggested by Fig. 66 (g). Although the scatter plot suggests the accumulation of data points satisfying the velocity criterion (Eq. 28) at moderate gap of 1.5 mm, it also however seems to suggest the same phenomenon at highest gap of 3 mm and lowest gap of 1 mm. This observation deviates from the general results available in literature and the same anomaly would be looked into in detail in future when this model is applied on different material combinations with varying geometry. Circuit parameters resistance and inductance

also play a role in deciding the peak velocity achievable by the flyer. Lower resistance in circuit reduces the damping coefficient and in turn higher current values are achieved. Thus decrease in resistance helps increase the impact velocity, the same being suggested in Fig. 66 (i) where the velocity criterion was satisfied by more data points at lower resistances (around 10 ohm to 120 ohm). Similar trend was also observed in case of the other circuit parameter i.e. inductance. Lower inductance values help increase the operating frequencies and also allow quick release of energy. This two factors in combine help the flyer cross the threshold required for the weld success. Higher accumulation of data points for inductance values of 2 nH to 5 nH was observed Fig. 66 (h).

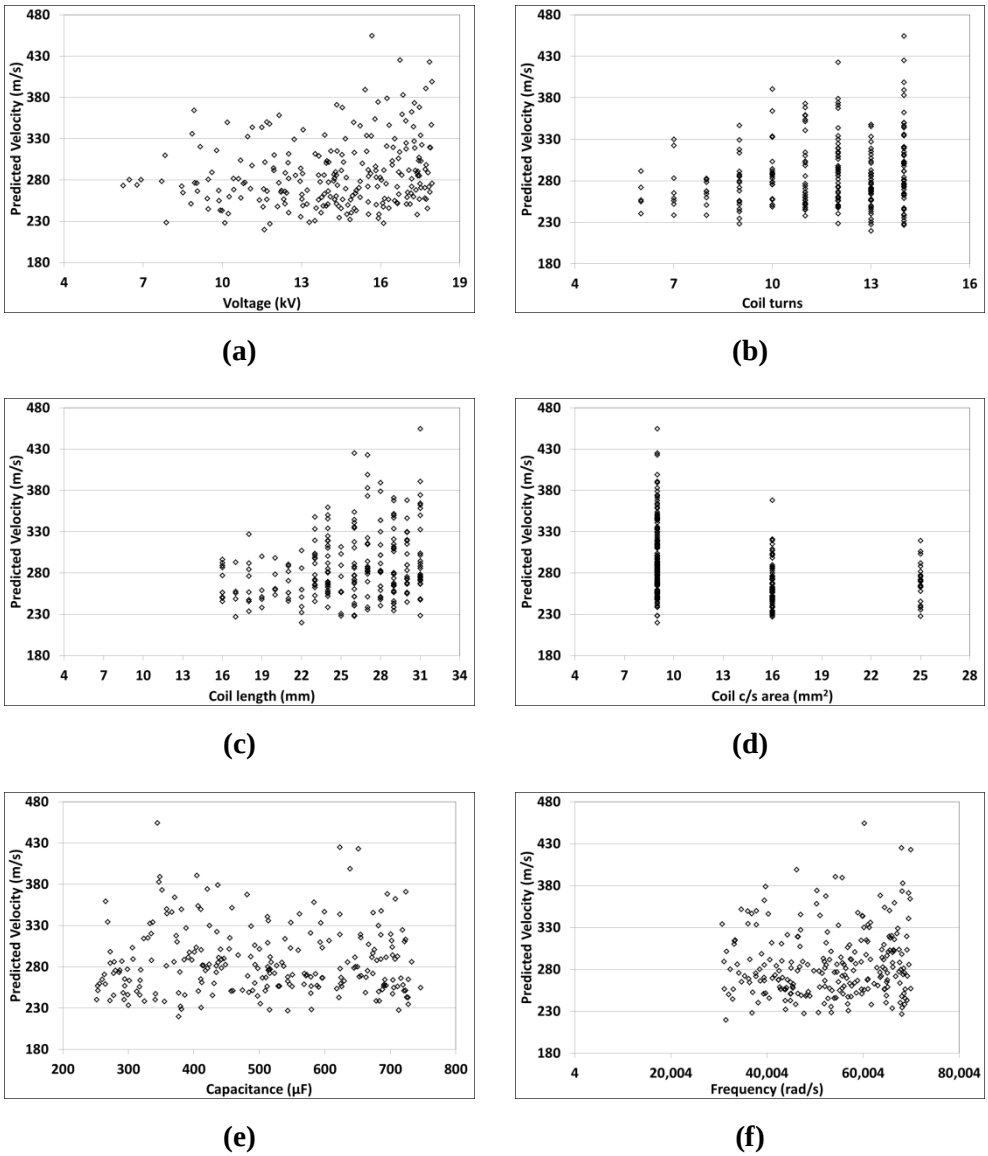

(a) **(b)**

(c) **(d)**

(e) **(f)**

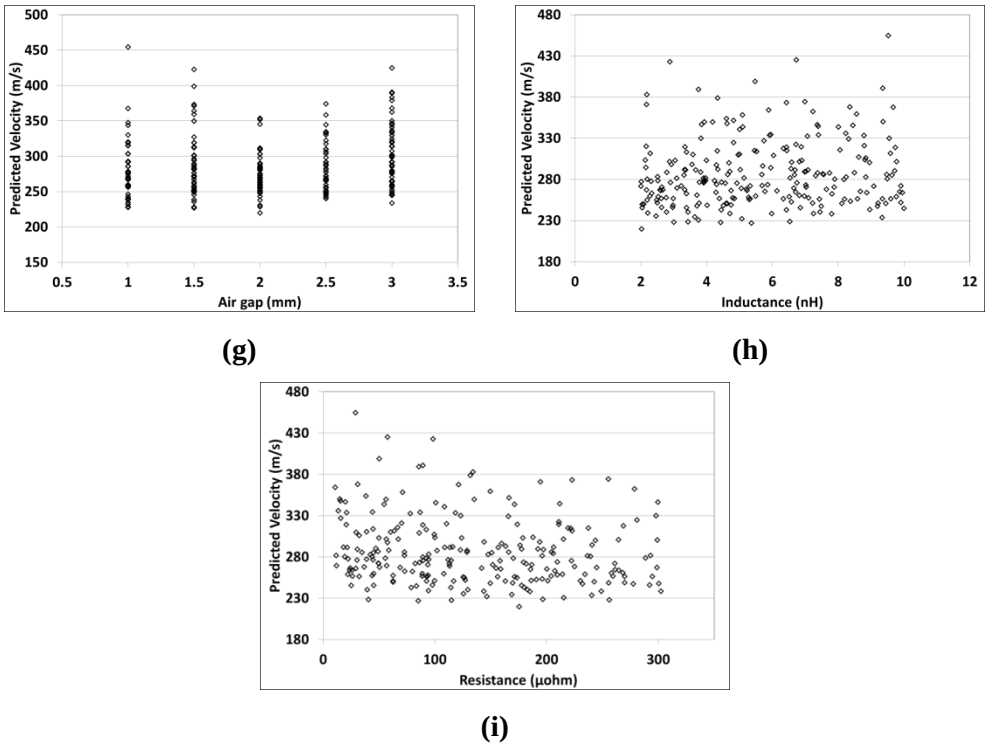

Fig. 66 (a) to (i) scatter plots of variation in velocity with process parameters for the considered case study

The case study conducted on the Al-SS 304 material combination by utilizing the ANN developed in the previous section helped the user to identify the exact combination of process parameters at which the impact velocity i.e. the weld validation criteria was satisfied. The conducted case study was verified experimentally in the next chapter. Single values of each of the nine process parameters at which impact velocity condition (Eq. 28) was satisfied and plotted in Figs. 66 (a) to (i) are selected and mechanical and metallurgical tests are conducted to validate the weldability of the joint. The material processing, welding of sample and various tests conducted along with discussion of the same is being given in the next chapter.

Chapter 4

Experimental Work

The previous chapter discussed the development of a FEM and impact velocity based predictive models which gave the end user the MPW process parameters at which successful weld might occur. To validate the findings of the numerical modelling and simulation work and the subsequently developed predictive model, experimental study has been carried out and the results have been discussed in this chapter. Two different sets of material combination were used for producing the welds in the present study viz. AA 2219-SS 321and Al- SS 304. The processing of the material, geometry and process parameters chosen, pulsed welding of the members followed by investigative tests to ascertain the weldability of the selected members is explained in details in the current chapter.

4.1 Method and material

4.1.1 AA 2219-SS 321 material pair

The chemical composition and properties of the material pair AA 2219- SS 321chosen for the study have been listed in Table 5 and Table 6 respectively. The geometry and configuration of the mating members is shown in Fig. 41 in the previous chapter. The material was subjected to processing to bring it desired shape and size (stage A) and subsequently pulse welded (stage B). The entire scheme of operations is discussed in the current section.

Stage A: Processing of the material

The material received in bar form was processed to prepare samples to perform MPW. A total of 10 ready to be welded specimens were generated from the material available, the dimensions of which are listed in Table 30. The material processing has been done in three steps as described in the flowchart (Fig. 67) below.

Table 30 Material and dimensions of the samples

Dimensions (AA 2219, Flyer tube)	Inner Dia (mm)	Outer Dia (mm)	Thickness (mm)	No of samples
	76	80	2	9
Dimensions (SS 321, Base tube)	Inner Dia (mm)	Outer Dia (mm)	Thickness (mm)	No of samples
	60	74	7	3
	60	73	6.5	4
	60	72	6	3
Length of all test pieces (mm) = 75				

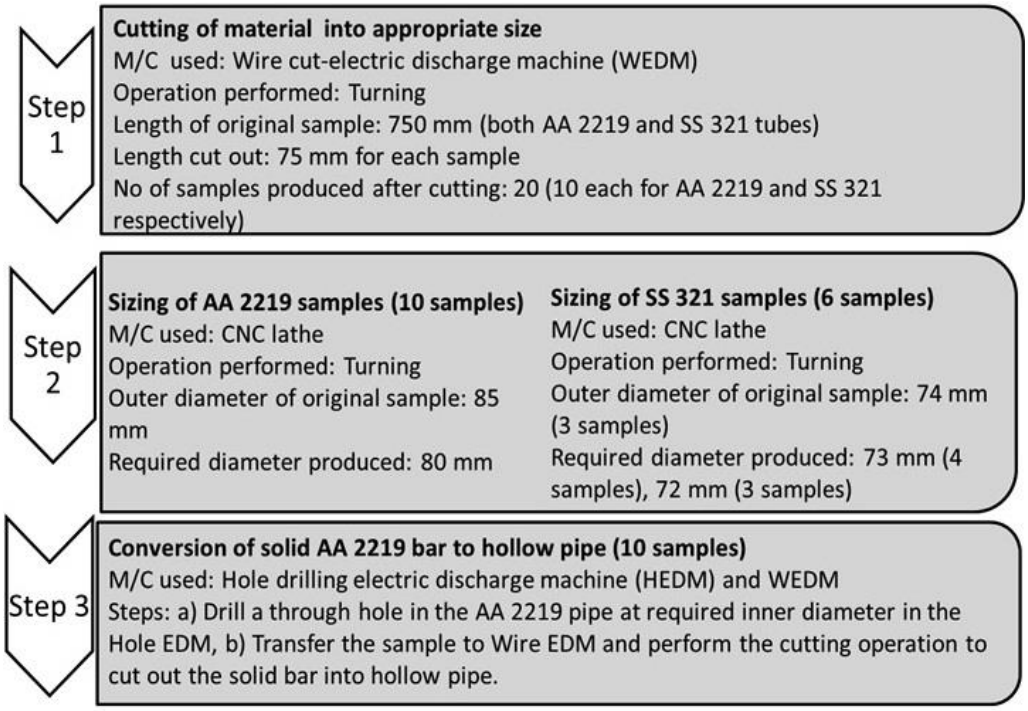

Fig. 67 Flowchart for material processing

Figs. 68 (a) to (f) show the processing of the material at various steps. Fig. 68 (a) shows a Sprintcut, Electronica make WEDM used in the present investigation. A zinc coated brass wire with wire diameter of 0.25 mm was used for all the operations mentioned in flowchart shown in Fig. 67. Fig. 68 (b) shows the AA 2219 (flyer tube) bar clamped in the WEDM for cutting into required length. A total of 20 samples (10 each of AA 2219 and SS 321) of 75 mm length each were cut in the WEDM. After this, each specimen underwent the operations mentioned in step 2 (Fig. 67). The Al

and steel members were subjected to turning operation in CNC lathe to produce the required diameter. The diameters were carefully chosen beforehand such that different air gaps between the mating members could be produced. All the AA 2219 samples were turned to an outer diameter of 80 mm whereas the SS 321 samples had a mix of outer diameters (Table 30) as per air gap required. The next step was to convert the solid Al bar into a hollow tube, which was done using a combination of WEDM and HEDM. A special fixture was prepared for the same as shown in Fig. 68 (c). A Speed II, Sparkonix make HEDM was used in the present study shown in Fig. 68 (d). An electrode with diameter 0.3 mm was used to drill the holes in the AA 2219 samples (Fig. 68 (e)), after which the sample along with the fixture was transferred to the WEDM to perform necessary cutting action to produce the required hollow Al tubes (Fig. 68 (f)). The inner of all the AA 2219 was kept fixed at 74 mm.

(a)

(b)

(c)

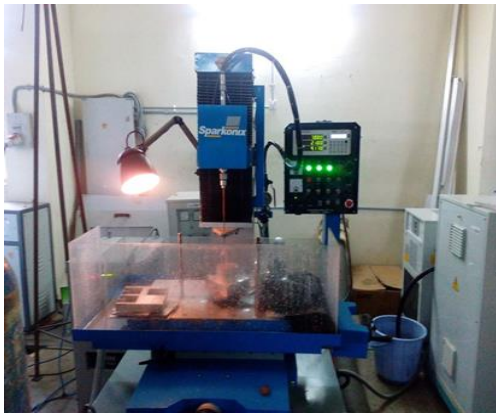

(d)

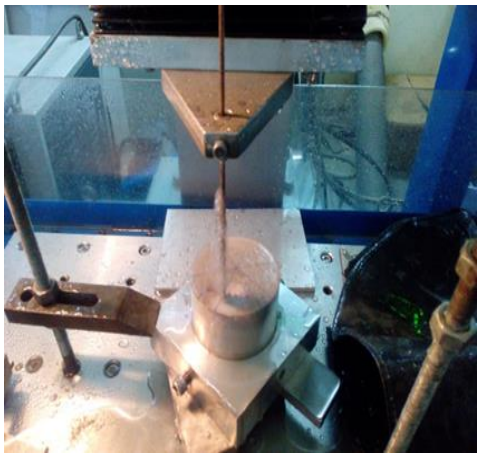

(e) **(f)**

Figs. 68 (a) to (f) processing of the material

Figs. 69 (a) to (e) shows the AA 2219 and SS 321 samples prepared after processing in stage 1. Figs. 69 (a) to (c) show the SS 321 samples with outer diameters 74 mm, 73 mm and 72 mm respectively while Fig. 69 (d) shows the AA 2219 samples. Fig. 69 (e) shows the configuration of an AA 2219-SS 321member at an air gap of 1.5 mm which was subjected to MPW. The welding of the samples along with machine specifications and selected process parameters is discussed next.

(a) **(b)**

(c)

(d)

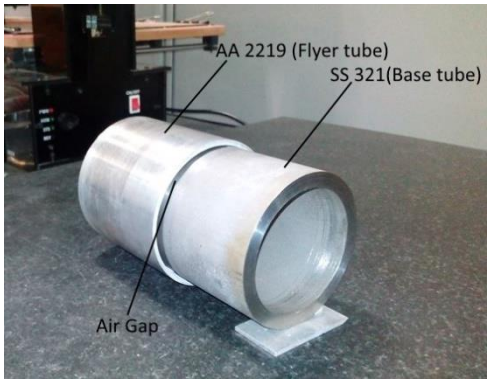

(e)

Figs. 69 (a) to (e) samples prepared for MPW

Stage B: MPW of prepared samples

The samples processed in the first stage were pulse welded using an electromagnetic forming (EMF) machine. The machine specifications are listed in Table 31.

Table 31 Machine specifications for MPW

Machine specifications	**Machine type:** Electromagnetic forming machine
	Operating voltage range: 3kV to 9kV
	Capacitance(μF): 320
	Charging energy (kJ): 12.96 (maximum)
	Peak current (kA): 150
	Operating frequency (kHz): 5.747
	Electromagnetic coil: Copper coil, 4 turn**, Outer dia (mm):** 240 **c/s:** circular**, c/s diameter:** Φ20 mm**, Length (mm):**125

The variable operating process parameters chosen for the study were voltage and air gap as depicted in Fig. 70. The parameters were selected such that it covered the entire range of machine capability. Low, Moderate to high air gaps and voltages were chosen for conducting the pulse welding of AA 2219-SS 321tubular members. It is known from literature and the numerical work conducted in the previous chapter that a moderate air gap and voltage results in a sound weld. A low air gap at higher voltage levels increases the possibility of damage in the mating members due to high speed impact within a very short duration of time. Also at lower voltages and higher air gaps the velocity reached at the impact time tends to be lower than threshold thus reducing the possibility of weld success. At low gaps and voltages the flyer impacts the target even before it reaches its peak velocity. To incorporate these stated facts the pulse welding of the selected members was conducted at air gaps ranging from 1 mm to 2 mm with a step size of 0.5 mm and voltage levels ranging from 3 to 9 kV with a step size of 1.5 kV. The aim of choosing this range of parameters was to study the effect of the same on the weld quality and further the mechanical and metallurgical properties. The idea was to validate the finding of the ANN developed in the previous chapter and at the same time ascertain particular process range where welding would be successful.

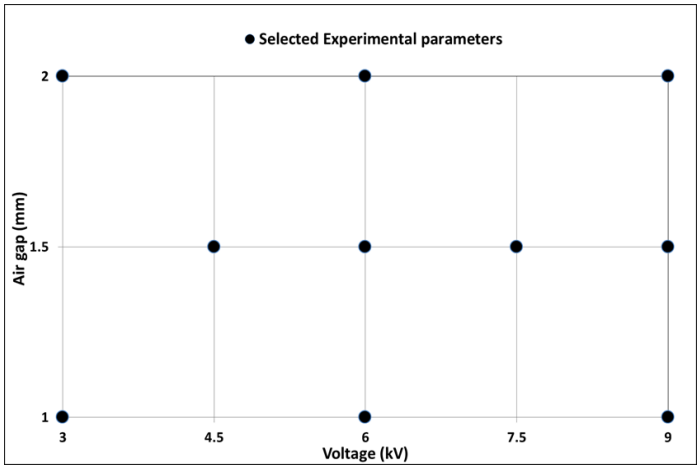

Fig. 70 Experimental parameters selected for MPW of AA 2219-SS 321tubular members

Figs. 71 (a) to (e) show the machine set up and the configuration of the flyer and base tubes for pulse welding of AA2219-SS321 dissimilar material combination. Fig. 71 (a) shows the entire EMF machine set up along with the electromagnetic coil used for the welding of the samples. During the course of the welding In situ measurement of current signal was done with the help of an oscilloscope which is connected to the coil via a Rogowski coil (Fig. 71 (b)). The current signals obtained from the

oscilloscope were used to calculate the peak current and operating frequency of the set up during each operation of welding. Based on the waveform calculation of circuit impedance and hence inductance were done. The coil used was a helical coil covered with insulation to prevent flux leakage. A field shaper was employed to concentrate the flux lines or the magnetic energy to a 10 mm length on the flyer tube (Fig. 71 (c)). The arrangement of the mating tubes (flyer and base) and the coil along with the field shaper is shown in Fig. 71 (d). The final position of the mating member's right before the machine was operated is shown in Fig. 71 (e)

(a)

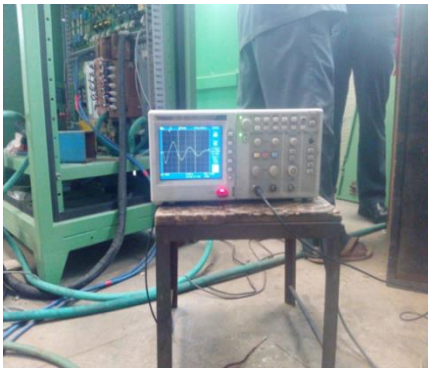

(b)

(c)

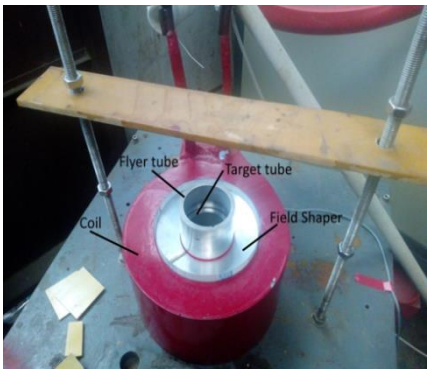

(d)

(e)

Figs. 71 (a) to (e) machine set up and the configuration of the flyer and base tubes for MPW

Figs. 72 (a) to (i) show the MPW welded AA 2219-SS 321 tubular members at various processing parameters. Out of the total eleven experiments performed, the experiments performed at a voltage level of 3 kV with air gaps of 1 mm and 2mm failed to produce any deformation of the flyer tube. Thus the sample with 1 mm gap was machined to create a gap of 1.5 mm and the same was reused for pulse welding at 9 kV. The other failed sample with 2 mm gap was reused and pulse welded at a voltage rating of 9kV. It can be observed from Figs. 72 (a) and (b) that the flyer showed very little deformation at 1 mm gap even at high voltage of 9 kV, whereas a clear deformation on the flyer tube surface can be observed on all the samples welded at 2 mm air gap (Figs. 72 (g-i)). At an air gap of 1.5 mm the tubes deformation increased with increase in voltage level (Figs. 72 (c-f)).

(a) 1 mm air gap/ 6 kV

(b) 1 mm air gap/ 9 kV

(c) 1.5 mm air gap/ 4.5 kV

(d) 1.5 mm air gap/ 6 kV

(e) 1.5 mm air gap/ 7.5 kV

(f) 1.5 mm air gap/ 9 kV



(g) 2 mm air gap/ 6 kV **(h) 2 mm air gap/ 9 kV** **(i) 2 mm air gap/ 9 kV**

Figs. 72 (a) to (i) MPW welded AA 2219-SS 321 tubular members

Figs. 73 (a) to (i) show the current waveforms generated during the pulse welding of the AA 2219-SS 321 tubular members. As mentioned earlier, this current waveform enables the user to calculate the peak current during the course of the welding and also the operating frequency and subsequently the circuit impedance. Calculation of these values is very important in the context of MPW as this in a way decide the weldability of the joint. To generate the required magnetic pressure, it is necessary to apply very high pulsed currents. The EMF machine capacitor bank needs to possess a sufficiently high capacitance in order to store enough energy, while the inductance of the discharge circuit should be low enough, in order to ensure a fast energy release and thus a larger current pulse when discharging the current through the coil. The impact velocity, one of the important weld validation criteria also depends on the magnitude of the pulsed current; a higher peak current value inducing higher magnetic pressure causing the velocity to reach peak values at the time of impact. The success of the welding also depends on the charging energy or voltage during applied during the course of the welding. The capacitor charging voltage is directly related to the energy level. The voltage level is a crucial parameter in the formation of the weld, as this parameter determines the impact velocity for a given a material combination. An increase in the voltage level results in an increase of the magnetic pressure on the flyer which aids the deformation and ensures higher impact velocity. The voltage level is the parameter which is user controllable and is the easiest to change during the experiments. It can be observed from the current waveforms that the peak current values increased with increase in voltage levels and were maximum at the maximum voltage of 9 kV at all air gaps (1 mm, 1.5 mm, 2 mm) (Figs. 73 (b), (f), (h), (i)). The waveforms obtained at 4.5 kV and 7.5 kV at an air gap of 1.5 mm also reveal the fact that the amplitude of the

current increases on increasing the voltage levels. It is also seen and further calculated from the waveforms that the current amplitude and frequency remained almost same at similar voltage levels (Figs. 73 (a), (d), (g)). It concludes the fact that the frequency of operation and the peak current achievable mostly depends on the circuit electrical parameters like voltage, inductance and energy and the air gap has a little or no effect on the same. The operating frequency is another important parameter which has a major effect on the success of MPW. The frequency determines the skin depth of the material which decreases with an increase of the frequency (Eq. 5). For conductive workpieces the skin depth values are generally very large and hence it becomes necessary to employ high operating frequencies. Apart from its effect on the skin depth, the frequency also influences the space distribution of the magnetic field, the peak value of the magnetic pressure and the pulse width of the magnetic pressure. The pulse width of the magnetic pressure influences the acceleration duration of the outer tubular workpiece. The longer it accelerates, the more the tube will increase its velocity. Lower frequencies lead to larger pulse width [22]. To be successful, the welding requires an accurate frequency of the pulse to avoid a diffusion of the magnetic field induced by the coil throughout the flyer.

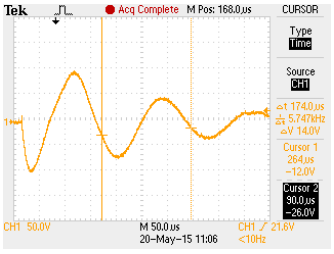

(a) 1 mm air gap/ 6 kV

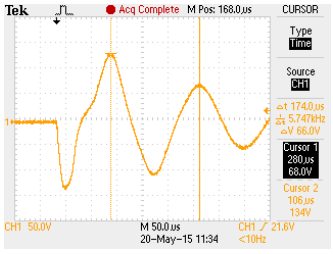

(b) 1 mm air gap/ 9 kV

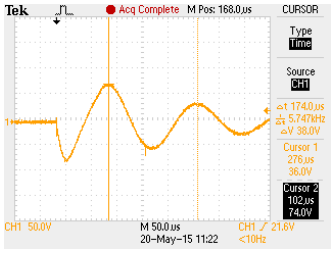

(c) 1.5 mm air gap/ 4.5 kV

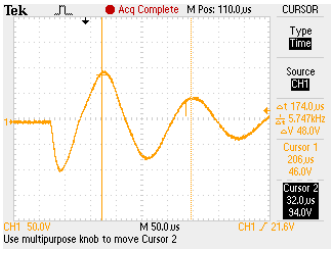

(d) 1.5 mm air gap/ 6 kV

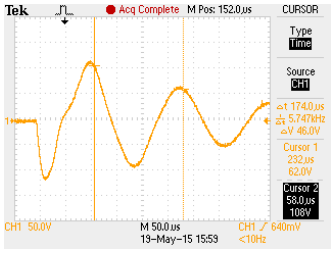

(e) 1.5 mm air gap/ 7.5 kV

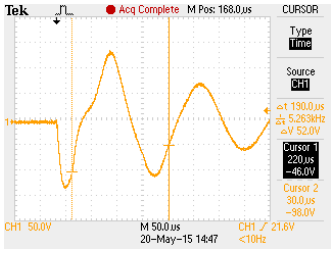

(f) 1.5 mm air gap/ 9 kV

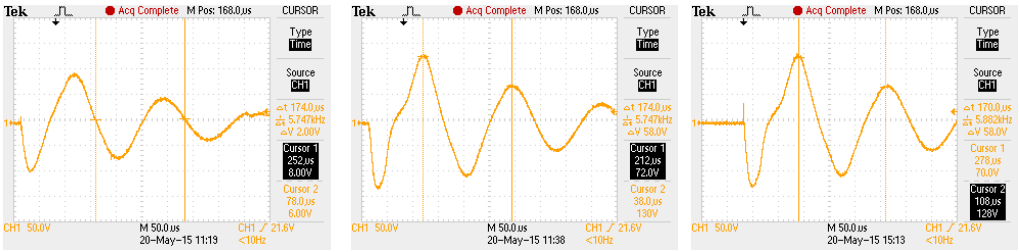

(g) 2 mm air gap/ 6 kV **(h) 2 mm air gap/ 9 kV** **(i) 2 mm air gap/ 9 kV**

Figs. 73 (a) to (i) current waveforms generated during MPW of the AA 2219-SS 321 tubular members

The AA 2219- SS321 joints were then cut along the length of the axis. From all the samples, traversed section specimens were cut using WEDM. It was observed that while the cut in WEDM was going on, the flyer and base tube sections separated from each and fell off once the cut reached halfway of the overlap length of the mating members. Figs. 74 (a) and (b) show the MPW sample from which the section was cut off and section which failed respectively. The same observation was made in all the rest of the samples and the pulse welding for AA 2219-SS 321 members had failed for all the experimental runs.

(a) **(b)**

Fig. 74 (a) MPW sample from which section was cut off and (b) failed section showing absence of any bonding (1.5 mm/9 kV)

The joint obtained for the AA 2219-SS 321samples resembled that of a shrink- fit joint with the absence of any physical and metallic bond between the members. The flyer tube was merely deformed and had a slight impact with the base tube. Upon crucial analysis of literature and based on the experience of the user it was found that a combination of factors led to failure of the joint. It was calculated from the current waveforms (Fig. 73 (a) to (i)) that the current reached a peak value of 150 kA for the

maximum voltage of 9 kV which is the below the average values recorded in literature where successful welds have been reported [10]. The current values were directly affected by the voltage limitation of the EMF machine available. As a result of low peak current values the magnetic forces generated were very low which could not accelerate the flyer tube to velocities beyond the threshold (Eq. (7-10)) which could ensure a weld at the interface. The current waveforms also led to the calculation of operating frequency of the setup. The operating frequency directly affects the skin depth as already mentioned. In order to maximise the magnetic pressure, the skin depth should be small relative to the workpiece wall thickness and ideally should be one third of the flyer tube thickness as suggested in literature [22]. For the present study the flyer tube thickness was 2 mm, and the operating frequency calculated from the waveforms was 5745 Hz. From Eq. (5) it is found that the skin depth for the chosen material and available set up is 1.3 mm which is way more than the ideal limit of one-third the flyer thickness. The use of a low frequency led to skin depth being on the higher side and it is highly likely that a great share of the magnetic field diffused through the wall thickness, thus reducing the pressure generated. Adjusting the frequency is only possible by making adjustments to the capacitor banks, but in the present case the EMF equipment had a single capacitor bank of 320 μF which could not be adjusted. As mentioned earlier an ideal MPW set up should have a low inductance value. The current waveforms in the present study suggest that the EMF machine carried a very high inductance value which made the energy release slower thus lowering the current pulse when discharging the current through the coil.

It is seen that inspite of choosing a wide range of process parameters and a highly conductive AA 2219 flyer for conducting the experiments no welds could be created as many other controllable and uncontrollable parameters were found to be out of ideal range. A limitation on the electrical parameters viz. voltage, capacitance, frequency and inductance and material parameters viz. skin depth led to the failure of the joints. In future the same process window (Fig. 70) would be tried again with necessary changes and modifications made with the available equipment.

Due to the failure of the first material pair combination (AA 2219- SS 321) another new material pair i.e. Al alloy and SS 304 was pulse welded with a new machine with a voltage and energy rating of 16 kV and 42 kJ respectively. The welding for this material pair and machine combination was successful. The sample

preparation along with the various investigative tests results is discussed in the next section.

4.1.2 Al-SS 304 material pair

The material chosen for the study and its properties have been listed in Table 6. The geometry and configuration of the mating members is shown in Fig. 40 in the previous chapter. From the process parameters given by the predictive model, MPW experiments were carried out at a charging voltage of 16 kV, discharge energy of 42 kJ with a capacitance value of 328 μF. An air gap of 1.5 mm was provided between the pure Al tube and the SS 304 tube so that the aluminum tube has time for acceleration before the first point of impact. It also helped create a favourable collision angle as the flyer collapsed against the base tube. The overlapping length between the two tubes was kept at 14 mm.

The welded sample was then tested using a simple mechanical lap shear test of the welded member. After confirmation of welding, the welded joint was cut along the length of the axis. From the welded samples, traversed section specimens were cut using WEDM (Fig. 75). These cut specimens were subjected to mechanical polishing using different grade emery papers followed by diamond polish up to 1 μm. Microhardness testing was conducted across the interface for the cut out sample. Metallographic examination of the welded surface was carried out on an Olympus STM6-LM optical microscope (OM) and Carl Zeiss AG-Supra 40 field electron scanning electron microscope (FESEM). Chemical etching of the samples was not carried out since the observation of micro structure at the welded surface is not considered for this study. Elemental distribution mapping at the welded interface was obtained though energy dispersive spectroscopy (EDS) analysis at the interface between the Al and SS 304 members. Surface mapping of the interface was also carried out to check for diffusion of one metal into the other in the zone of interest (welded interface).

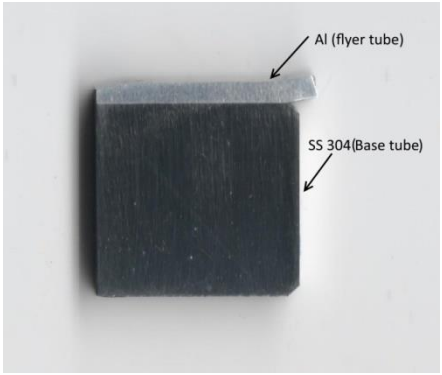

Fig. 75 Cross section of the MPW welded member cut out using WEDM for hardness measurement and metallographic observation

4.2 Mechanical investigation

4.2.1 Lap shear test

The mechanical property of MPW joint was measured by the lap shear test. The lap shearing test is similar to tensile test, but the tensile axis is parallel to the welded interface as shown in Fig. 76. Four dog bone specimens were prepared by slicing the welded tubes using WEDM. The applied load generates shear stress on the welded region; the load and displacement being recorded during the test. The joint strength (MPa) was calculated by dividing the load with shearing area. The elongation (%) was determined from the measured displacement.

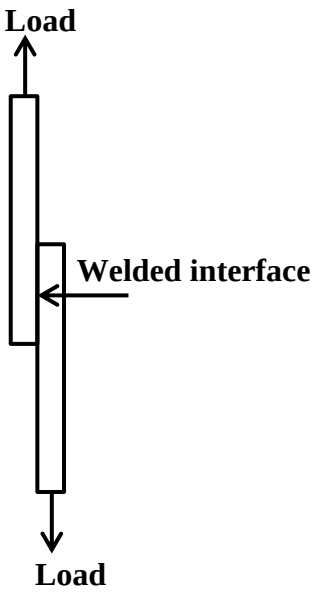

Fig. 76 Illustration of lap shear test

Table 32 lists the yield and the ultimate tensile strengths along with percentage elongation and hardness values of the investigated base materials in as-received state. Table 33 lists the mechanical properties of the pulse welded Al-SS 304 joint obtained from the lap shear test. It can be seen that the ultimate tensile strengths of the all MPW samples were greater than that of the weaker of the base metals i.e. Al. It was found that for the pulse welded joints of Al and SS 304 subjected to mechanical lap shear all the prepared specimens the fractured outside the welded region and broke at weaker of the base metals i.e. Al proving that the weld is sound. The maximum pull-off strength of the joint obtained was 111 MPa corresponding to a pull-off force of 1.697 kN, which is higher than that of pure Al tube (as shown in Tables 32 and 33).

Table 32 Mechanical properties of base materials

Material	**0.2% Yield strength (MPa)**	**Ultimate tensile strength (MPa)**	**% Elongation**	**Hardness (HV)**
Pure Al (flyer tube)	98	52	48	55
SS 304 (base tube)	205	515	42	210

Table 33 Mechanical properties of pulse welded Al-SS 304 joint

Sample No.	**Ultimate tensile strength (MPa)**	**Peak load (kN)**	**Failure location**
1	101	1.759	Outside welded zone at Al side
2	111	1.697	Outside welded zone at Al side
3	101	1.527	Outside welded zone at Al side
4	99	1.498	Outside welded zone at Al side

4.2.2 Hardness mapping

Hardness testing is a method to estimate weld quality as it enables evaluation of mechanical properties at very small distances. The common feature of the weld interface region created during the MPW process is the increase of hardness in the weld interface. The interface layer shows an increase in hardness relative to the base material (Fig. 77). This can be attributed to severe plastic deformation or to a new fine-grained microstructure produced by melting and rapid solidification of the weld

interface. This interface layer may support two possible mechanisms of bond formation: bonding as a result of solid-state processes based on accelerated mass transfer due to intensive plastic deformation at very high rates, and bonding as a result of solid-liquid interaction and based on the formation of a thin layer of molten metal between the components

The specimens under discharge voltage of 16 kV (42 kJ discharge energy) and radial gap of 1.5 mm were chosen to measure the micro-hardness with micro-indentation machine. The microhardness measurement across the interface was done with 100 gf load and 15s dwell time As illustrated in Fig. 77, on both sides of the transition zone, points were chosen every 75 μm in the direction vertical to the interface to measure the micro-hardness. The transition zone has the highest hardness value of 302 HV. The micro-hardness increases promptly in the region both sides of the transition zone and it tends to be constant beyond the above regions, which is similar to the results given in literature [4, 31]. It is attributable to the severe plastic deformation of the base metal in the interface that contributes to serious work hardening and grain refinement. With increasing distance from the interface, the plastic deformation decreases that leads to a subsequent decrease in the micro-hardness values. In addition, some kind of high hardness intermetallics produced in the transition zone might result in the higher hardness value than the base metals.

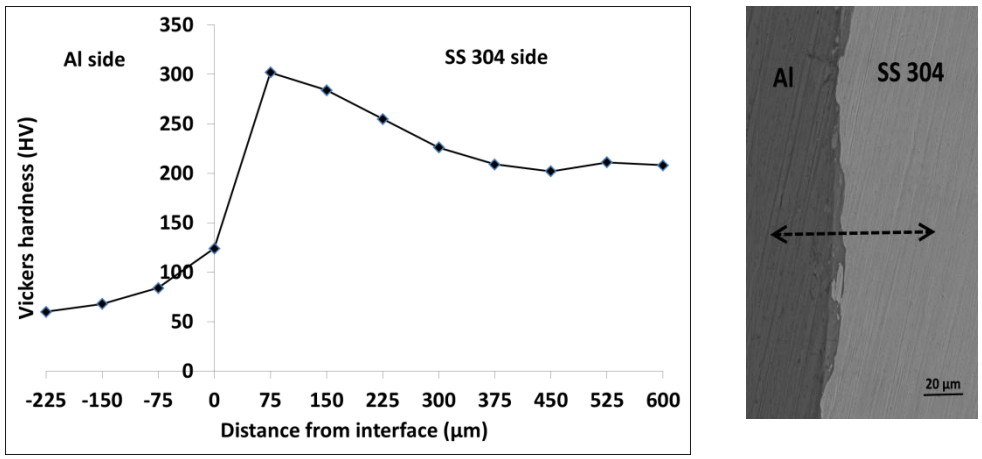

(a) **(b)**

Fig. 77 (a) variation of microhardness across the interface of the pulse welded members and (b) micrograph illustrating the path of microhardness testing (the dotted black line)

4.3 Metallurgical investigation

In MPW severe plastic deformation occurs in the colliding members along the interface due to the high velocity impact of the flyer tube onto the base tube. The impact and the plastic deformation are two key factors that lead high quality MPW joints. The impurity on the tube surfaces in the form of oxides, absorption etc. are broken up by the severe plastic deformation, which then are blown off by the jet generated between the two tubes. Therefore, new, pure and clean surfaces are obtained that are opposite to each other. Under the transient impact, both surfaces approach to the atomic distance and hence realize an atomic binding force [30]. While most of the plastic deformation energy transforms into heat, which improves the interface temperature, enforces the atomic activity, then makes for the solid state diffusion of interface atoms [68], even local melting and solidification.

The mechanical properties of the MPW joints are closely related to the interface morphology. Metallurgical analysis of MPW bonded member reveals various types of joint morphologies: flat interfaces, wavy interfaces, no bond zone etc. The interfacial layer morphology is determined by interface evolution during this ultrafast welding process [87]. In order to gain in-depth understanding of the interface evolution during MPW the Al-SS 304 joint is examined by advanced characterization methods. The major focus of this investigation is characterizing the interface in the Al-SS 304 pulse welded member.

4.3.1 Optical imaging and scanning electron microscopy

The quality and morphology of the pulse welded joint changes continuously along the interface from start to end. Generally, the start and end zones of the welds exhibit no or only limited bonding whereas the middle section of the welds showed good bonding. The insufficient bonding at the start and the end of the weld zone is a typical feature of MPW cylindrical parts and according to literature not critical for many applications [21, 40]. However the unbonded sections can act as strong notch points at the weld, which would be very detrimental under cyclic load or corrosive environment. The interface of the welded members has a characteristic wavy appearance in MPW and the process of wave formation along the interface strongly depends on sample geometry and to a lesser extent also on the process parameters.

Fig. 78 shows a stitched optical microscopy image of the cross-section of Al-SS 304 pulse welded joint. The Al-SS 304 welded members used in the present study showed distinct bonded and unbonded zones together with the characteristic wavy interface especially in the middle section of the welds. The unbonded zone to the left of the bonded centre zone is known as the Run-in zone whereas the unbonded zone to the right of the bonded centre zone is known as the Run-out zone. The presence of these three distinct zones is a characteristic feature of pulse welded tubular joint. Fig. 80 shows the images of optical microscopy observations along the length of the interface. The presence of several distinct zones can be easily identified. The interface at the beginning of the weld (Fig. 79 (a)) where the metals were in contact showed absence of any metallic bonding. This was followed by the centre region Fig. 79 (b), where the wavy pattern typical to that of the MPW process appeared. The length and amplitude of the waves tend to evolve along the welding direction. The amplitude of the wave is highly reliant on collision angle and its dependency on collision velocity is negligible. The bonded centre zone with the presence of the wavy interface was followed by a somewhat flat-end region. This was followed by an unbonded zone (black region in Fig. 79 (c)) suggesting that the welding did not take place over the entire length of the sample.

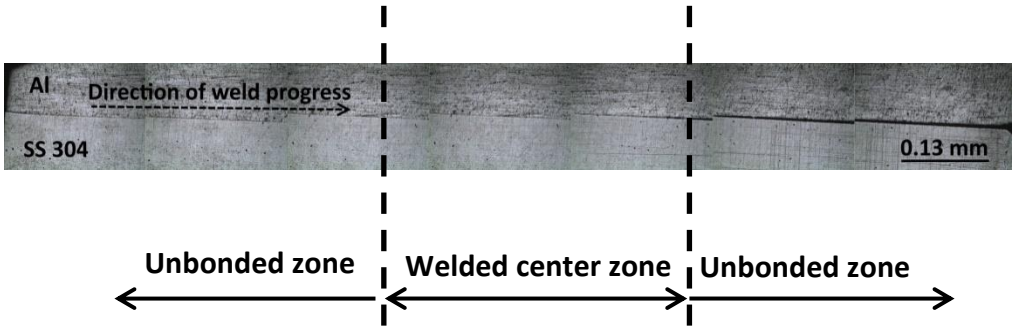

Fig. 78 Stitched OM image showing the cross-section of Al-SS 304 pulse welded joint

(a)

(b)

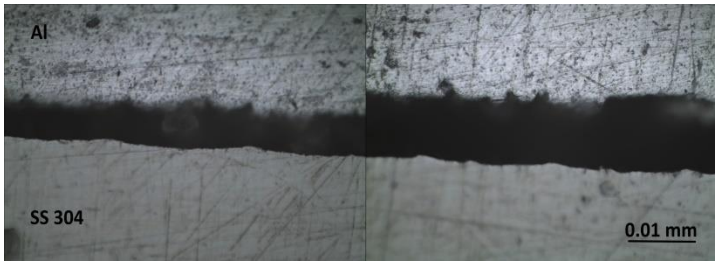

(c)

Fig. 79 Stitched OM images showing (a) unbonded zone at the beginning of weld, (b) welded center zone and (c) unbonded zone at the end of the weld

In MPW a minimum flyer workpiece velocity is necessary to generate the optimum contact pressure required to obtain a successful weld or a bonded zone. Likewise, the minimum kinetic energy imparted to the flyer workpiece must be such that the strain energy necessary to cause dynamic yield in the stronger of the mating members is exceeded. An upper limit of impact energy is imposed by phenomena such as the formation of intermetallic compounds or excessive melting at the interface, which lead to weakening of the joint [114]. A critical value of impact energy is thus required to achieve welding. However, a unique value of impact energy does not exist for all thicknesses of flyer workpiece and for constant impact energy the weld quality decreases with decrease in flyer workpiece velocity [3]. It has been proved [145] that the kinetic energy is directly proportional to the strain energy required for dynamic yield of the stronger of the materials being welded.

$$Kinetic\ energy\ (K.E) = \frac{K_m \sigma_D^2}{2Y} = \frac{\rho_f\ t_f V_f^2}{2} \tag{29}$$

where σ_D is the dynamic yield stress, Y is the Young's modulus, K_m is a constant, ρ_f is the density of the flyer workpiece (kg/m^3), t_f is the flyer workpiece thickness (mm) and V_f is the flyer velocity.

Figs. 79 (a) to (c) depict stitched images showing the bonded centre zone with transition to the unbonded zone on either side of it. In the unbonded zone, where normal compressive loading through tube thickness occurred, the oxide layer is still present. In the oblique collision, the removal of oxide is normally accomplished through jetting. As a result, at the oxide disappearance location, jetting of oxides and contaminates must begin to occur. The morphology of the joint, i.e. from the unbonded zone to the bonded centre zone and then to the unbonded outer zone, is similar to the observations of Watanabe and Kumai [8].

Fig. 80 shows scanning electron images of the interface of magnetic pulse welds between aluminum and SS 304. Fig. 80 (a) shows the unbonded zone at the beginning of the weld and as we move along the interface, the welded zone starts to appear. The bonded/welded zone is characterized by the presence of a wavy interface, as we move further along the interface the wavy nature tends to decrease and the interface assumes a flat shape. Figs. 80 (b-e) show the presence of a wavy pattern at the interface of the pulse welded members whereas Figs. 80 (f-h) represent the transition from wavy to flat interface. The bonded centre zone is succeeded by an unbonded zone as represented by Figs. 80 (i-l). Due to differences in density and electrical conductivity the aluminium side of the welded member has a dark contrast whereas the SS 304 side has a bright contrast.

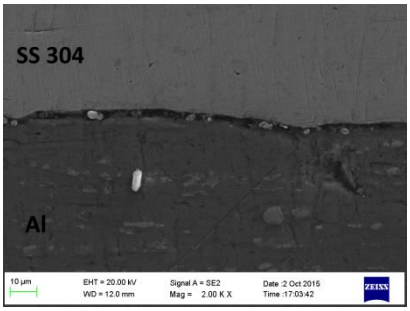

(a)

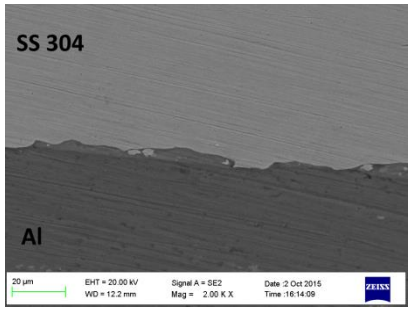

(b)

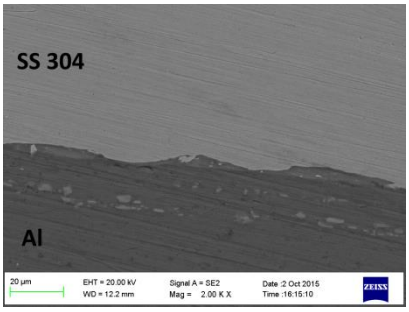

(c)

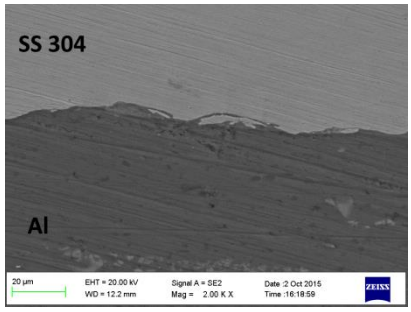

(d)

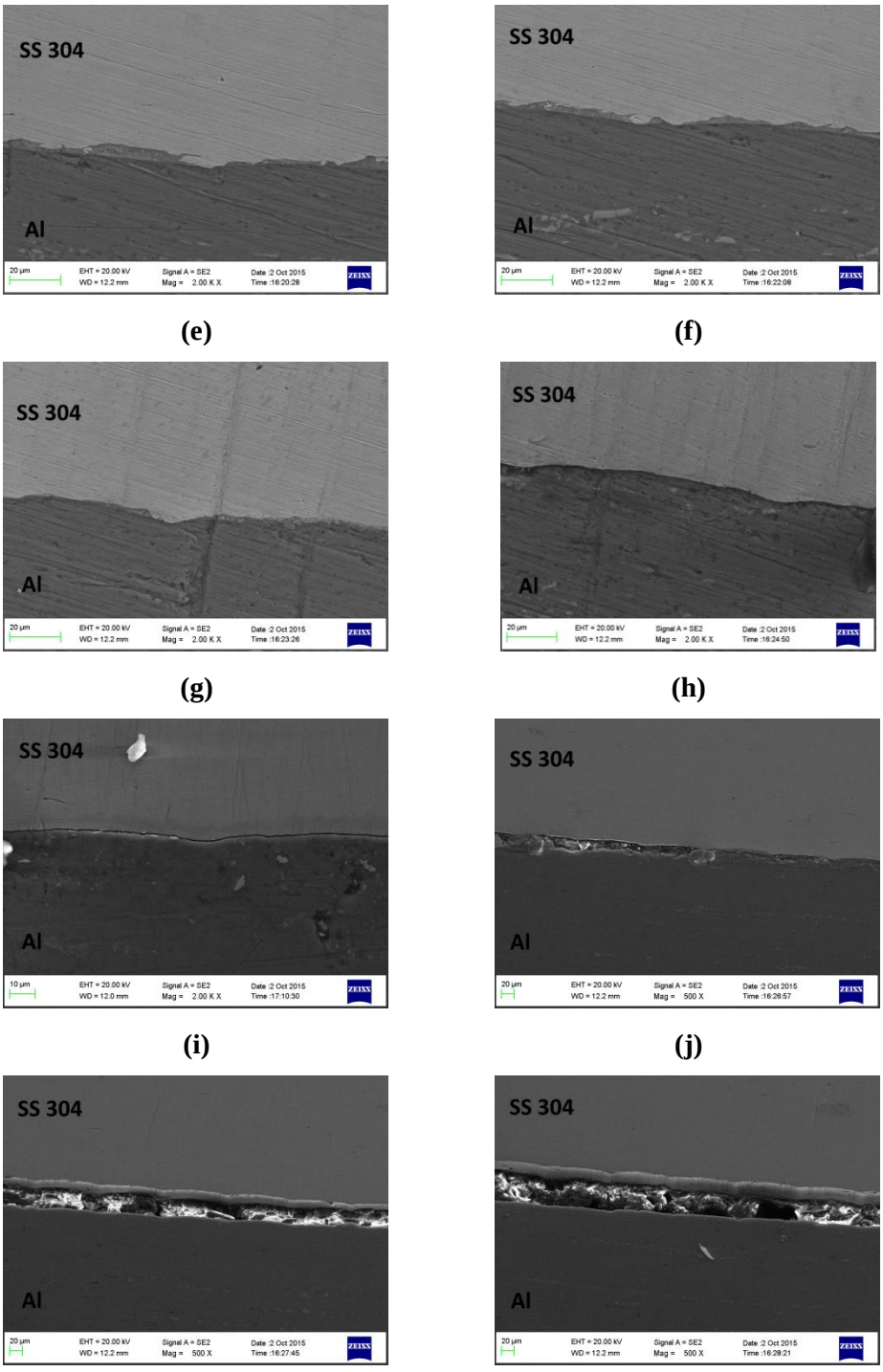

Fig. 80 (a) to (l) scanning electron images of the interface of magnetic pulse welds between aluminum and SS 304

In MPW process to achieve a successful weld the collision point velocity must be kept well below the sonic velocity and within a range appropriate to the materials and the flyer workpiece being used. Welding parameters like collision velocity, collision

angle, flyer and target workpiece thickness and shape of the flyer workpiece affect the nature of interface formed and often decide the changeover from smooth to a wavy interface. When the collision point velocity falls below a particular value, the weld interface becomes flat, whilst with increasing collision point velocity, the volume of trapped jet increases, which suppresses the formation of waves. At intermediate collision point velocities, the jet behaviour is regular, a steady-state wave pattern at the interface is established and the maximum bond strength is obtained. The value of the collision-point velocity at which the interface just becomes flat is known as the transition velocity,V_{WT}, its value depending upon the particular properties of the mating members and is given by the relationship [114]:

$$V_{WT}^2 = \frac{2(H_f+H_t)\, Re \times 10^7}{(\rho_f+\rho_t)} \tag{30}$$

where Re is the Reynolds number, H_f is the hardness of the flyer tube (kgf/mm^2), H_t is the hardness of the target tube (kgf/mm^2), ρ_f is the density of the flyer tube (kg/m^3), ρ_t is the density of the target tube (kg/m^3).

In general, welds obtained at a collision velocity v_w equal to 1.25 V_{WT} are found to be satisfactory [146]. The collision-point velocity depends upon the tube velocity, the detonation velocity and the dynamic angle of collision. Cowan et al. [28] reported that a transition from a wavy to smooth bond zone occurred with increasing collision angle. This is due to the fact that as the collision angles were increasing the collision velocities were decreasing.

From the optical and scanning electron images, it is evident that the wave formation was more pronounced in the mid region than the beginning and end of the welded interface, where the bonding was minimal. This wave formation is similar to that one observed in EXW and the associated mechanisms could be related. The variation of wave length along the length of the weld is caused due to the variation of collision angle between the flyer tube and the base tube. Also, the formation of maximum amplitude and wavelength at the interface tends to increase with the increase in measured impact velocity and estimated the magnetic pressure acting on the interface. Figs. 80 (f, g) show the relatively flat or straight interface of the bond zone of samples produced using 42 kJ discharge energy. Meanwhile, the bond of these welds is initially wavy (Figs. 80 (b-e) but gradually developed into a flat interface.

These waves are commonly observed phenomenon in MPW. Available literature [147] shows that there exists a certain range of collision angles and velocities over which a solid-state weld with a wavy interface can be formed. This range is commonly referred to as the weldability window, and varies for each material combination. The straight interface occurs only when the collision conditions are at or near the lower limit of jetting and welding, the preferred MPW interface would contain a larger portion of wavy than straight interface.

Ben-Artzy et al. [40] suggested that the interface wave's result due to flow velocity discontinuities based on the instability mechanism derived by Kelvin and Helmholtz. Due to the discontinuities waves are generated across the interface of the welded members. The theory suggests that interaction of two fluids with dissimilar velocities result into instabilities at the interface which subsequently leads to mass flow from one material to other Figs. 81 (a and b). The instability has a certain direction and velocity (energy) and causes a movement of material from one side of the interface to the other and vice versa. In fact, the elements diffusion during MPW process by the high energy impact is inevitable. It is mainly due to the sudden change from one metal to another across the interface that is the primary term for the element diffusion. In addition, the irreversible severe plastic deformation for high velocity impact causes the transient process with high temperature and high pressure, which makes for the mutual diffusion of basic elements across the interface. The diffusion zone is dependent on the energy transfer relation during the MPW Therefore; more than one factor simultaneously results in the basic elements diffusion during process. Figs. 81 (a and b) depict the surface EDS maps of the Al and SS 304 welded members taken at two locations of the bonded centre zone of the weld as depicted in. The surface EDS maps give clear evidence of material transfer between the two base materials at the crests and troughs of the waves. Figs. 81 (a) and (b) demonstrates that there was unequal distribution of constituent elements across the interface and aluminium and SS 304 did not take an equal part in weld formation. The transfer of material between the flyer and base materials results into several phenomena. One of the reasons for the increase in hardness (Fig. 77) in the interface layer or transition zone can be attributed to the material transfer between the mating members as a result of the high speed impact. It is clear from literature that during MPW the formation of IP at the welding interface cannot be avoided. The composition, arrangement and extent of the intermetallics formed depend on the process parameters chosen and is

partly connected with the structure of the interface. The intermetallic zone formation could be a direct result of atomic diffusion of one metal into the other.

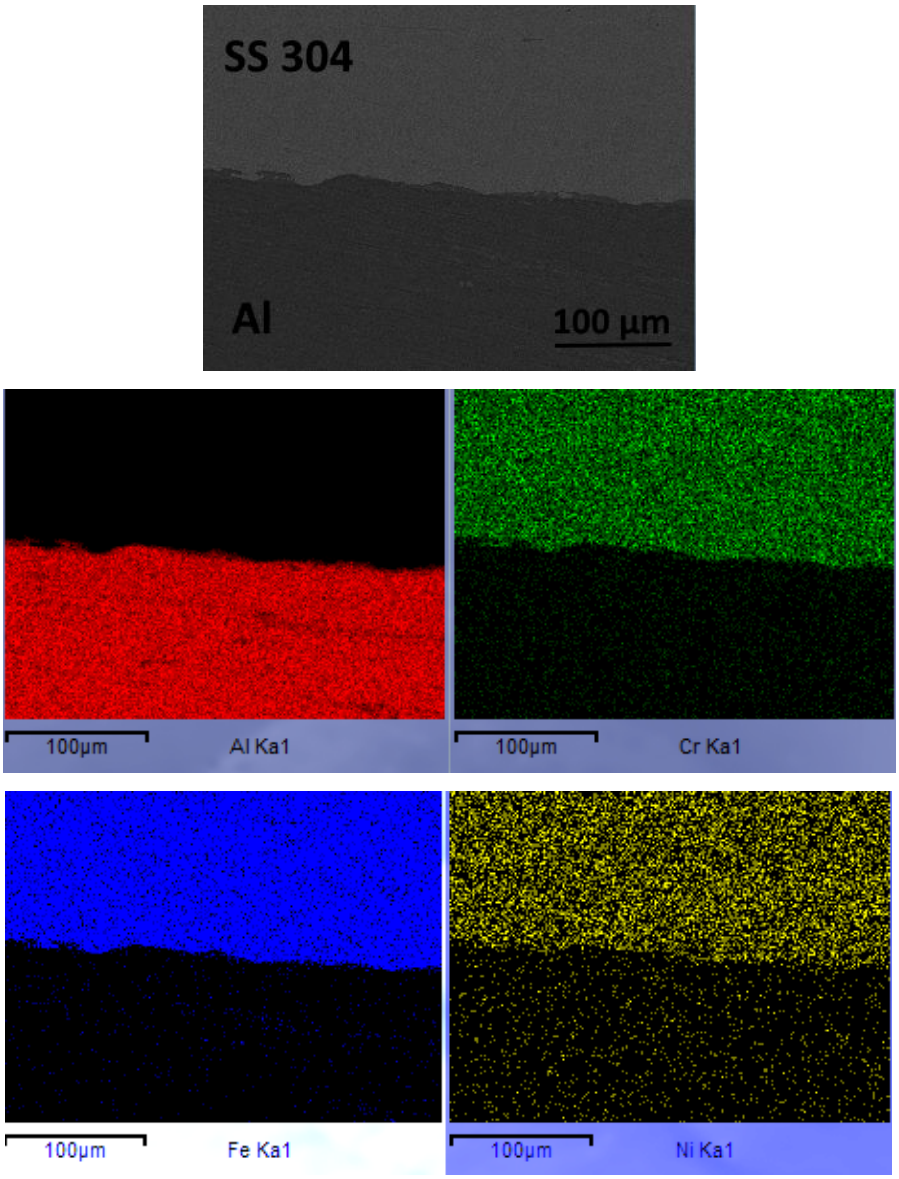

(a)

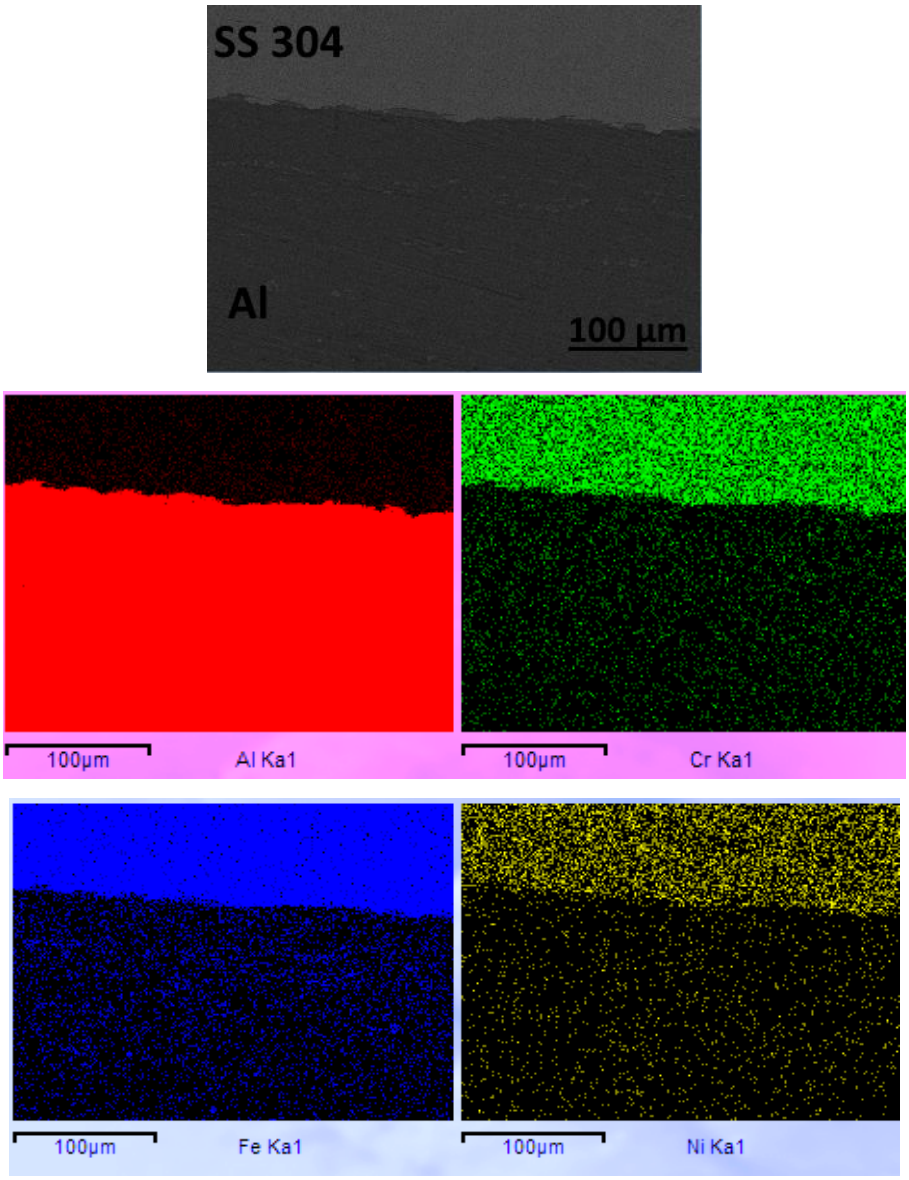

(b)

Fig. 81 (a) and (b) Surface EDS map of the interface of the Al–SS 304 weld taken at two different locations of the bonded centre zone showing material transfer

EDS was used to determine the distribution of aluminium and SS 304 across the weld interface for the bonded centre zone. The line analysis was performed across the IML, as shown in Figs. 82 (a), (c) and (e). The upper side is SS 304 member and the lower side is Al member. The distribution gradient of the basic elements across the zone is not uniform. The area between the broken lines corresponds to the IML region. The composition of elements changed sharply at the IML region, as shown in Figs. 82 (b), (d), (f) proving the fact that the bonding in this joint not only depends on basic element diffusion but also on severe plastic deformation. In the area outside and away

from the broken lines, composition of each element was almost constant, although the distribution of elements was not uniform due to metal diffusion across the interface (Fig. 81 (a) and (b)) indicated by the peaks and valleys in the line scan results (Figs. 82 (b, d, f). The absence of compositional gradients indicates that aluminium and SS 304 rearranged themselves to establish a new microstructure with no more chemical driving force. The regions of zero compositional gradients might be an indication of regions with new phases.

Three different locations along the length of the bonded zone were chosen to perform the line analysis as shown by the yellow coloured lines in Figs. 82 (a), (c), and (e). The width of the IML changed with the location where the line scan was being performed. This change in the width of IML indicates presence of IP of varying thickness along the length of the bonded zone. Fig. 82 (b) shows the distribution of elements for the line scan performed along the crest of a wave, the measurement done from the Al side towards SS 304 side. The obtained width of the IML in this case is approximately estimated to be 9 μm form Fig. 82 (b). The next measurement was carried along a trough of the wavy interface. The line scan result for this measurement is presented in Fig. 83 (d). It can be observed that the IML width increased slightly and is found to be around 12 μm. In this IML region the distribution of Al changed gradually for several μm and then sharply decreased to zero, as seen in Fig. 82 (d). For the third and final scan the measurement was done along a flat interface (Fig. 82 (e)), the measurement being done from SS 304 side towards Al side. There was a considerable decrease in the width of the IML and the same is found to be around 5 μm (Fig. 82 (f)).

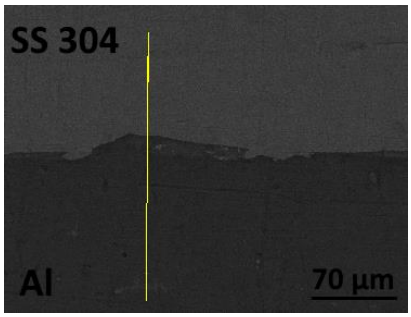

(a)

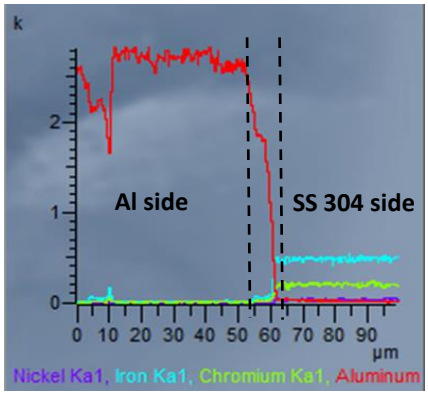

(b)

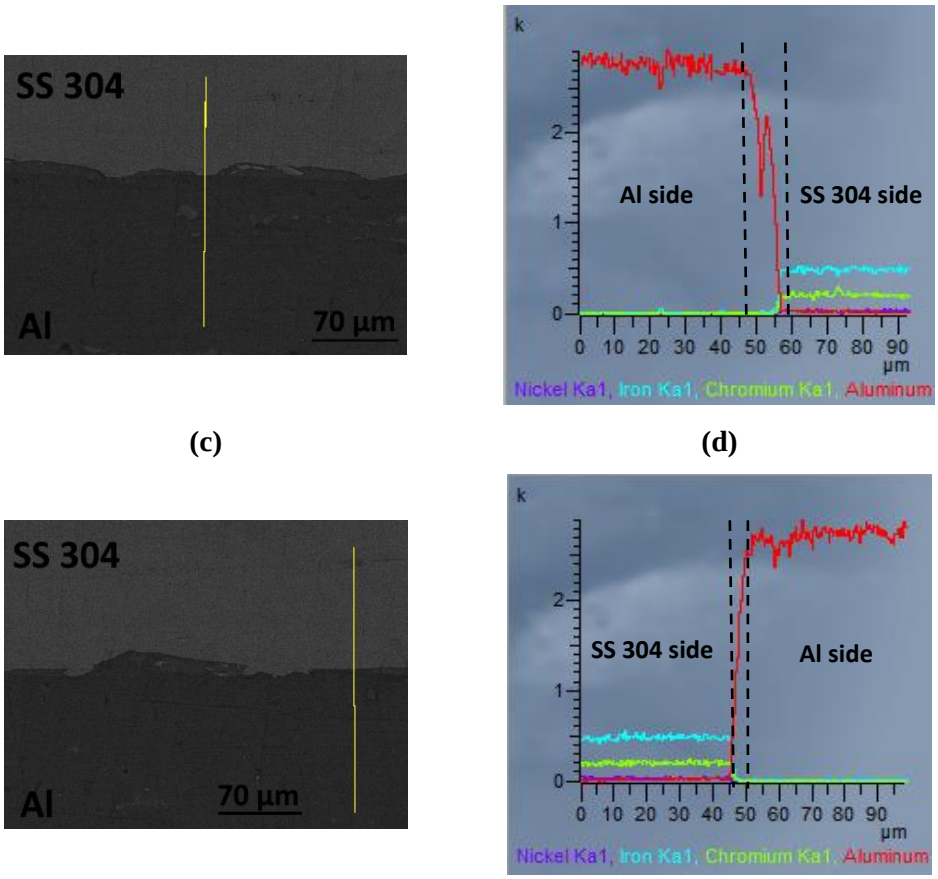

Fig. 82 SEM and EDS of welded interface for the weld created between Al-SS 304 members using MPW

In MPW the formation of IP is inevitable as suggested by literature [74]. Researchers have found out that if the welded interface shows a wavy appearance, the intermetallics formed are mainly concentrated the crests of the waves (so called "melt pockets") and the trough of the waves, whereas if the interface if flat, IP forms a film of thin thickness [74]. These facts have also been observed in the present investigation. The EDS line scan conducted over the crest and trough of the waves (Figs. 82 (a) and (c)) in the wavy zone of the interface shows presence of a thicker IP (9 µm and 12 µm) (Figs. 82 (b) and (d)), whereas the line scan performed across the flat interface (Fig. 82 (e)) shows presence of a thinner IP with a width of 5 µm. The formation of the intermetallic phase is likely due to the local heating, melting, and rapid solidification in the interface [148]. The chances of IP formation increases with increase in discharge energies while for low discharge energies a relatively thin IP is formed. It has been found out by researchers that an IP with film thickness of around 5 microns leads to a very good bonding. For a thickness in and around 5 microns the IP rarely contains any

macro cracks, voids or pores. In the present study, an IP with a width of 5 μm was seen in the transition zone across the flat interface devoid of any cracks, voids or pores. For higher discharge energies the maximum thickness of the IP can increase above 25 microns which is detrimental to the weld quality and strength [74]. However in the present study the IP had a maximum thickness of around 10-12 μm and thus the interface is free from any detrimental effects. The presence of thicker IP is usually observed for an interface exhibiting a wavy appearance. In the present study a thicker IP produced at the so called "melt pockets" (wave crests) and the wave trough (Figs. 82 (b) and (d)) led to increase of temperature of steel locally as well as leading to a higher content of constituent elements of steel in the IP as observed from Fig. (81). It can be concluded that some intermetallics, such as $FeAl_3$ is likely to have formed in this region and other similar parts of the diffusion zone. Fig. 83 shows the scanning electron image of an Al-SS 304 welded interface. In this micrograph, SS 304 appears bright and Al dark and fragments in grey stand out in the corner of the wave vortex. The grey regions are the mixtures of the base metals SS 304 and Al and show the concentration of IP at the wave pockets. The diffusion of constituent elements from one mating member to the other also plays a part in the IP formation.

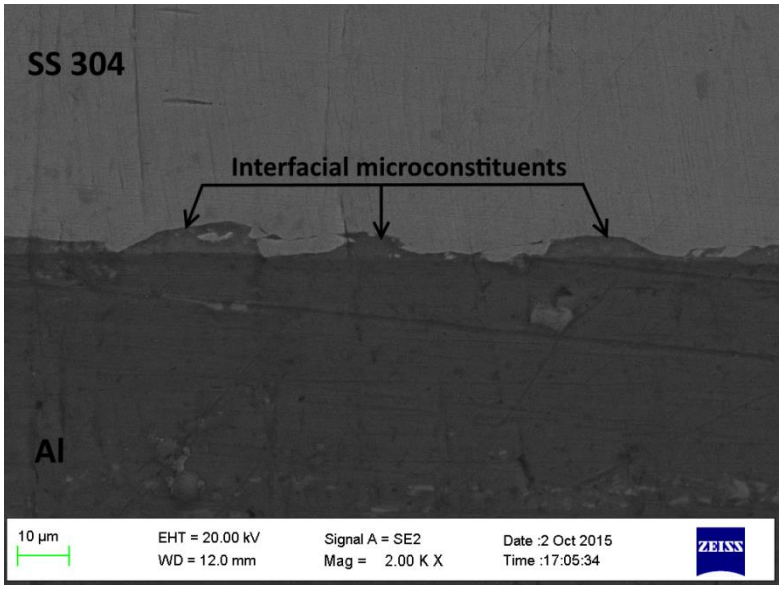

Fig. 83 scanning electron image showing regions (wave pockets) where IP formation is present

The presence of IP of varying width has already been observed in this investigation and the same has been confirmed through the EDS line scan results (Figs. 82 (b), (d), (f)). The nature of the interface (flat or wavy) largely decides the IP width

which then decides the quality of the weld. The hardness increase on both sides of the interface as seen in Fig. 77 also depends largely on the width of the IP. Figs. 84 (a), (b) and (c) show the presence of IP with varying width along the length of the welded portion proving the fact that bonding quality and the diffusion of elements across the members varied widely along the length of the bonded zone. Fig. 84 (a) shows the interface of Al-SS 304 weld with a near flat shape accompanied by a very thin IP as stated earlier. Figs. 84 (b) and (c) show presence of a wavy interface with increasing amplitude. The width of the IP varies directly with the wave amplitude and a clear increase is observed in the width of IP as the wave amplitude increases. It can also be observed that the distribution of intermetallics was not even along the length of the interface

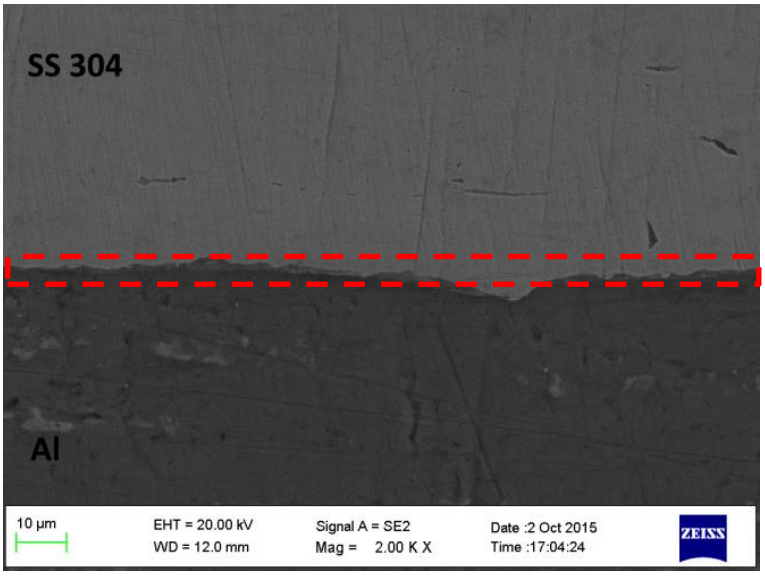

(a)

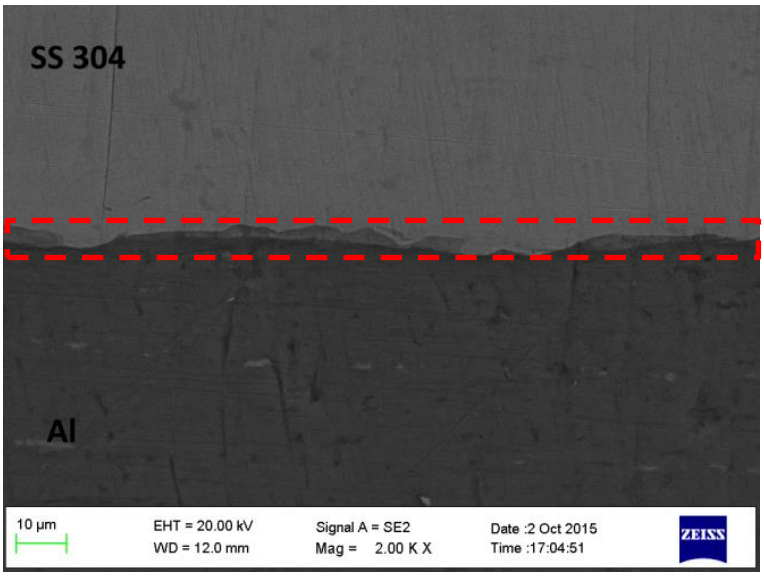

(b)

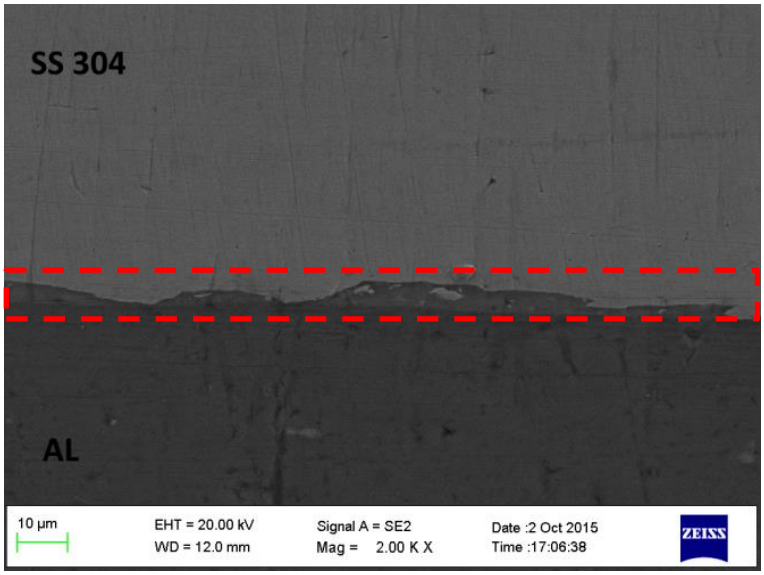

(c)

Fig. 84 Micrographs of the MPW joint: (a) with very thin diffusion zone; (b) with narrow diffusion zone and (c) with wide diffusion zone.

In has been concluded by many researchers in the past that the wavy appearance is a pre requisite to a successful bond, however it has been proved recently [74] that the formation of wavy interface does not guarantee a high quality bond. On the contrary, the best weld quality is achieved if a very thin intermetallic film, whose thickness does not exceed 5 microns, is formed. In the welds without wavy interfaces perfectly bonded zones exist without any detrimental disturbances and defects. In the transition zone the flat interface is correlated with the high-bonding-strength zone. However it is

very difficult to achieve a thin IP (small wavy morphology) along the entire length of the weld as localized interfacial melting seems to be a prerequisite for a successful bond. The formation of pulse welds between Al and SS 304 used in the present study appears to be largely caused by interfacial heating.

It has been stated in literature [63] that mechanical interlocking aids the process of bonding in MPW. A high speed collision leads to the formation of a discontinuous interface (mostly wave), where vortices of the waves take part in mechanical interlocking and the same acts as a joining mechanism [63] (Fig. 85). The wavy morphology increases the intimate contact area and forms the interlocking between two metal surfaces for strong joining [94]. In line with other processes successful and sound electromagnetic welds will be characterized by the proper amount of intermetallic phases and interlocking. In the present study the interlocking was most likely promoted by the relative low strength and high ductility of Al compared to SS 304. Mechanical interlocking caused by the plastic deformation at the interface and formation of IP appear to be the primary factors dictating properties of MPW joints. The vortex wave forms a pocket-shaped interface shown in the micrograph of Fig. 85.

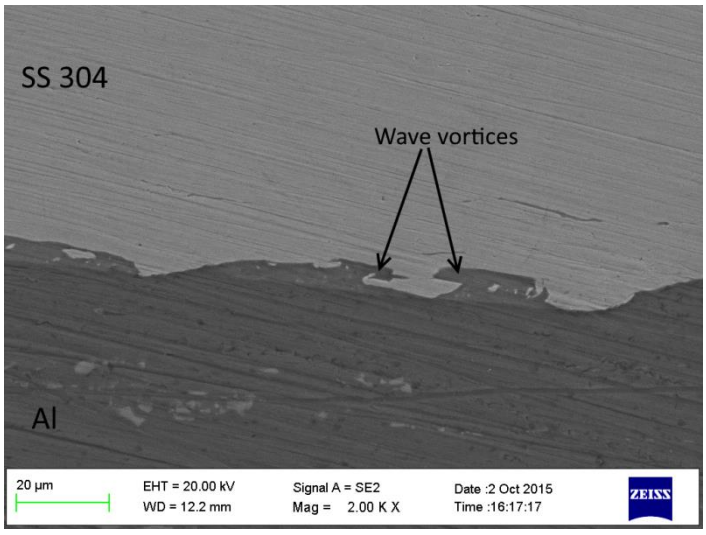

Fig. 85 Scanning electron image of vortex formed during MPW of Al–SS 304

The experimental results (optical imaging and scanning electron microscopy) have much similarity with the FEM developed in the previous chapter. Both the FEM and experimental results show similar weld interface characteristics which are in complete agreement with the available literature. It is clear from Figs. (78 and 79) that a tubular magnetic pulse welded joint has separate bond and no-bond zones. The same has been well predicted by the FEM (Fig. 41) which validates the same. The micrographs (Fig.

48 (a)) clearly show the presence of a characteristic wavy pattern at the weld interface which the FEM also has been able to predict upto great similarity (Fig. 48 (b)). The closeness in the results predicted by the FEM gives the end user the confidence to use to predict suitable process parameters for successful welding at the same making the model practical and shop floor applicable. The following chapters discuss the main conclusions of the present work and possibility of further investigation in MPW respectively.

Chapter 5

Conclusions

High velocity impact welding technologies like MPW are important because they can be easily applied in typical manufacturing environments, and therefore offer new prospects for dissimilar material welding. MPW is a complex combination of electromagnetism, mechanics and impact welding. The process has been on the growth in the last decade and over the next few years, the further development of this process will allow for a standard implementation in different industries. With advancement in technology and rising demand for newer environmentally friendly welding techniques, the MPW equipment is being made more reliable, cheap, safer, durable and user friendly. Introduction of in situ process control techniques e.g. programmable logic controller (PLC), PDV system etc. have helped the end user to have a better control on the process. The process is capable of welding a large variety of similar and dissimilar metals in microseconds without the use of filler materials, emission of shielding gases or much preparation of the workpieces. MPW is affected by a large number of parameters and the interpretation of the effect of all the parameters is often difficult, as they influence the process through several physical phenomena.

The objective of the current chapter is to describe the major conclusions drawn from the thesis. The succeeding chapter discusses the possibilities ahead for research in MPW. The investigation carried out during the present study result in some generic and specific conclusions. The following section lists these conclusions.

5.1 Generic and specific conclusions

The modelling of the MPW process through FEA and ANN has resulted in some generic conclusions listed as follows:

- Finite element models developed in this study help predict accurate values of weld validation criteria for a wide range of process parameters and for different combinations of similar and dissimilar materials with varying geometry. The demonstrated methodology of developing a weldability window

(single criteria/ multi-criteria) through FEA would save cost and time spent in production of product using MPW.

- Statistical modelling processes like regression analysis are unable to capture the multivariable nature of the MPW process. The impact velocity can be predicted more accurately by ANN model as compared to the statistical model.
- Predictive modelling of weld validation criteria i.e. impact velocity using ANN provides practical and shop-floor applicable models. The models are validated in the present study and are found to be precise for implementation at shop floor.
- The development of an ANN model provides an alternative to statistical and mathematical modelling. The major advantage of ANN over statistical and mathematical models is that a single ANN model can handle quantitative as well as qualitative process parameters. It can also accurately and quickly predict results for a large data set which would otherwise consume lot of time and effort when done through experiments or finite element modelling.
- Sensitivity analysis provides feedback as to which input channels are the most significant thereby helping the user to prune the input space by removing the insignificant channels. Sensitivity analysis provides a way of quantifying the effect of process parameters over the entire chosen range and helps understand the precedence of process parameters.
- A successful weld occurring in MPW depends upon the specific material and process parameters chosen. For a given material and geometry, a weld can be achieved by different combinations of process parameters. The same range of process parameters may not result into a successful weld with other materials. In other words the process is material, geometry and parameter specific. In MPW the flyer workpiece velocity and subsequently the kinetic energy imparted to the flyer workpiece must be high enough to obtain a successful bond.
- Simulation of complex phenomena occurring during MPW, lack of literature on coil design and cost estimation are some of the issues that need to be addressed in order to successfully apply MPW in more technologically challenging situations.

In addition to the above stated generic conclusions, some specific conclusions have been reached at, and are listed below:

- The numerically computed impact velocities by the developed FEM were within the within a range of ±10% variation ascertaining the validity of the model and making it shop floor applicable.
- A pulse welded tubular joint was found to consist of distinct bonded and unbonded zones through experiments. The presence of a bonded centre zone and unbonded zones viz. run-in zone and run-out zone respectively on either side of the centre zone was well predicted by the FEM and the same was in agreement with the experimental results.
- The MPW joint showed a wavy pattern at the impact zone. The FEM developed for the present study also predicted similar results and clearly showed a wavy morphology at the interface of the two mating members.
- Two different types of weldability windows were developed for different material combinations and type of MPW process employed. The first considered only impact velocity as the weld criteria. It was found that compression welded members dominated the range of values crossing the threshold over the expansion joints. The second type employed all the available weld criteria viz. impact velocity, effective plastic strain and the direction and magnitude of the shear stress. It was found that all the three criteria have a significant role in MPW of tubular joint. Existence of process parameters which can simultaneously satisfy the three foregoing criteria is non-trivial. A comprehensive approach considering each of the foregoing weldability criteria for MPW should be adopted.
- Regression models for impact velocity employing best subset selection in multiple regression were developed for the two material combinations viz. Al-SS 304 and AA 2219-SS 321chosen for the present study. The best coefficient of determination values were obtained for a total number of 19 and 20 terms for the two developed models which indicated that the data was over-fitted. It was found that none of the models could predict data where error was in the ± 10% variation range.
- The impact velocity in MPW was modelled within ±10% variation for the two material combinations chosen with ANN modelling. Multilayer modular feed forward networks were developed in the present study and the same were able to accurately model the effect of the weld validation criteria viz. impact velocity; however, they required much iteration to get trained.

- For both the material pair's viz. Al-SS 304 and AA 2219- SS 321, the parameters viz. coil c/s area, coil turns, voltage and air gap affected the process in a major way. The effect of coil c/s area, coil turns and voltage was more profound for AA 2219-SS 321material pair, while air gap affected the process more in Al-SS 304 pair. Two other parameters viz. coil length and resistance had a moderate effect on the process for Al–SS 304 pair while the same parameters had a negligible effect for AA 229- SS 321 material combination. All other parameters had a negligible effect on the MPW process as predicted by sensitivity analysis in the ANN.
- A case study to better understand the developed neural networks and to present its applicability in shop floor applications of MPW was conducted for Al-SS 304 material pair. The conducted case study helped the user to identify the exact combination of process parameters at which the impact velocity i.e. the weld validation criteria was satisfied.
- Two different sets of material combination were used for producing the welds in the present study viz. AA 2219-SS 321and Al- SS 304. All the AA 2219-SS321 joints failed and no visible bonding was observed among the mating members. A limitation on the electrical parameters viz. voltage, capacitance, frequency and inductance and material parameters viz. skin depth led to the failure of the joints. In future the same material combination and geometry would be tried again with necessary changes and modifications made with the available equipment.
- The Al-SS 304 MPW joint subjected to lap shear tests resulted in fracture occurring out of the welded region and broke at the weaker of the base metals i.e. pure Al. The ultimate tensile strengths of the MPW samples were greater than that of the weaker of the base metals i.e. Al. Maximum pull-off strength of 111 MPa corresponding to a pull-off force of 1.697 kN was obtained for the joint.
- There was considerable increase in the hardness values in and around the interface zone of the Al-SS 304 joint similar to the results given in literature with the highest value of 302 HV recorded near the interface on SS 304 side which is attributable to the severe plastic deformation of the base metal in the interface that contributes to serious work hardening and grain refinement. In addition, some kind of high hardness IP produced in the transition zone might

result in the higher hardness value than the base metals. It can be concluded that some intermetallics, such as $FeAl_3$ is likely to have formed in this region and other similar parts of the diffusion zone.

- The OM and FESEM micrographs of the Al-SS 304 joint showed presence of a welded centre zone with a characteristic wavy pattern at the interface proving the weldability of the joint using MPW. The length and amplitude of the waves evolved along the welding direction and the wavy interface was followed by a somewhat flat-end region. The amplitude of the wave is highly reliant on collision angle and its dependency on collision velocity is negligible. It is clear from the experiments that welding did not take place over the entire length of the sample.
- From the optical and scanning electron images, it is evident that the wave formation was more pronounced in the mid region than the beginning and end of the welded interface, where the bonding was minimal. The surface EDS map of the Al-SS 304 joint gave clear evidence of material transfer between the two base materials at the crests and troughs of the waves. The transfer of material between the flyer and base materials resulted into several phenomena, one of them being the increase in hardness in the interface layer or transition zone, the other being the formation of IP at the weld interface.
- The EDS line scan conducted over the crest and trough of the waves in the wavy zone of the interface showed presence of thicker IP (9 μm and 12 μm) whereas the line scan performed across the flat interface showed presence of a thinner IP with a width of 5 μm. In the present study a thicker IP produced at the so called “melt pockets” (wave crests) and the wave trough led to increase of temperature of steel locally as well as leading to a higher content of constituent elements of steel in the intermetallic phase.
- The welded bonds in the present investigation were aided by mechanical interlocking. The wave vortices took part in mechanical interlocking and the same acted as a joining mechanism.
- The experimental results (optical imaging and scanning electron microscopy) have much similarity with the developed FEM. Both the FEM and experimental results showed similar weld interface characteristics which are in complete agreement with the available literature.

Chapter 6

Future research directions

Until date, the use of MPW as a potential and economically feasible technology in industries has been very limited. This can be attributed to the fact that there remain a lot of open queries and unanswered problems, which incites the necessity for additional research work. Some of the open questions and unsolved problems together with future research directions are listed below:

- At present tools that facilitate the user to assess the viability of a special industrial task by means of MPW are very limited. To make such an assessment and estimating accurate process dimensioning together with robust process design requires experience and technical expertise. Finite element software packages that are user friendly and can make accurate predictions regarding feasibility of the process are very limited. The commercially available software packages can be used to make simple 2-dimensional or simple 3-dimensional models of the process and are mostly not able to model complex industrially relevant applications. Some researchers have been able to model complex problems relating to MPW but even those require extremely long calculation time, making them economically unviable.
- FEA based simulation for MPW must include thermodynamic simulation at micrometer scale to understand the short range diffusion and phase transformation along the welded interface during high pressure impact.
- The electromagnetic coil is one of the major components of an MPW system. Very limited literature is available which talk about coil design and ways to enhance coil lifetime. Recently, some literature has been reported which suggest ways to enhance the durability of the coil and some encouraging results have been stated, but they still talk about special case studies. Thus, explicit studies and development of guidelines for coil design are required.
- The weld quality evaluation methods should be further optimised as none of the evaluation methods suggested in literature can confirm the weld quality with 100% certainty. Several tests are mentioned in the literature, but so far

there are no international specifications defining the quality control of the MPW process. Further research on this subject is strongly recommended.

- The measurements of the wave pattern should be compared to the finite element simulations. Hence, the influence of different process parameters on the wavelength and amplitude can be further investigated.
- Development of suitable weldability windows and weldability criteria specific to MPW for a varying material combination and geometry of mating members needs to be carried out. A multi-scale study would be required to fully determine the interchangeability of process windows developed from this tool to other impact welding techniques.
- Although researchers have carried out MPW for varying material combination and process parameters, sufficient studies are needed to be carried out in order to properly understand the welding mechanism and its relationship with the process parameters. Further tests are necessary to completely understand the effect of process parameters on the joint strength, weld quality and integrity, weld length, joint metallurgy and the interface properties.
- Development of instrumental measurement for the spatial and temporal temperature changes during impact welding is necessary which would the help understand the microstructure evolution. Further research is still required to continue detailing the microstructural changes in the parent materials and the mechanical properties of dissimilar welds. Further Transmission electron microscopy (TEM) work is required to study the structure of the mixture along the welded interface.
- The formation of IP at the welding interface in MPW is inevitable and is partly connected with the structure of the interface. An extensive study regarding the composition, structure, arrangement and extent of the intermetallics formed must be carried out. Until now it is not clear if the intermetallic films in the weld regions are too thin to be properly detected by metallographic methods. For this reason TEM investigations of the weld interface must be carried out in future work. Special attention should be paid to melting zones and IP, and whether these are or aren't influenced by the process parameters.
- The implementation of stricter environmental protection laws by various environmental protection societies and the rising gas prices has driven the need of application of lightweight construction concepts. Reduction of product

weight requires an eclectic mix of dissimilar materials, which need to be joined to each other. The most applicable material for each distinct element has to be recognized and applied. However, this makes the design highly complex and realization of such complex components through conventional welding processes is very difficult. Thus, the need for innovative and technologically and economically viable joining processes has become the need of the hour. The use of electrically conductive materials such as aluminium alloys is most evident in lightweight manufacturing concepts, thus making MPW an encouraging technology.

- The success of MPW as an industrially viable process depends upon technologically and economically oriented aims. The use of MPW as an alternative to conventional processing technologies in order to process materials that are difficult to be achieved by other methods and simultaneously reduce production costs has to be the prime focus for researchers in this technologically driven modern era. In future MPW can be successfully applied to those circumstances that are technologically driven. The widespread application of MPW in industries combined with ongoing investigative studies can definitely solve the problems currently unsolved and answer all the questions. To endorse this technology, successful enactments in manufacturing for which MPW is especially suitable should be published. In the end, the newly gathered experience will contribute to a favourable implementation of MPW in those cases that are economically driven.
- The manufacturing sector in today's time is cost oriented. Sufficient calculations to determine the underlying costs of running the process have become very necessary keeping in mind the efficiency of the process. Some people have worked in this regard but the few specifications available contradict each other, as the process itself is strongly influenced by a large number of parameters. Investigative studies bearing in mind the energy transfer in the course of the process is must to make the process economically viable, but here ample parametric studies are crucial to construct a trustworthy database [78].

References

[1] Zhang, Y., Babu, S.S, Prothe, C., Blakely, M., Kwasegroch, J., LaHa, M. and Daehn, G.S. 'Application of High Velocity Impact Welding at Varied Different Length Scales', *J. Mater. Process. Tech.*, 2011, **211**, 944–952.

[2] Weddeling, C., Woodward, S., Nellesen, J., Psyk, V., Marre, M., Brosius, A., Tekkaya, A. E., Daehn, G. S. and Tillmann, W. 'Development of design principles for form-fit joints in lightweight frame structures', Proc. of the 4th Int. Conf. on High speed forming , March 9th - 10th, 2010 , Columbus, Ohio, USA.

[3] Shribman, V. 'Magnetic pulse welding of automotive HVAC parts', 2007, Pulsar Ltd.

[4] Stern, A. and Aizenshtein, M. 'Bonding zone formation in magnetic pulse welds', *Sci. Technol. Weld. Joi.*, 2002, **7(5)**, 339-342.

[5] Aizawa, T., Kashani, M. and Okagawa, K. 'Application of Magnetic Pulse Welding for Aluminum Alloys and SPCC Steel Sheet Joints', *Weld. J.*, 2007, **86**, 119-124.

[6] Shribman, V. 'Magnetic Pulse Welding of Automotive HVAC Parts', Pulsar-Magnetic pulse solutions, 2007, 1-31.

[7] Epechurin, V.P. 'Properties of bimetal joints by magnetic pulse welding', *Weld Prod.*, 1974, **21(5)**, 4–12.

[8] Watanabe, M. and Kumai, S. 'Interfacial Morphology of Magnetic Pulse Welded Aluminum/Aluminum and Copper/Copper Lap Joints', *Mater. Trans.*, 2009, **50(2)**, 286-292.

[9] Casalino, G. and Ludovico, A.D. 'Finite element simulation of high speed pulse welding of high specific strength metal alloys', *J. Mater. Process. Tech.*, 2008, **198**, 301–305.

[10]Raoelison, R.N., Buiron, N., Rachik, M., Haye, D. and Franz, G. 'Efficient welding conditions in magnetic pulse welding process', *J. Manuf.*, 2012, **14**, 372-377.

[11] Kore, S.D., Date, P.P. and Kulkarni S.V. 'Electromagnetic impact welding of aluminum to stainless steel sheets', *J. Mater. Process. Tech.*, 2008, **208**, 486-493.

[12] Tomas, B.M.C. 'Magnetic Pulse welding MPW', PhD thesis, Universidade Nova de Lisboa, Lisbon, Portugal, 2010.

[13] Kore, S.D., Date, P.P. and Kulkarni, S.V. 'Effect of process parameters on electromagnetic impact welding of aluminum sheets', *Int. J. Impact Eng.*, 2007**, 34**, 1327–1341.

[14] Desai, S.V., Kumar, S., Satyamurthy, P., Chakravartty, J.K. and D.P. Chakravarthy, 'Analysis of the effect of collision velocity in electromagnetic welding of aluminum strips', *Int. J. Appl. Electrom.*, 2010, **34**,131-139.

[15] Kleiner, M., Beerwald, C. and Homberg, W. 'Analysis of Process Parameters and Forming Mechanisms within the Electromagnetic Forming Process', *CIRP Ann. Manuf. Technol.*, 2005, **54**, 225-228.

[16] Masumoto, I., Tamaki, K. and Kojima, M. 'Electromagnetic welding of aluminium tube to aluminium or dissimilar metal cores'. *Trans. Jpn. Weld. Soc*., 1985, **16(2)**, 110-116.

[17] Kamal, M. 'A Uniform Pressure Electromagnetic Actuator for Forming Flat Sheets', Master's thesis, The Ohio State University, 2005.

[18] Broeckhove, J. and Willemsens, L. 'Experimental research on magnetic pulse welding of dissimilar metals', Master's Thesis, Ghent University, Ghent, Belgium, 2009-2010.

[19] Aizawa, T. and Kashani, M. 'Magnetic Pulse Welding (MPW) Method for Dissimilar Sheet Metal Joints', Tokyo metropolitan college of technology, Department of Electronic and Information Engineering, 2004, Tokyo, Japan.

[20] Miranda, R. M., Tomas, B., Santos, T. G. and Fernandes, N. 'Magnetic pulse welding on the cutting edge of industrial applications' *Soldag. insp. [online]*, 2014, **19(1)**, 69-81.

[21] Marya, M., Marya, S., and Priem, D. 'On the Characteristics of Electromagnetic Welds between Aluminium and other Metals and Alloys', *Weld World,* 2005, **49(5-6)**, 74-84.

[22] Faes, K., Tube welding, 2011, https://www.researchgate.net/publication/ 230757399 Electromagnetic pulse tube welding (sited 17/7/2014).

[23] Daehn, G.S., 2006. ASM Handbook, Metalworking: Sheet Forming- Appendix D. ASM International, **14 (b)**, 405-418.

[24] Wonterghem, and Vanhulsel, P. 'Magnetic pulse crimping of mechanical joints', Master's thesis, Ghent University, 2010-2011.

[25] Pulsar Ltd., MPW 50 25 Magnetic Pulse System, User guide.

[26] Vaidyanathan, P.V. and Ramanathan, A.R. 'Design for quality explosive welding', *J. Mater. Process. Tech.,* 1992, **32**, 439-448.

[27] Grignon, F., Benson, D., Vecchio, K. S. and Meyers, M. A. 'Explosive Welding of Aluminum to Aluminum: Analysis, Computations and Experiments', Proc. 13th APS Topical Conference on 'Shock Compression of Condensed Matter', Portland, Oregon, USA, July 2004, 1098-1101.

[28] Cowan, G.R., Bergmann, O.R. and Holzman, A.H. 'Mechanism of bond zone formation in explosion-clad metals', *Mater. Trans.,* 1971, **2**, 3145–55.

[29] Markashova, L.I., Arsenyuk, V.V. and Grigorenko, G.M. 'Relationship governing plastic deformation in pressure welding dissimilar metals', *Weld Int.,* 2005,**19(1)**, 68–72.

[30] Ben-Artzy, A., Stern, A., Frage, N. and Shribman, V. 'Interface phenomena in aluminum–magnesium magnetic pulse welding', *Sci. Technol. Weld. Joi.,* 2008, **13(4)**, 402–409.

[31] Watanabe, M., Kumai, S., Hagimoto, G., Zhang, Q. and Nakayama, K. 'Interfacial Microstructure of Aluminum/Metallic Glass Lap Joints Fabricated by Magnetic Pulse Welding', *Mater. Trans.* 2009, **50**, 1279-1285.

[32] Watanabe, M., Kumai, S., Okagawa, K. and Aizawa, T. 'In-situ observation of magnetic pulse welding process for similar and dissimilar lap joints using a high-speed video camera', Proc. 11th Int. Conf. on 'Aluminium alloys', Aachen, Germany, 2008, 1992–1997.

[33] Lee, K.J., Kumai, S., Arai, T. and Aizawa, T. 'Interfacial microstructure and strength of steel/aluminum alloy lap joint fabricated by magnetic pressure seam welding', *Mat Sci Eng A-Struct,* 2007, **471**, 95-101.

[34] Bazdenkov, S. V., Demichev, V. F., Morozov, D. K. and Pogutse, O. P. 'Possible mechanism Possible mechanism of wave formation in explosive welding', *Combust. Explo. Shock,* 1985, **21(1)**, 124–130.

[35] Zlobin, B. S. 'Explosion Welding of Steel with Aluminum', *Combust. Explo. Shock.,* 2002.

[36] Shribman, V. 'Magnetic Pulse Welding for Dissimilar and Similar Materials', Proc. 3rd Int. Conf. on 'High Speed Forming', Dortmund, Germany, March 2008, University of Dortmund, 13-22.

[37] Reid, S. R. 'Wake instability mechanism for wave formation in explosive welding', *Int. J. Mech. Sci.,* 1978, **20(4)**, 247–253.

[38] Holtzman, A.H. and Cowan, G.R. 'Bonding of metals with explosives', *Weld. Res. Counc. Bull.,* 1965, **21**, ISBN: #1-58145-103-2.

[39] Hampel, H. and Richter, U. 'Formation of interface waves in dependence of the explosive welding parameters', Proc. Int. Conf. on 'High energy rate fabrication', Leeds, UK, 1981, 89–99.

[40] Ben-Artzy, A., Stern, A., Frage, N., Shribman, V. and Sadot, O. 'Wave formation mechanism in magnetic pulse welding', *Int. J. Impact Eng.,* 2010, **37,** 397-404.

[41] Hokari, H., Sato, T., Kawauchi, K. and Muto, A. 'Magnetic impulse welding of aluminum tube and copper tube with various core materials', *Weld Int.,* 1998, **12(8)**, 619–626

[42] Reid, S. R. and Sherif, N.H. 'Prediction of the wavelength of interface waves in symmetric explosive welding', *J. Mech. Eng. Sci.*, 1976, **18(2)**, 87-94.

[43] Lucas, W., Williams, D.J. and Crossland, B. 'Some metallurgical observations on explosive welding', Proc. 2nd Int. Conf. on 'High energy forming', Denver, USA, 1969, 22–37.

[44] Reid, S. R. 'A discussion of the mechanism of interface wave generation in explosive welding', *Int. J. Mech. Sci*., 1974, **16**, 399-413.

[45] Hunt, M. 'Wave formation in explosive welding', *Phil. Mag.*, 1968, **17(148)**, 669–680.

[46] Robinson, J.L. 'The mechanics of wave formation in impact welding', *Phil. Mag.*, 1975, **31(28)**, 587–597.

[47] Chadwick, M.D. and Jackson, P.W. 'Explosion welding in planary geometry', Proc. 6th Int. Conf. on 'High energy rate fabrication', Essen, Germany, 1978.

[48] Bahrani, A.S., Black, T.J. and Crossland, B. 'The mechanism of wave formation in explosive welding', *Weld Process Roy. Soc.*, 1967, **A296**, 123–36.

[49] Kore, S.D., Dhanesh, P., Kulkarni, S.V. and Date, P.P. 'Numerical modeling of electromagnetic welding', *Int. J. Appl. Electrom.*, 2010, **32**, 1–19.

[50] Jassim, A. K. 'Magnetic Pulse Welding Technology', Proc. 1st Int. Conf. on 'Energy, Power and Control (EPC-IQ)', Basrah, Iraq, December 2010, University of Basrah, 363-373.

[51] Jassim, A.K., 'Comparison of Magnetic Pulse Welding with Other Welding Methods', *Journal of Energy and Power Engineering*, 2011, **5**, 1173-1178.

[52] Livshiz, Y. and Gafri, O. 'Technology and equipment for industrial use of pulse magnetic fields, Pulsar, 1999, 475-478.

[53] Raoelison, R.N., Rachik, M., Buiron, N., Haye, D., Morel, M., Sanstos, B. D., Jouaffre, D. and Frantz, G. 'Assessment of Gap and Charging Voltage Influence on Mechanical Behaviour of Joints Obtained by Magnetic Pulse Welding', Proc. of the 5th Int. Conf. on 'High Speed Forming', Dortmund, Germany, 2012, 207-216..

[54] Chelluri, B. and Knoth, E. ‘Powder forming using Dynamic Magnetic compaction’, Proc. of the 4th Int. Conf. on ‘High speed forming’, Columbus, USA, 2010, 26–34.

[55] Shribman, V. and Blakely, M, ‘Benefits of magnetic pulse process for welding dissimilar metals’, *Weld. J.,* 2008, **87(9)**, 56-59.

[56] Weber, A. ‘The cold welding process is being used for more and more high volume applications’, *Assembly Mag.,* 2002.

[57] Shribman, V. and Spitz, B. ‘Magnetic pulse welding for tubular applications: Discovering new technology for welding conductive materials’, *The Tube & Pipe Journal*, July 2001.

[58] Hirose, S., Itoh, T., Makita, M., Fujii, S., Arai, S., Sasaki, K. and Saka, H. ‘Defect structure of deformed Fe_2Al_5 intermetallic compound’, *Intermetallics*, 2003, **11(7)**, 633-642.

[59] SCOPUS documents, http://www.scopus.com.citation, sited 19/3/2014.

[60] Lysenko, D.N., Ermolaev, V.V. and Dudin, A.A. ‘Method of Pressure Welding’, US Patent 3520049, 1970.

[61] Zhang, P. ‘Joining enabled by high velocity deformation’, Ph.D. Thesis, The Ohio state university, 2009.

[62] Zhang, P., Kimchi, M., Shao, H., Gould, J.E. and Daehn, G.S. ‘Analysis of the electromagnetic impulse joining process with a field concentrator’, *Numiform*, 2004, 1253-58.

[63] Marya, M. and Marya, S. ‘Interfacial microstructures and temperatures in aluminum – copper electromagnetic pulse welds’, *Sci. Technol. Weld. Joi.,* 2004, **9(6)**, 541–547.

[64] Shribman, V., Stern, A., Livshitz, Y. and O. Gafri: ‘Magnetic pulse welding produces high strength aluminum welds’, *Weld J*., 2002, **81(4)**, 33–37.

[65] Aizawa, T. and Okogawa, K. ‘Impact seam welding with magnetic pressure for Aluminum sheets’, *Mater. Sci. Forum*, 2004, **465**, 231–236.

[66] Zhang, Y., Babu, S.S., Zhang, P., Kenik, E.A., and Daehn, G.S. 'Microstructure characterisation of magnetic pulse welded AA6061-T6 by electron backscattered diffraction', *Sci. Technol. Weld. Joi.*, 2008, **13(5)**, 467–471.

[67] Zhang, Y., Eplattenier, P.L., Geoff, T., Vivek, A., Daehn, G.S. and Babu, S.S. 'Numerical Simulation and Experimental Study for Magnetic Pulse Welding Process on AA6061 and Cu 101 Sheet', Proc. 10th Int. LSDyna Users Conf., 2008.

[68] Kore, S.D., Date, P.P., Kulkarni, S.V., Kumar, S., Kulkarni, M.R., Desai, S.V., Rajawat, R.K., Nagesh, K.V. and Chakravarty, D.P. 'Electromagnetic Impact Welding of Al-to-Al-Li Sheets', *J. Manuf. Sci. E.-T. ASME*, 2009, **131,** 1-4.

[69] Brown, W.F., Bandas, J. and Olson, N.T. 'Pulsed magnetic welding of breeder reactor fuel pin and closures', Proc. of the AWS 59th Annual Meeting , New Orleans, USA. 1978.

[70] Shribman, V., Tomer, Y. 'Magnetic pulse technology for improved tube joining and forming', *Tube & Pipe Technology*, 2006, 91–95.

[71] Hisashi, S., Isao, S., Sherif, R. and Hidekazu, M. 'Numerical study of joining process in magnetic pressure seam welding', *Trans. JWRI*, 2009, **38 (1)**, 63–68.

[72] Uhlmann, E. and Ziefle, A. 'Modelling pulse magnetic welding processes—an empirical approach', Proc. of the 4th Int. Conf. on 'High Speed Forming', 2010, Columbus, USA, 108–116.

[73] Kore, S.D., Imbert, J., Worswick, M.J. and Zhou, Y. 'Electromagnetic Impact Welding of Mg to Al Sheets', *Sci. Technol. Weld. Joi.*, 2009, **14(6)**, 549–553.

[74] Gobel, G., Kaspar, J., Herrmannsdorfer, T., Brenner, B. and Beyer, E. 'Insights into intermetallic phases on pulse welded dissimilar metal joints', Proc. of the 4th Int. Conf. on 'High Speed Forming', 2010, Columbus, USA, 127–136.

[75] Wu, X. and Shang, J. 'An Investigation of Magnetic Pulse Welding of Al/Cu and Interface Characterization', *J. Manuf. Sci. E.-T. ASME*, 2014, **136**, 051002-1- 051002-11.

[76] Nassiri, A., Chini, G. and Kinsey, B. 'Spatial stability analysis of emergent wavy interfacial patterns in magnetic pulsed welding', *CIRP Ann. Manuf. Technol.*, 2014, **63**, 245-248.

[77] Cui, J., Sun, G., Li, G., Xu, Z. and Chu, P. K. 'Specific wave interface and its formation during magnetic pulse welding', *Appl. Phys. Lett.*, 2014, **105**, 221901-1-221901-4.

[78] Psyk, V., Risch, D., Kinsey, B.L., Tekkaya, A.E. and Kleiner, M. 'Electromagnetic forming—A review', *J. Mater. Process. Tech*., 2011, **211**, 787–829.

[79] Uhlmann, E., Prasol, L. and Ziefle, A. 'Potentials of pulse magnetic forming and joining', *Adv. Mat. Res.*, 2014, **907**, 349-364.

[80] Watanabe, M., Kumai, S., and Aizawa, T. 'Interfacial microstructure of magnetic pressure seam welded Al–Fe, Al–Ni, and Al–Cu lap joints', *Mater. Sci. Forum*, 2006, **519–521**, 1145–1150.

[81] Groche, P., Wagner, M.F.X., Pabst, C. and Sharafiev, S. 'Development of a novel test rig to investigate the fundamentals of impact welding', *J. Mater. Process. Tech.*, 2014, **214**, 2009-2017.

[82] Elsen, A., Ludwig, A., M., Schaefer, R. and Groche, P. 'Fundamentals of EMPT welding', Proc. of the 4th Int. Conf. on 'High Speed Forming', Columbus, USA, 2010, 117 126.

[83] Psyk, V., Gershteyn, G., Demir, O.K., Brosius, A., Tekkaya, A., Schaper, M. and Bach, F. W. 'Process analysis and physical simulation of electromagnetic joining of thin-walled parts', Proc. of the 3rd Int. Conf. on 'High Speed Forming', Dortmund, Germany, 2008, 181–190.

[84] Faes, K., Baaten, T., Waele, W. D. and Debroux, N. 'Joining of Copper to Brass Using Magnetic Pulse Welding', Proc. of the 4th Int. Conf. on 'High Speed Forming', Columbus, USA, 2010, 84–96.

[85] Haiping, Y.U., Zhidan, X.U., Zhisong, F., Zhixue, Z. and Chunfeng, L.I. 'Mechanical property and microstructure of aluminum alloy-steel tubes joint by magnetic pulse welding', *Mat Sci Eng A-Struct*, 2013, **561**, 259–265.

[86] Haiping, Y.U., Zhidan, X.U., Wei, J.H., Zhixue, Z. and Chunfeng, L.I. 'Magnetic pulse joining of aluminum alloy−carbon steel tubes', *Trans. Nonferrous Met. Soc. China,* 2012, **22**, s548−s552.

[87] Stern, A., Aizenshtein, M., Moshe, G., Cohen, S.R. and Frage, N. 'The Nature of Interfaces in Al-1050/Al-1050 and Al-1050/Mg-AZ31 Couples Joined by Magnetic Pulse Welding (MPW)', *J. Mater. Eng. Perform.*, 2013, **22**, 2098–2103.

[88] Raoelison, R.N., Racine, D., Zhang, Z., Buiron, N., Marceau, D. and Rachik, M. 'Magnetic pulse welding: Interface of Al/Cu joint and investigation of intermetallic formation effect on the weld features', *J. Manuf.*, 2014, **16**, 427-434.

[89] Kore, S.D., Date, P.P., Kulkarni, S.V., Kumar, S., Rani, D., Kulkarni, M.R., Desai, S.V., Rajawat, R.K., Nagesh, K.V. and Chakravarty, D.P. 'Electromagnetic impact welding of copper-to-copper sheets', *Int. J. Mater. Form.*, 2009, **3**, 117–121.

[90] Berlin, A., Nguyen, T. C., Worswick, M. J. Zhou, and Y. 'Metallurgical analysis of magnetic pulse welds of AZ31 magnesium alloy', *Sci. Technol. Weld. Joi.*, 2011, **16(8)**, 728- 734.

[91] Kumar, S., Desai, S.V. and Chakravarthy, D.P. 'Characterisation of electromagnetic welding equipment', *Int. J. Appl. Electrom.*, 2012, **40**, 293-300.

[92] Aizawa, T., Matsuzawa, K., Okogawa, K. and Ishibashi, M. 'Parallel Seam Welding of Aluminum Sheets by Magnetic Pulse Welding Method with Collision between Metal Jets', *Mater. Sci. Forum*, 2014, **767**, 171-176.

[93] Shim, J.Y., Kang, B.Y., Kim, I.S., Kang, M.J., Park, D.H. and Kim, I.J. 'A study on distributions of electromagnetic force of the dissimilar metal joining in MPW using a FEM', *Adv. Mat. Res.*, 2010, **83-86**, 214-221.

[94] Haiping, Y.U., Zhisong, F. and Chunfeng, L.I. 'Magnetic pulse cladding of aluminum alloy on mild steel tube', *J. Mater. Process. Tech.*, 2014, **214**, 141– 150.

[95] Aizawa, T. and Kashani, M. 'Experimental and numerical study on magnetic pulse welding to improving the life time of one-turn flat coil', Proc. Int. Symposium on Interfacial Joining and Surface Technology (IJST2013), IOP Conf. Series: Materials Science and Engineering, 2014, **61**, doi:10.1088/1757-899X/61/1/012028.

[96] Zaitov, O. and Kolchuzhin, V.A. 'Bitter coil design methodology for electromagnetic pulse metal processing techniques', *J. Manuf.,* 2014, **16**, 551-562.

[97] Shim, J.Y. and Kang, B.Y. 'Distribution of Electromagnetic Force of Square Working Coil for High-Speed', *Mater. Sci. Appl.,* 2013, **4**, 856-862.

[98] Zhidan, X.U., Junjia, C., Haiping, Y.U. and Chunfeng, L.I. 'Research on the impact velocity of magnetic impulse welding of pipe fitting', *Mater. Design*, 2013, **49**, 736–745.

[99] Zhang, Y., Daehn, G.S., Eplattenier, P.L. and Babu, S.S. 'Experimental study and numerical simulation on magnetic pulse welding for pre-flanged AA6061- T6 and Cu101 Sheets', Proc. of the 8th Int. Conf. on 'Trends in Welding Research', Georgia, USA, 2008, 715–720.

[100] Uhlmann, E., Ziefle, A., Konig, C. and Prasol, L., 'Coupled FEM-Simulation of Magnetic Pulse Welding for Nonsymmetric Applications', Proc. 5th Conf. on 'High Speed Forming', Dortmund, Germany, 2012, 303-314.

[101] Miyazaki, M., Sasaki, K. and Okada, M. 'Influence of gap length on collision angle and collision point velocity of magnetic pressure seam welding', *Mater. Sci. Forum*, 2014, **767**, 166-170.

[102] Vivek, A., Liu, B.C., Hansen, S.R. and Daehn, G.S. 'Accessing Collision Welding Process Window for Titanium/Copper Welds with Vaporizing Foil Actuators and Grooved Targets', *J. Mater. Process. Tech*., 2014, **214(8)**, 1583-1589.

[103] Raoelison, R.N., Buiron, N., Rachik, M., Haye, D., Franz, G. and Habak, M. 'Study of the Elaboration of a Practical Weldability Window in Magnetic Pulse Welding', *J. Mater. Process. Tech.*, 2013, **213**, 1348–1354.

[104] Deng, W., Lu, M. and Tian, X. 'Simulation of Explosive Welding with Reasonable Gap Based on ALE Method', *Int. J. Mod. Eng. Res.*, 2013, **3(6)**, 3621-3625.

[105] Ghomi, M.T., Mahmoudi, J., Khalkhali, A. and Liaghat, G., 'Explosive welding of unequal surface using groove method', *T. Can. Soc. Mech. Eng.*, 2012, **36(2)**, 113-125.

[106] Alipour, R. and Najarian, F. ‘A FEM Study of Explosive Welding of Double Layer Tubes’, *World Academy of Science, Engineering and Technology*, 2011, **49**, 801-803.

[107] Chizari, M., Al-Hassani, S.T.S. and Barrett, L.M. ‘Effect of flyer shape on the bonding criteria in impact welding of plates’, *J. Mater. Process. Tech.*, 2009, **209**, 445–454.

[108]Akbari Mousavi, S.A.A., Halvaee, A. and Khanzadeh, R. ‘Experimental Investigations of Explosive Welding of Three-Layer Cylinder Composites-Part 1’, *Mater. Sci. Forum*, 2008, **580-582**, 323-326.

[109] Akbari Mousavi, S.A.A. ‘Numerical Studies of Explosive Welding of Three-Layer Cylinder Composites-Part 2’, *Mater. Sci. Forum*, 2008, **580-582**, 327-330.

[110] Akbari Mousavi, S.A.A. and Al-Hassani, S.T.S. ‘Finite element simulation of explosively-driven plate impact with application to explosive welding’, *Mater. Design*, 2008, **29**, 1–19.

[111] Chizari, M., Al Hassani, S.T.S., Barrett, L.M. and Wang, B. ‘3-D Finite Element Modelling of Water Jet Spot Welding’, Proc. of the World Congress on Engineering, London, U.K., 2007.

[112] Akbari Mousavi, S.A.A. and Al-Hassani, S.T.S. ‘Numerical and experimental studies of the mechanism of the wavy interface formations in explosive/impact welding’, *J. Mech. Phys. Solids*, 2005, **53**, 2501–2528.

[113] Akbari Mousavi, S.A.A., Burley, S.J. and Al-Hassani, S.T.S. ‘Simulation of explosive welding using the Williamsburg equation of state to model low detonation velocity explosives’, *Int. J. Impact Eng.*, 2005, **31**, 719-734.

[114] Krishnan, J. and Kakodkar, A. ‘An experimental investigation into tube to tube-plate welding using the impactor method’, *J. Mater. Process. Tech.*, 1990, **22**, 191-201.

[115] Thibaudeau, E. and Kinsey, B.L., ‘Analytical design and experimental validation of uniform pressure actuator for electromagnetic forming and welding’, *J. Mater. Process. Tech.*, 2015, **215**, 251-263.

[116] Groche, P., Wohletz, S., Brenneis, M., Pabst, C. and Resch F. 'Joining by forming—A review on joint mechanisms, applications and future trends', *J. Mater. Process. Tech.*, 2014, **214**, 1972-1994.

[117] Althoff, J.L., Lorenz, A., Gies, S., Weddeling, C., Goebel, G., Tekkaya, A. E. and Beyer, E. 'Magnetic Pulse Welding by Electromagnetic Compression: Determination of the Impact Velocity', *Adv. Mat. Res.*, 2014, **966-967**, 489-499.

[118] Kapil, A. and Sharma, A.: "Coupled Electromagnetic Structural Simulation of Magnetic Pulse welding", ADVANCES IN MATERIAL FORMING AND JOINING, Edited by Uday Shanker Dixit and R. Ganesh Narayanan, 06/2015, Chapter 13: Pages 255-272; DOI 10.1007/978-81-322-2355-9_13, ISBN: 978-81-322-2354-2.

[119] Kapil, A. and Sharma, A. 'Coupled Electromagnetic Structural Simulation of Magnetic Pulse Welding', Proc. 5th Int. and 26th All India Manufacturing Technology, Design and Research Conference (AIMTDR 2014), Guwahati, Assam, India, Indian Institute of Technology Guwahati, 2014, 249(1)-249(6).

[120] Zhang, Y., Babu, S.S. and Daehn, G. S. 'Impact Welding in a Variety of Geometric Configurations', Proc. 4th Int. Conf. on 'High Speed Forming', Columbus, USA, March 2010, 97-107.

[121] Verstraete, J., Waele, W.D. and Faes, K. 'Magnetic Pulse Welding: Lessons to Be Learned From Explosive Welding', *Sustainable Construction and Design*, 2011, **2(3)**, 458-464.

[122] Haiping Y.U. and Chunfeng L.I. 'Effects of current frequency on electromagnetic tube compression', *J. Mater. Process. Tech.*, 2009, **209**, 1053–1059.

[123] Szekely, G., Henriques, B., Gil, M., Ramos, A. and Alvarez, C. 'Design of experiments as a tool for LC MS/MS method development for the trace analysis of the potentially genotoxic 4-dimethylaminopyridine impurity in glucocorticoids, *Biomed. Anal.*, 2012, **70**, 251-258.

[124] Dejaegher, B. and Heyden, Y.V. 'Experimental designs and their recent advances in set-up, data interpretation, and analytical applications', *J. Pharm. Biomed. Anal.*, 2011, **56,** 141-158.

[125] Lingjian, Y., Songsong, L., Sophia T. and Lazaros, G.P. 'Mathematical Programming for Piecewise Linear Regression Analysis', *Expert Syst. Appl.*, (2015), doi: 10.1016/j.eswa.2015.08.034.

[126] Sharma, A., Arora, N and Mishra, B.K. 'Statistical modeling of deposition rate in twin-wire submerged arc welding', *Proc. IMechE,* 2009, **223**, 851-863.

[127] Yarlagadda, P.K.D.V. and Chiang, E.C.W. 'A neural network system for the prediction of process parameters in pressure die casting', *J. Mater. Process. Tech.*, 1999, **89-90 (3)**, 583-590.

[128] Mathews, P.G. and Shunmugam, M.S. 'Neural-network approach for predicting hole quality in reaming', *Int. J. Mach. Tool. Manu.*, 1999, **39**, 723-730.

[129] Guessasma, S., Montavon G. and Coddet, C. 'Plasma spray process modelling using artificial neural networks; Application to Al2O3-TiO2 (13% by weight) ceramic coating structure', *J. Phys. IV*, 2004, **120**, 363-370.

[130] Son, J.S., Lee, D.M., Kim, I.S. and Choi S.K., 'A study on genetic algorithm to select architecture of an optimal neural network in the hot rolling process', *J. Mater. Process. Tech.*, 2004, **153-154 (3)**, 643-648.

[131] Raj, K.H., Sharma, R.S., Setia, R., Upadhyay, V. and Verma, A.K. 'Modeling of micro end-milling operations with artificial neural networks', *Int. J. Agile Manuf.*, 2006, **9 (2)**, 99-103.

[132] Sterjovski, Z., Pitrun, M., Nolan, D., Dunne, D. and Norrish J. **'**Artificial neural networks for predicting diffusible hydrogen content and cracking susceptibility in rutile flux-cored arc welds', *J. Mater. Process. Tech.*, 2007, **184 (3)**, 420-427.

[133] De, A., Jantre, J. and Ghosh, P.K. 'Prediction of weld quality in pulsed current GMAW process using artificial neural network', *Sci. Technol. Weld. Joi.*, 2004, **9 (3)**, 253-259.

[134] Mendoza, R.A.R., Morales-Menendez R., and Cantu-Ortiz F.J. **'**Neural nets modelling for automotive welding process', Proc. of the IASTED Int. Conf. on Modelling and Simulation, 2005,459-464.

[135] Chang, C.C., Chen, P.L., Chiu, F.R. and Chen, Y.K. 'Application of neural networks and kanos method to content recommendation in web personalization', *Expert Syst. Appl.*, 2009, **36**, 5310–5316.

[136] Hsieh, K.L. 'Employing a recommendation expert system based on mental accounting and artificial neural networks into mining business intelligence for study abroad p/s recommendations', *Expert Syst. Appl.*, 2011, **38(12)**, 14376–14381.

[137] Anderson, J.A. 'An Introduction to Neural Networks', *MIT Press*, 1995.

[138] Reed, R. and Marksii, R.J. 'Neural Smithing: Supervised Learning in Feedforward Artificial Neural Networks, *MIT Press*, 1999.

[139] Vitek, J.M., Iskander, Y.S. and Oblow, E.M. 'Improved ferrite number prediction in stainless steel arc welds using artificial neural network-Part 1: neural network development', *Weld. J.*, 2000, **79(2)**, 33s-40s.

[140] Najafi, H. and Woodbury, K.A. 'Online heat flux estimation using artificial neural network as a digital filter approach', *Int. J. Heat Mass Tran.*, 2015, **91**, 808–817.

[141] Harrington, P.B. 'Sigmoid Transfer Functions in Backpropagation Neural Networks', *Anal. Chem.*, 1993, **65**, 2167-2168.

[142] Li, X., Chen, F., Sun, D. and Tao, M. 'Predicting menopausal symptoms with artificial neural network', *Expert Syst. Appl.*, 2015, **42**, 8698–8706.

[143] Esfe, M.H., Saedodin, S., Sina, N., Afrand, M. and Rostami, S. 'Designing an artificial neural network to predict thermal conductivity and dynamic viscosity of ferromagnetic nanofluid', *Int. Commun. Heat Mass.*, 2015, **68**, 50–57.

[144] Sharma, A. 'Process modeling of twin-wire submerged arc welding' PhD thesis, Indian Institute of Technology Roorkee, India, 2007.

[145] Wylie, H.K., Williams, P.E.G and Crossland, B. 'An experimental investigation of explosive welding parameters', Proc. of Int. Symp. On Explosive Cladding, Czechoslovakia, 1970, 45-67.

[146] Thyobe, K.C., Seest, K. and Alting, L. ‘Explosive welding of tube to tube plates, *Weld. J.*, 1973, **5**, 412-419.

[147] Deribas, A.A., Simonov, V.A. and Zakcharenko, I.D. ‘Investigations on Explosive Welding Parameters for Arbitrary Combinations of Metals and Alloys’, Proc. 6th Int. Conf. of High Energy Rate Fabrication, 1975, **4**, 1024.

[148] Rajani, H.R.Z. and Mousavi, S.A.A. ‘The effect of explosive welding parameters on metallurgical and mechanical interfacial features of Inconel 625/plain carbon steel bi-metal plate’, *Mat. Sci. Eng. A-Struct*, 2012, **556**, 454–464.

Appendix 1

Weight matrix for ANN models of impact velocity (Section 3.6.3)

a) Al - SS 304 material pair

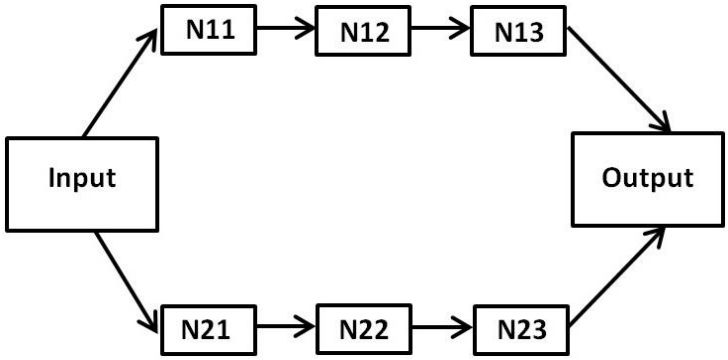

		Weights							
Input to N11	Voltage	0.855	-0.215	1.590	-0.468	0.819	-1.441	-0.798	1.769
	Coil turns	-1.811	-1.155	0.961	0.651	-1.401	1.674	-1.260	-0.208
	Coil length	-1.051	0.200	-0.794	0.528	-1.314	-0.721	-1.262	0.884
	Coil C/s area	-1.378	1.066	-1.883	-0.160	-1.311	1.429	0.792	-1.462
	Capacitance	0.511	0.420	1.559	0.933	0.829	-0.066	-1.426	-0.026
	Frequency	-0.587	1.248	-0.089	-0.647	-0.740	1.135	-1.162	-1.631
	Air gap	1.707	1.871	-0.507	0.028	-0.027	0.142	-0.991	1.165
	Inductance	-1.914	0.838	0.677	-1.989	1.166	-1.474	0.944	0.295
	Resistance	-1.423	-0.960	1.21	1.629	-1.513	-0.865	-0.011	-1.690
Bias		-1.451	1.835	-1.462	0.566	-0.254	-2.031	-1.771	0.480

	Weights					
N11 to N12	1.885	0.685	-1.282	1.495	0.483	1.071
	-0.424	-1.203	1.290	-0.427	0.463	0.504
	-0.749	1.187	0.335	1.874	0.058	-1.368
	1.772	-0.870	0.681	1.359	1.873	-0.282
	1.609	0.854	-0.588	-0.358	-0.211	-1.495
	-0.891	-0.943	-1.448	1.629	1.865	-1.138
	-1.194	-1.377	-1.462	-1.998	0.518	1.913
	-0.993	1.503	1.284	0.791	-0.550	0.110
Bias	-1.908	-0.473	1.093	0.679	-1.887	0.290

	Weights			
N12 to N13	-0.734	-1.139	-0.557	1.449
	1.443	-0.298	-0.743	0.398
	0.112	1.583	-1.371	0.728
	0.151	1.616	-1.810	-1.594
	1.592	-1.606	0.721	1.524
	0.633	-1.341	-1.139	0.017
Bias	0.866	1.167	0.529	1.355

		Weights					
Input to N21	Voltage	0.989	1.841	1.864	-1.327	0.013	1.394
	Coil turns	-1.208	1.440	0.719	-1.326	-1.315	-0.006
	Coil length	1.698	-0.902	1.441	-0.197	-1.603	-1.479
	Coil C/s area	1.153	-1.166	-1.316	1.223	-1.288	-0.101
	Capacitance	0.513	-0.416	-0.523	-0.092	1.278	1.316
	Frequency	-1.331	-0.411	0.134	1.5399	-0.298	-0.800
	Air gap	0.285	1.741	0.764	1.423	0.817	0.653
	Inductance	1.246	1.190	-1.292	-0.658	-1.481	1.276
	Resistance	0.337	-0.657	-0.315	0.265	-1.152	-1.774
Bias		-1.748	-1.451	-1.639	-0.374	1.011	0.223

	Weights			
N21 to N22	-1.187	-1.782	-1.169	-1.496
	-0.555	1.134	-1.938	-1.4914
	0.726	0.045	-1.299	-1.563
	-1.569	-1.931	0.378	-0.138
	1.755	0.940	0.716	1.419
	0.933	0.327	0.1277	0.610
Bias	0.742	-1.117	-1.389	1.767

	Weights			
N22 to N23	-1.033	-1.779	1.774	-1.303
	0.833	0.568	1.039	1.664
	-0.762	-1.063	0.653	0.703

	-1.936	-1.535	-0.404	1.143
Bias	1.618	1.734	1.271	-1.120

	Weights		Weights		Weights
Input to output	-1.690	N13 to output	-0.181	N23 to output	1.246
	-0.865		-1.838		1.067
	-0960		0.701		-1.361
	-1.314		-1.304		1.694
	-0.724				
	-1.015				
	-1.441				
	-0.468				
	-0.160				
Bias	0.651	Bias	1.665	Bias	-1.549

b) AA 2219 - SS 321 material pair

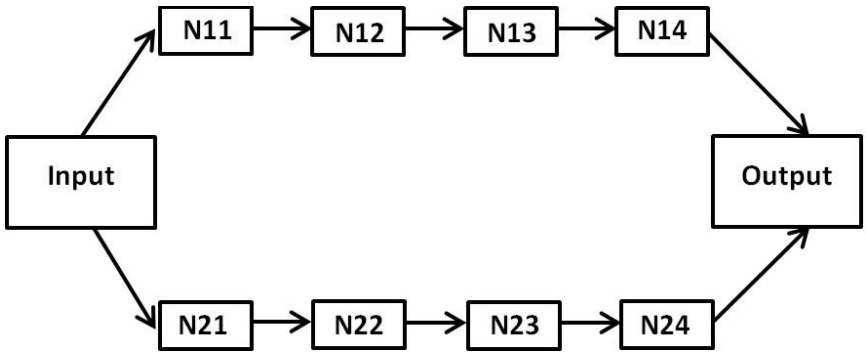

		Weights											
Input to N11	Voltage	-1.033	1.167	0.265	-1.088	-0.037	0.121	0.324	-1.367	-1.540	-1.424	-1.140	0.314
	Coil turns	-1.443	0.061	-0.565	-1.431	0.735	1.046	-0.701	0.192	1.334	-1.134	1.245	1.536
	Coil length	0.964	-1.451	-0.891	1.699	0.732	-1.187	0.895	-0.664	0.220	1.157	1.836	-0.633
	Coil C/s area	0.279	-0.936	1.155	-1.343	-1.575	1.438	-1.898	-0.112	1.147	0.459	-1.528	-0.419
	Capacitance	0.180	0.520	-0.137	-1.318	1.204	0.878	-1.053	0.690	1.797	0.993	0.997	0.419
	Frequency	-1.206	0.244	-1.403	-1.213	1.361	1.526	1.170	1.632	-0.762	-0.007	0.750	0.427
	Air gap	1.413	-0.201	1.062	0.996	1.467	-1.873	1.583	-1.644	0.662	-0.299	-1.265	1.836
	Inductance	-2.032	1.212	0.835	-1.488	-1.729	-0.962	0.219	-1.029	1.674	0.374	1.966	1.930
	Resistance	-0.203	-0.610	1.687	0.865	-0.543	-1.599	-0.354	-1.319	0.390	-1.136	-1.226	1.300
Bias		1.602	-1.814	-1.801	0.947	-1.296	1.021	-0.987	-1.546	-1.901	-1.590	-1.141	-1.948

	Weights							
N11 to N12	-1.591	1.528	-1.418	0.522	-0.631	0.319	-0.220	0.973
	-1.080	1.439	0.008	0.956	-0.450	-1.748	1.302	-1.813
	-1.493	0.450	1.091	-0.206	1.149	1.335	-1.360	1.111
	-0.512	1.973	-0.565	1.141	-0.215	-0.197	1.178	1.256
	-0.045	-1.511	1.558	1.444	-1.550	-1.282	0.848	0.011
	-1.400	-0.317	-1.620	0.394	0.115	0.792	-0.653	-1.125
	1.921	-1.398	-0.962	1.397	0.129	-0.106	0.095	1.481
	0.272	-1.365	-1.829	0.038	-1.484	1.004	0.208	-1.315
	-0.385	-1.326	0.025	-0.600	0.888	1.049	1.174	-0.682
	-1.138	-0.220	-1.414	1.702	-1.463	0.391	1.646	1.584
	0.374	-1.605	-1.541	0.797	0.433	-0.775	1.816	-0.212
	0.361	-0.918	1.540	-1.453	-1.734	-0.124	0.870	-1.062
Bias	-0.640	0.519	1.645	-0.0571	1.499	0.910	-1.178	0.360

	Weights							
N12 to N13	0.557	1.367	1.340	-0.496	-0.684	1.456	1.386	-1.188
	1.493	-1.887	-0.528	-1.905	0.182	-1.673	-1.297	-0.684
	0.746	0.862	1.195	1.221	0.819	-1.411	-0.108	-1.851
	0.437	-1.155	0.363	-1.838	-1.372	1.564	1.710	-1.269
	1.760	0.343	-1.530	0.425	1.042	1.646	-0.200	-1.381
	1.883	-1.354	1.229	0.415	-0.628	-1.761	0.601	-0.692
	1.518	-1.876	-1.985	-0.163	0.062	-0.414	-1.363	1.756
	0.974	-1.929	1.930	1.418	-1.891	-1.110	0.539	-0.045
Bias	1.053	0.657	-0.595	1.551	1.498	-0.934	0.028	-0.742

	Weights					
N13 to N14	-1.119	-0.605	0.905	0.934	0.226	-1.319
	1.978	1.391	0.255	-1.122	-1.391	-1.331
	0.786	-1.477	-1.625	1.577	1.775	-0.809
	0.588	-0.914	1.848	1.111	-0.024	-1.638
	1.628	-0.647	1.034	1.580	-1.945	-1.195
	-1.421	0.445	1.405	0.122	-1.441	1.054
	0.847	-1.596	-1.683	1.183	0.698	-1.409
	-1.550	-1.216	-1.045	0.916	-1.273	-1.620
Bias	0.625	0.327	-1.412	-1.501	0.984	-0.593

		Weights					
Input to N21	Voltage	-1.304	-0.795	0.112	1.432	0.019	-0.911
	Coil turns	0.066	0.294	-0.803	-1.015	0.811	-0.084
	Coil length	-0.600	-1.849	-1.020	-1.089	-1.206	1.422
	Coil C/s area	-0.431	-1.619	-0.712	0.727	-1.353	1.705
	Capacitance	-0.821	-0.617	-1.628	0.813	-1.778	1.026
	Frequency	-1.447	-0.943	0.691	-1.300	0.039	1.034
	Air gap	1.807	0.831	0.865	-0.552	-1.056	-0.088
	Inductance	-1.203	1.346	0.594	0.972	1.109	-0.351
	Resistance	-0.956	0.825	1.319	0.824	1.300	0.804
Bias		1.554	1.260	0.900	0.749	1.177	-0.359

	Weights				
N21 to N22	1.170	1.004	0.107	1.120	-1.078
	1.161	-1.067	0.733	-0.461	-1.710
	1.502	0.780	1.504	1.021	0.947
	0.961	1.771	1.771	0.667	1.735
	-0.147	0.780	-1.912	1.243	-1.089
	-1.455	1.255	0.901	1.189	-1.634
Bias	-1.698	-1.908	-0.992	-1.586	-0.726

	Weights			
N22 to N23	1.099	1.234	0.403	1.459
	0.904	-1.257	1.118	-1.838
	-1.158	-0.721	1.356	1.331
	1.180	1.737	0.354	1.054
	0.876	-1.603	1.690	-1.469
Bias	-0.998	1.452	-1.687	0.499

	Weights			
N23 to N24	-1.207	-0.692	-0.543	0.064
	0.424	-1.877	-1.715	1.168
	-0.156	-0.529	1.549	1.639
	-1.731	-1.753	-1.0523	0.942
Bias	1.815	0.742	1.492	-1.648

	Weights		Weights		Weights
Input to output	0.727	N14 to output	-1.372	N24 to output	-0.904
	-1.089		-1.542		0.596
	1.705		-0.690		-1.883
	-0.911		-1.425		-1.412
	0.294		-0.267		
	-0.351		-1.174		
	0.813				
	-1.307				
	-1.849				
Bias	0.824		-0.967		-1.901